THE CHARACTERIZATION OF HUMAN γD-CRYSTALLIN MUTANTS AND THEIR DIFFERENTIAL INTERACTIONS WITH THE LENS CHAPERONE αB-CRYSTALLIN

By
Kate L. Moreau

B.A. Molecular Biology and Biochemistry
Rutgers University, 2004

SUBMITTED TO THE DEPARTMENT OF BIOLOGY
IN PARTIAL FULFILLMENT OF THE REQUIREMENTS
FOR THE DEGREE OF

DOCTOR OF PHILOSOPHY
AT THE
MASSACHUSETTS INSTITUTE OF TECHNOLOGY

FEBRUARY 2011

Signature of Author_____
Department of Biology
October 2010

Certified by_____
Jonathan A. King
Professor of Molecular Biology
Thesis Supervisor

Accepted by_____
Stephen P. Bell
Co-Chair, Department Committee on Graduate Students

THE CHARACTERIZATION OF HUMAN γD-CRYSTALLIN MUTANTS AND THEIR DIFFERENTIAL INTERACTIONS WITH THE LENS CHAPERONE αB-CRYSTALLIN

by

Kate L. Moreau

Submitted to the Department of Biology
on October 13, 2010 in Partial Fulfillment of the
Requirements for the Degree of
Doctor of Philosophy in Biology

ABSTRACT

Cataract, the leading cause of blindness worldwide, is the opacification of the eye lens. In age-related cataract, as well as roughly one half of congenital cataract cases, aggregation or precipitation of crystallin proteins results in the formation of large structures that scatter light, preventing the pinpoint focusing on the retina normally accomplished by the lens.

The human eye lens is composed of fiber cells packed with crystallins up to 450 mg/ml. Human γD-crystallin (HγD-Crys) is a monomeric, two-domain protein, predominantly localized to the lens nucleus. Both domains of this long-lived protein have double Greek key β-sheet folds with well-packed hydrophobic cores. Three mutations resulting in amino acid substitutions in the γ-crystallin buried cores—two in the N-terminal domain (N-td), and one in the C-terminal domain (C-td)—cause early-onset cataract in mice. It has not been possible to identify the aggregating precursors within lens tissues, and the question persists as to the nature of structure and stability changes in the crystallins leading to their increased propensity for aggregation and cataract formation within the lens environment. To compare *in vivo* cataract-forming phenotypes with *in vitro* unfolding and aggregation of γ-crystallins, mouse mutant substitutions were introduced into HγD-Crys.

WT HγD-Crys unfolds *in vitro* through a three-state pathway, exhibiting an intermediate with the N-td unfolded, and the C-td native-like. L5S and V75D also displayed three-state unfolding pathways, with the first transition, unfolding of the N-td, shifted to significantly lower denaturant concentrations. I90F was globally destabilized and the overall unfolding transition was shifted to lower denaturant concentrations. During thermal denaturation, the mutant proteins exhibited lowered thermal stability compared with WT. Kinetic unfolding experiments further confirmed this destabilization.

The cataract phenotype of increased protein aggregation could be a direct property of the mutation, or could reflect an inability to be recognized by the α-crystallin chaperone. We have therefore carried out experiments comparing the interactions of WT HγD-Crys, V75D and I90F with a major component of the lenticular chaperone system, the small heat shock protein human αB-crystallin. Suppression levels of the aggregation that competes with the refolding pathway after dilution from GdnHCl were indistinguishable between WT and mutant proteins. However, dramatic differences among the mutants were observed under different conditions, including physiological conditions in the absence of denaturant and partially destabilizing acidic conditions such as those that may exist in the vicinity of degrading lysosomes in maturing lens fiber cells. In particular, incubation under physiological conditions highlighted differential interactions between the lens chaperone and the mutant HγD-Crys proteins themselves. Destabilized precursors to the cataractous state may populate various non-native structural conformations that, although aggregation-prone, elude recognition by α-crystallin and efficiently continue along the aggregation pathway.

Coupled with the observation of different unfolding pathways for the mutant crystallins, these results support the existence of multiple pathways for cataract formation in which partially unfolded species are differentially recognized by the passive lens chaperone system. While these observations were made utilizing destabilized mutant proteins, the same mechanisms may underlie the formation of age-related cataractous aggregates induced *in vivo* by covalent modification of the lens proteins.

Thesis Supervisor: Jonathan A. King
Title: Professor of Molecular Biology

ACKNOWLEDGEMENTS

None of this would have been possible without the assistance, encouragement and support of many people. First, I would like to thank my advisor, Professor Jonathan King, for giving me a place in his lab. You have been not only a scientific advisor, but you've shared your perspectives on life and responsibilities inside and outside of the lab. Your passion for science and education is inspiring. While offering your opinions, you have been supportive of my decisions, or sometimes the lack thereof. Thank you for your encouragement and confidence building—I'm working on that.

I would also like to thank my thesis committee members. Professors Bob Sauer and Amy Keating, thank you for giving your perspectives and suggestions, as well as your time, over the past several years. Professor Thomas Schwartz and Dr. Caroline Shamu, thank you for taking the time to read my thesis and serve on my defense committee.

To the entire King lab, thank you for creating such an interesting, fun and memorable working environment! Thank you to Dr. Kelly Knee for being a most excellent bay-mate. You are always ready to listen, whether I need to work through an experiment, vent my frustrations or share a gross story. I hope that we can continue to share our brand of humor and our love of the Clover truck. To Dr. Ligia Acosta-Sampson, thank you for sharing your vast α-crystallin knowledge. You are always ready to answer questions or help troubleshoot and I certainly would not have completed the experiments in this thesis without your advice. To Dessy Raytcheva, good luck as you approach the end of your graduate career! Your upbeat outlook is inspiring and your ability to TA every semester amazes me. You have such a great perspective on graduate school and science, and I enjoy our overlapping tea breaks during the day. To Fanrong Kong, good luck with all of your mutants! You are the next bird on the crystallin tree. To Nathaniel Schafheimer and Oksana Sergeeva, good luck as you both progress through your graduate studies. Your enthusiasm is refreshing! To Drs. Ishara Mills-Henry, Jiejin Chen and Yongting Wang, thank you for all your help as I started in the King lab. You all have answered my many questions with patience and excellent advice. Thank you to Dan Goulet for being the lab socialite and getting us all out to see The Maquis. Thank you to Cammie Haase-Pettingell for answering countless random questions and encouraging our lab outings. You are always ready to lend a hand. Thank you to all other members of the King lab, including Jeannie Chew, Cindy Woolley, Ginger Yang, Althea Hill, Dr. Takumi Takata, Professor Jacqueline Piret, and Lisa Guisbond, for creating such a fun and unique lab!

I cannot ever express the importance of the friendships I have made at MIT. As a first year student, I quickly bonded with my classmates Crystal Lee, Jamie Newman and Gina Lafkas. Thank you for the (in)sanity that you provided, the laughter we have shared (oh my!) and the amazing support system that you have been throughout my time here. Crystal, I don't know how you fit it all into a 24-hour day, but your hard work and perseverance are inspiring. To top it off, you are an excellent baker! Thank you for all the laughs we've shared, for making sure I made it home through all of our first year and

for listening to my wacky, often winding rants. Jamie, you are an amazing listener. You are always there for a much needed break with words of encouragement. I will never forget you laughing yourself into tears, and I hope we can continue to do so (just minus the stress of graduate school).

I must also thank my friends back in New York and New Jersey. Shana Dworken, you have been my PR person and my cheerleader since high school! I cannot thank you enough for supporting my decisions, giving thoughtful advice and encouragement and being such a fun roommate. Amy Chiaravallo, I'm so glad we became close friends, even if it didn't start out that way. Thank you for being there through thick and thin, you have truly seen my ups, my downs and the messes in between, and have always been there with advice and humor (and probably a much needed beer). Marisa Montemorano, thank you for being such a supportive friend, keeping me on my toes with your pranks and introducing me to new music and films.

I absolutely must thank my family for their unwavering support. To my mom, Diane Drahos, thank you for never pressuring me, but allowing me to follow my own path. I am so happy we have become friends as well as family. We certainly share the same sense of humor! To my sister, Colleen Drahos, thank you for your support and encouragement. We have become much closer over the past few years and I hope we continue to do so. Thank you to my father, Steve Drahos, for encouraging me to take the harder math class. Although my math usage is rather minimal now, thank you for pushing me. Finally, to my Nana, the funniest 90 year old ever (who does not have cataracts). You have been a constant presence in my life, always encouraging, always supportive, and always truthful. I am incredibly thankful for you.

Last, but certainly not least, to my husband Mark Moreau. Thank you for moving to Massachusetts. Thank you for believing in me (and jet packs), for making me laugh and for being there every day. I know I have your confidence when my own falters. I love you.

This research was supported by National Institutes of Health grants EY015834 and GM17980 awarded to Jonathan A. King.

BIOGRAPHICAL NOTE

Education

Ph.D. Expected 2011	Massachusetts Institute of Technology, Department of Biology Cambridge, MA
B.A. June 2004	Rutgers University, Department of Molecular Biology and Biochemistry, New Brunswick, NJ Major: Molecular Biology and Biochemistry, *with Highest Honors*

Research and Professional Experience

2006-2010	Graduate Research Assistant in the laboratory of Professor Jonathan King, MIT Department of Biology, Cambridge, MA
2004-2005	Proteomics Research Associate, Alfa Wassermann Proteomic Technologies, LLC, West Caldwell, NJ
Summer 2003	Research Intern in the Department of Ion Channels Merck and Co., Inc., Rahway, NJ
Summer 2002	Research Intern, Provid Pharmaceuticals, North Brunswick, NJ
2001-2004	Undergraduate Research Assistant in the laboratory of Professor Gaetano Montelione, Rutgers University, New Brunswick, NJ *Thesis: Protein Expression and Folding Optimization for High-Throughput Proteomics*

Publications

Moreau, K.L. and King, J. 2009. Hydrophobic Core Mutations Associated with Cataract Development in Mice Destabilize Human γD-Crystallin. *J. Biol. Chem.* **284**(48): 33285-33295.

TABLE OF CONTENTS

LIST OF FIGURES

CHAPTER 1

CHAPTER 2

CHAPTER 3

CHAPTER 4

CHAPTER 6

LIST OF TABLES

LIST OF ABBREVIATIONS

(*in alphabetical order*)

αA: human αA-crystallin
αB: human αB-crystallin
AD: Alzheimer's disease
AFM: atomic force microscopy
bis-ANS: 4,4'-bis(1-anilinonaphthalene 8-sulfonate)
CD: circular dichroism
CRABP1: cellular retinoic acid binding protein 1
CR: Congo Red
C-td: C-terminal domain
CV: column volume
DTT: dithiothreitol
EDTA: ethylenediaminetetraacetic acid
FPLC: fast protein liquid chromatography
FRET: fluorescence resonance energy transfer
GdnHCl: guanidinium hydrochloride
HbS: sickle cell form of human hemoglobin (containing E6V substitution)
HγC-Crys: human γC-crystallin
HγD-Crys: human γD-crystallin
HγS-Crys: human γS-crystallin
HSQC: heteronuclear single quantum coherence
Ig: immunoglobulin
IPTG: isopropyl-β-thiogalactoside
MγB-Crys: murine γB-crystallin
MγD-Crys: murine γD-crystallin
MγS-Crys: murine γS-crystallin
NaPi: sodium phosphate
NMR: nuclear magnetic resonance
N-td: N-terminal domain
PrP^{C}: human prion protein cellular form
PrP^{Sc}: human prion protein infectious scrapie form
RDC: residual dipolar coupling
SDS-PAGE: sodium dodecyl sulfate polyacrylamide gel electrophoresis
SEC: size exclusion chromatography
sHSP: small heat shock protein
TEM: transmission electron microscopy
ThT: Thioflavin T
Tris: Tris(hydroxymethyl)-amino methane
TTR: Transthyretin
UV: ultraviolet
WT: wild type

CHAPTER 1:

INTRODUCTION

A. The Human Eye

The human eye is a chambered eye that uses refraction to focus light. Light first passes through the cornea, the outer transparent layer of the eye where about two-thirds of refraction takes place (Oyster 1999). The cornea maintains its transparency by way of an ordered arrangement of collagen fibers (Oyster 1999). Light next enters the pupil, whose size is controlled by contraction and expansion of the surrounding iris, thereby controlling the amount of light that enters. The transparent lens sits behind the cornea and pupil and accounts for the remaining one-third of the eye's refractive power (Oyster 1999). The lens is responsible for fine-focusing of light onto the retina and its transparency is vital for visual acuity. Its transparency is maintained in a different manner than that of the cornea and is discussed further in the following section. Light exits the lens, passes through the vitreous humor and is focused on photoreceptor cells of the retina (Oyster 1999). Activation of these cells results in signal relay through the optic nerve and processing in the brain, resulting in our visual perception. Figure 1-1 is a schematic diagram of the eye. Its major structures are denoted.

B. Lens Development, Structure and Transparency

Lens development occurs in humans around gestational day 28. It begins with formation of the lens placode from surface ectoderm and its subsequent invagination to form the lens vesicle (Figure 1-2) (Augusteyn 2010). The anterior of the lens vesicle is lined with a single layer of epithelial cells and the remainder is composed of elongated primary fiber cells, known as the embryonic nucleus. The epithelial cells may be thought of as lens stem cells, both maintaining the anterior epithelial layer and undergoing mitosis to produce daughter cells that migrate to the lens equator where they begin to differentiate into fiber cells (Figure 1-2) (Augusteyn 2010). The differentiating cells elongate to form long, thin ribbon-like structures that surround the embryonic nucleus. At this time, major intracellular changes occur, including high-level expression of the soluble crystallin proteins followed by degradation of all organelles, including the nucleus and ribosomes (Augusteyn 2010). Epithelial cells continue to differentiate

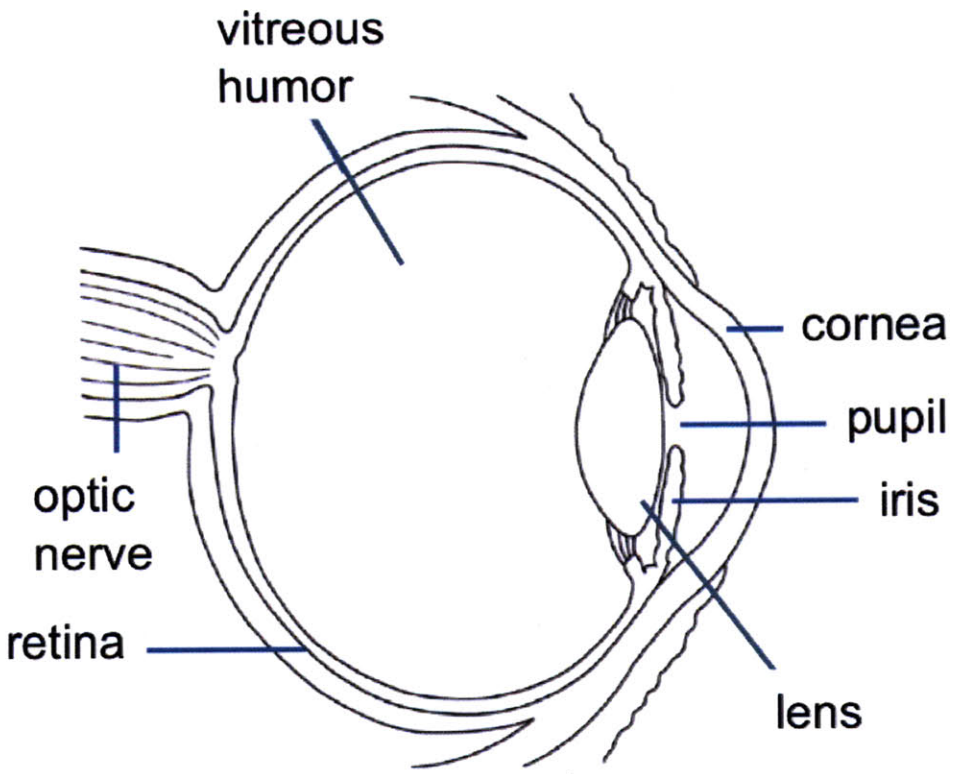

Figure 1-1: Schematic diagram of the human eye

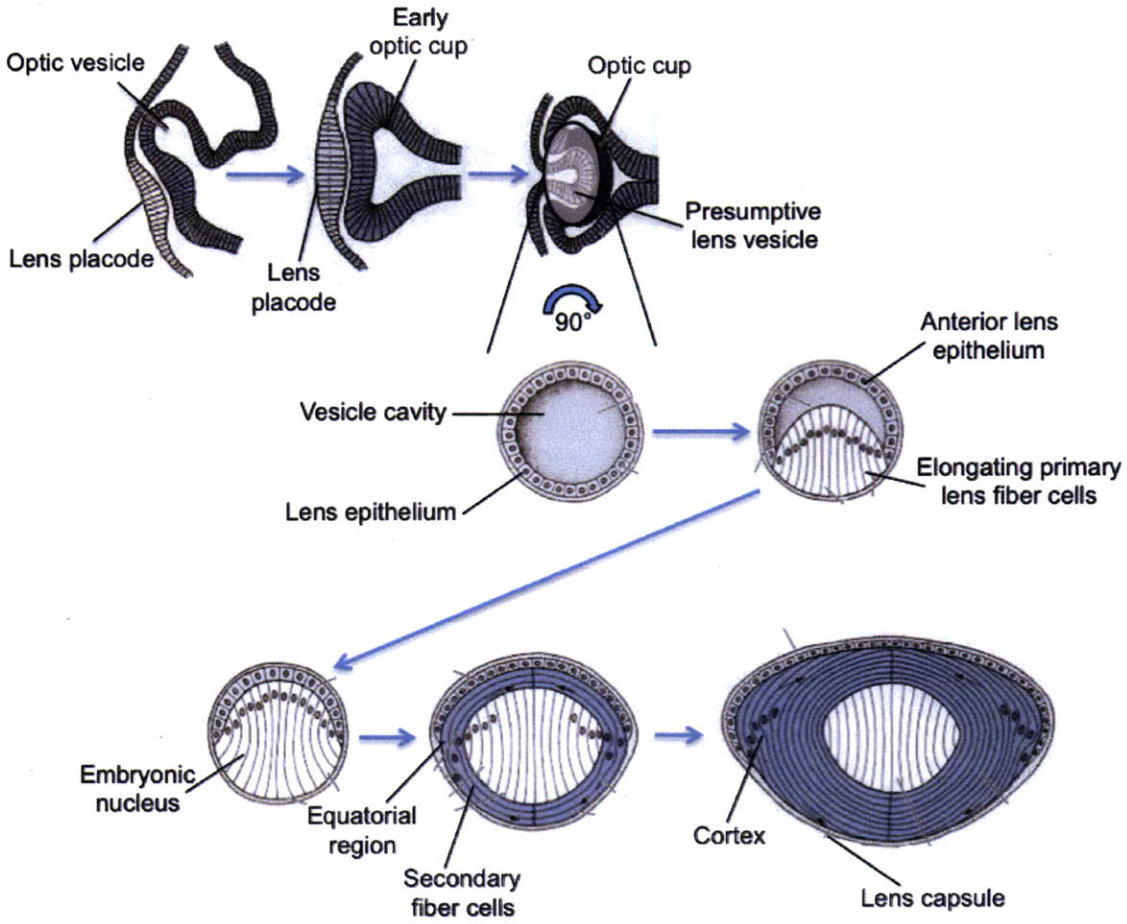

Figure 1-2: The stages of lens development. The first row depicts initial formation of the lens vesicle beginning with the lens placode. The second and third rows depict the continued formation of the lens.

throughout life, layering over existing fiber cells in shells similar to the layers of an onion. The embryonic nucleus and the surrounding layers formed *in utero*, as well as secondary fiber cells formed early after birth are collectively known as the lens nucleus. The cortex layer surrounds the nucleus and the cells in these outer layers maintain some level of protein synthesis and metabolic activity. The entire lens is surrounded by a collagenous lens capsule, making it a truly isolated tissue that is completely lacking in both arterial and venous blood flow (Figure 1-2) (Oyster 1999). The development and structure of the lens is such that it contains some of the oldest cells and proteins in the entire body that must maintain their molecular structure and organization over the lifetime of the individual.

The lens must remain transparent to visible light and numerous strategies are employed to reduce or remove light-scattering structures from the tissue. Fiber cells comprising the nucleus are compacted as new layers are added, thinning the interdigitated cell membranes and diminishing intercellular space to maintain a refractive index similar to the cytoplasm, thus reducing light scatter (Michael et al. 2003). In the cortex, fiber cells have a regular hexagonal shape to allow tight packing that achieves the same goal (Michael et al. 2003). Coordinated organelle degradation is initiated during fiber cell maturation to remove these large structures, which have a higher refractive index than the cytoplasm (Bassnett 2002). Crystallin protein expression is highly upregulated during fiber cell differentiation as they comprise 90% of proteins in the mature lens. Short-range ordered packing of the crystallins at concentrations of 250-450 mg/ml results in soluble fiber cell interiors with uniform density. This short-range order is responsible for transparency of the concentrated solution and a polydisperse mixture of crystallins avoids crystallization within the lens (Delaye and Tardieu 1983; Oyster 1999).

C. The Lens Crystallins

The crystallins are the major soluble proteins of the human lens, and they play an indispensible role in maintaining lens transparency. Human lenses, as well as those of all mammals, contain the ubiquitous α-, β- and γ-crystallins. Because the lens is formed *in utero* and mature fiber cells lack protein synthesis and degradation machinery, a major

requirement of the crystallins is superior solubility and stability of their native conformations.

1. The Small Heat Shock Protein α-Crystallin

α-Crystallin is a member of the small heat shock protein family of chaperones. Two different genes encode the homologous proteins αA- and αB-crystallin (herein αA and αB), which share 57% identity. Both monomers are approximately 20 kDa and together they form polydisperse hetero-oligomeric complexes ranging in size from 300 – 1000 kDa (Reddy et al. 2006). Isolated recombinant αA and αB formed homo-oligomers that have chaperone activity *in vitro* (Sun et al. 1997). αA is lens-specific while αB is expressed widely in both mouse and rat, in especially high levels in the heart and skeletal muscle (Dubin et al. 1989; Iwaki et al. 1990). Both proteins are found in the lens epithelium and their expression is highly upregulated in fiber cells during differentiation (McAvoy 1978; Van Leen et al. 1987).

a. α-Crystallin Structure

The small heat shock proteins (sHSPs) comprise a large family of 12-43 kDa proteins that form highly varied oligomers. They are present across all archea, eubacteria and metazoans with few exceptions (Narberhaus 2002), and in higher organisms multiple genes encode a range of sHSPs, including 10 in humans (Haslbeck et al. 2005). All sHSPs possess unstructured N-terminal domains (N-td) whose sequences are not well conserved and they share a common structural feature known as the α-crystallin domain. This domain has an immunoglobulin (Ig)-like, β-sandwich structure (Bagnéris et al. 2009). Crystal structures of the isolated α-crystallin domains of both rat Hsp20 and human αB revealed that α-crystallin domains formed dimers by aligning their β6/7 strands to form an extended, continuous sheet (Figure 1-3A). This dimeric assembly also created a groove lined with non-polar residues and the authors suggested that the N-tds (truncated in these constructs to allow for crystallization) would fill these grooves

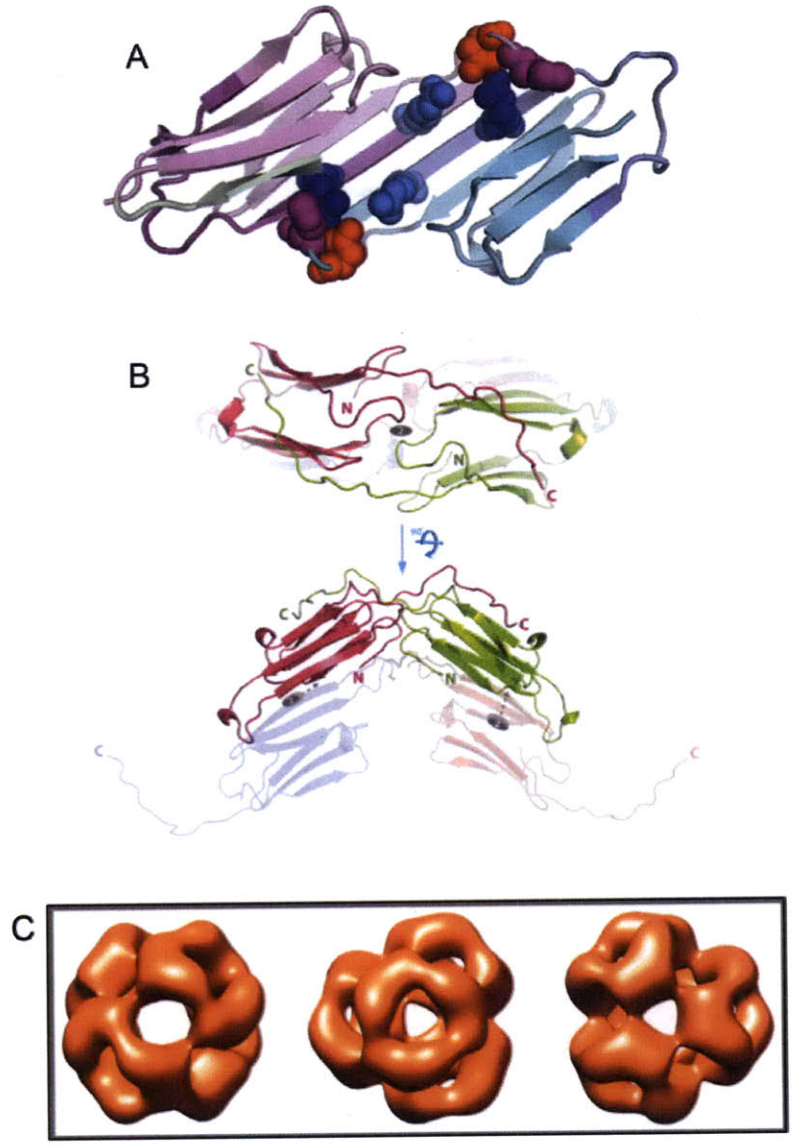

Figure 1-3: Structures of human αB-crystallin. **(A)** Crystal structure of truncated α-crystallin domain dimer highlighting the antiparellel β-sheet interface. Specific residues are shown in spacefill. R116 (light blue) and R120 (deep blue) are residues that are substituted in congenital cataract and cardiomyopathies. D109 (red) forms an ion pair with R120. Reprinted and modified with permission from Elsevier (Bagnéris *et al.* 2009). **(B)** Crystal structure of dimers including the interactions of the C-terminal extensions. Reprinted and modified with permission from Laganowsky *et al.* (2010). **(C)** Cryo-EM reconstruction of a 24 subunit complex modified from Peschek *et al.* (2009).

(Bagnéris et al. 2009). The overall structure was the same for both proteins, although the β-strands from each subunit aligned in different registers for the rat and human proteins, resulting in a more compact structure for human αB (Bagnéris et al. 2009). Further structural analysis of human αA and αB constructs that included portions of the C-terminal tail identified varied conformations of a flexible hinge loop and the palindromic sequence E-R-T-I-X-I/V-T-R-E, where the middle region I-X-I/V (the identity of X often being proline) is particularly well conserved (Laganowsky et al. 2010). These physical properties of the protein contribute to the inherent polydispersity of α-crystallin (Figure 1-3B).

Crystal structures of monodisperse sHSPs have been determined for wheat Hsp16.9 (van Montfort et al. 2001), which formed a dodecamer composed of two stacked discs, and *Methanococcus jannaschii* Hsp16.5 (Kim et al. 1998), whose structure was different, forming a 24-subunit hollow sphere. Unfortunately, the polydisperse nature of α-crystallin has long hindered crystallization of the assembled complex. Transmission electron microscopy (TEM) of recombinant αA and αB confirmed that even the isolated subunits form polydisperse mixtures. Cryo-electron microscopy reconstruction was possible for αB and the complex was roughly spherical and composed of 24 subunits (Figure 1-3C) (Peschek et al. 2009).

b. α-Crystallin Function

Murine Hsp25 and bovine α-crystallin were the first sHSPs shown to exhibit chaperone activity by suppressing the thermal aggregation of a number of model substrates (Horwitz 1992; Jakob et al. 1993). α-Crystallin suppresses aggregation in an ATP-independent manner and it does not appear to refold its bound substrates. Substrates remain bound to the chaperone, sequestered from other aggregating molecules, although in some cases these interactions are thought to be transient (Hatters et al. 2001). There is *in vitro* evidence that sHSPs maintain bound substrates in a folding-competent state and shuttle them to ATP-dependent chaperone systems where refolding is initiated (Lee et al. 1997; Tanksale et al. 2002). Raman *et al.* described the temperature dependence of chaperone activity for α-crystallin (1995). At 27.6°C α-crystallin was

unable to suppress aggregation of insulin B chain at a 1:1 ratio, but at 40.6°C aggregation was completely suppressed. Along with an increase in activity, changes in quaternary structure were observed by an increased binding of the hydrophobic probe 4,4'-bis(1-anilinonaphthalene 8-sulfonate) (bis-ANS) at temperatures above 30°C, indicating greater exposure of hydrophobic surfaces (Raman et al. 1995). An increase in chaperone function was accompanied by irreversible structural changes identified by increased binding of bis-ANS at temperatures over 50°C. These changes were maintained upon cooling to physiological temperature or below (Das and Surewicz 1995; Kumar et al. 2005). Further analysis of the individual subunits αA and αB showed that these changes occurred specifically in αA and the chaperone function of αA exceeded that of αB after heating (Reddy et al. 2000; Kumar et al. 2005). Although αA expression is no longer heat-inducible within the lens environment, it has maintained the structural plasticity associated with heat stress.

As briefly described in the preceding section, α-crystallin and all sHSPs can be divided into three regions of primary sequence: (1) an N-terminal region, consisting of residues 1-67 of αB, that is unstructured and poorly conserved; (2) the conserved α-crystallin domain, which spans residues 68-148 of αB and is the defining feature of all sHSPs; and (3) a flexible C-terminal extension (residues 149-175 of αB). Upon first glance, the conservation of the α-crystallin domain suggests that this region is the site of chaperone function, binding aggregation-prone intermediates. However, several studies have shown that various functions are shared throughout the three regions of sHSPs.

Dynamic structures that readily undergo subunit exchange are a hallmark of the sHSPs. Fluorescence resonance energy transfer (FRET) experiments using two populations of αA demonstrated that reversible subunit exchange occurred between oligomers (Bova et al. 1997). The rate of exchange was positively correlated with temperature (Sun et al. 1998). The presence of substrate reduced subunit exchange in a size-dependent manner, with larger substrate proteins having a more profound effect (Bova et al. 1997). Wheat Hsp16.9 and *M. jannaschii* Hsp16.5 also readily underwent subunit exchange (Bova et al. 2002; Sobott et al. 2002) making this a property of both mono- and polydisperse sHSPs.

Subunit-subunit interactions are crucial for the proper assembly and subunit exchange of sHSPs. The N-terminal domains of both αA and αB are implicated in subunit interactions. Truncation of the first 19 residues of αA had no effect on complex assembly, while removal of the following 36 residues resulted in improper assembly, and the dominant species consisted of trimers and tetramers that did not undergo exchange (Bova et al. 2000). Pasta *et al.* identified a narrow region of the N-td in both αA (residues 20-28) and αB (residues 21-29) that, when deleted, resulted in the formation of smaller oligomers that exhibited faster subunit exchange (Pasta et al. 2003). These oligomers were larger than those observed by Bova and colleagues and still underwent exchange, suggesting that residues of the N-td outside of the deleted sequence specifically mediated this function. Various truncations of the final nine residues of the C-terminal extension of αA resulted in the formation of somewhat smaller sHSP complexes with greatly reduced rates of subunit exchange with either WT αA or αB (Aquilina et al. 2005; Kallur et al. 2008). The C-terminal extension is also indicated in increasing solubility of the α-crystallin complex (Smulders et al. 1996). Slight decreases in subunit exchange were observed for the congenital cataract mutants R116C αA and R120G αB (both found within the α-crystallin domain); these findings may be due to the location of these residues at the interface of the dimeric structure rather than direct contribution of this domain to subunit exchange (Cobb and Petrash 2000; Liang and Liu 2006). Destabilization of the dimeric structure would likely affect subunit exchange and oligomerization (Michiel et al. 2009). These processes are clearly driven by a combination of factors, and regions in the N-terminal domain modulate subunit exchange.

In terms of substrate binding, mutagenesis studies implicate the hydrophobic, phenylalanine-rich N-terminal domain as critical for binding. Amino acid substitutions that altered selected N-terminal phenylalanine residues completely abolished the chaperone activity of murine αB (Plater et al. 1996). More direct binding studies using a heterobifunctional cross-linker identified two regions of αB, 57-69 in the N-td (just overlapping with the α-crystallin domain) and 93-107 in the α-crystallin domain, that are in close proximity to the bound substrate protein, alcohol dehydrogenase in this case (Sharma et al. 1997). Further binding studies utilizing protein pin arrays identified seven

regions important for substrate binding, two regions corresponding to the N-td, four from the α-crystallin domain and a single region from the C-terminal extension (Ghosh et al. 2005). Proteolytic protection assays also confirmed that four sites within the N-td and one region in the C-terminal extension of αB were shielded from cleavage in the presence of bound reduced α-lactalbumin (Aquilina and Watt 2007). Further support for the role of the N-td in substrate binding comes from studies on a variety of other sHSPs including wheat Hsp16.9, *M. jannaschii* Hsp16.5 and PsHsp18.1 from the pea plant. Cross-linking of substrate with PsHsp18.1 revealed several bound sites in the N-terminal arm of this protein (Jaya et al. 2009). Chimeras with exchanged N-terminal regions between wheat Hsp16.9 and PsHsp18.1 exhibited differential aggregation suppression abilities against a set of substrate proteins, suggesting that this domain plays a major role in substrate binding (Basha et al. 2006). These results indicate that substrate-interacting regions span the entire protein but are concentrated in the N-terminal domain.

Detailed studies of the binding site(s) on α-crystallin were undertaken by McHaourab and colleagues. Using a series of increasingly destabilized T4 lysozyme mutants, two different "binding modes" were identified, the first corresponding to a high-affinity/low capacity state and the second to a low-affinity/high capacity state (McHaourab et al. 2002; Koteiche and McHaourab 2003). They later demonstrated that the complexed T4 lysozyme molecules were mostly unfolded and bound in a distinct manner where the C-terminal domain was protected from solvent while the N-terminal domain was exposed (Claxton et al. 2008). Experiments with the lenticular substrates βB1- and βB2-crystallin demonstrated that α-crystallin recognized and bound monomeric forms of both proteins and promoted their dissociation and unfolding (Sathish et al. 2004; McHaourab et al. 2007). In addition, these studies showed that the two binding modes are in fact distinct sites, and both have the ability to bind the predominantly unfolded conformation of T4 lysozyme (Claxton et al. 2008).

The substrate binding sites of α-crystallin recognize a wide range of proteins. This begs the question: what substrate features are being recognized? Like Trigger factor and the ATP-dependent Hsp70/40 system and the chaperonins GroEL/S and TriC, the sHSPs including α-crystallin recognize and bind exposed hydrophobic regions of partially unfolded and destabilized proteins (Bloemendal et al. 2004; Hartl and Hayer-

Hartl 2009). Studies using the substrate α-lactalbumin showed that α-crystallin only binds to intermediates or molten globule structures that are unstable in solution and aggregation-prone. No significant binding was observed for stable molten globule structures, such as the partially reduced species of α-lactalbumin (Lindner et al. 1997). Carver *et al.* demonstrated that soluble, stable, but unfolded proteins did not interact with α-crystallin. Both α-casein and α-ovalbumin bound bis-ANS, indicating exposure of hydrophobic patches, but neither of these proteins interacted with α-crystallin, nor did they aggregate in solution (Carver et al. 1995).

Despite the general characterization of structural requirements for the substrate, identification of specific interacting regions on substrates is lacking. Studies using bovine α-crystallin cross-linked to bound yeast alcohol dehydrogenase identified two distinct peptides as probable substrate binding sites, indicating that upon destabilization and partial unfolding specific protein regions are recognized (Santhoshkumar and Sharma 2002). A short peptide derived from βA1/A3-crystallin (residues 102-117) bound α-crystallin and inhibited chaperone function (Rao et al. 2008), which suggests that this region may be a recognition site in the full-length protein. The identification of specific binding regions, in particular those of the physiological lenticular substrates, are of great interest as this information could potentially aid in the development of preventive cataract medication.

α-Crystallin is the sole chaperone system of lens fiber cells. Due to the lack of protein synthesis machinery, the supply of α-crystallin is finite. Its increased localization to the water-insoluble fraction of aged normal and cataractous lenses (Harrington et al. 2004; Harrington et al. 2007) suggests that with age, its bound substrate load becomes saturating and the chaperone-substrate complex aggregates and precipitates within fiber cells. αA knockout mice displayed a cataract phenotype with inclusions containing both αB- and γ-crystallins (Brady et al. 1997); however, αB knockouts were afflicted with skeletal muscle degeneration without cataract and suffered from dramatically shortened lifespan (Brady et al. 2001). It was therefore impossible to examine the importance of αB in the aging lens and it may be critical for maintenance of long-term fiber cell structure and lens transparency.

In addition to its chaperone role, α-crystallin is also a structural protein in the lens, interacting with plasma membranes and the lens-specific cytoskeletal proteins BFSP1 (filensin) and BFSP2 (CP49). The lens-specific beaded filaments are intermediate filament-like structures composed of BFSP1 and 2; they are heavily decorated with "beads" which have been identified as α-crystallin oligomers (Carter et al. 1995). α-Crystallin is required for the *in vitro* formation of native-like beaded filaments (Carter et al. 1995). In non-lens cells, intermediate filaments are associated with a host of proteins including chaperones and the proteasome, and they are crucial to plasma membrane stability (Song et al. 2009). They no doubt play a role in maintaining the unique structure of fiber cells in the lens nucleus and cortex. Although the precise role of the α-crystallin interaction with BFSP1 and 2 is unclear, both components are crucial for proper lens function.

It is well documented that proteins of the aging human lens are significantly modified through covalent damages including oxidation, deamidation and truncation. These destabilizing modifications result in partial unfolding and population of aggregation-prone intermediates that, as discussed in this section, are prime targets for sequestration by α-crystallin. As the fixed amount of free α-crystallin is diminished, the buffer capacity of the lens to prevent protein aggregation is reduced and there may be a threshold above which protein aggregation dominates. Adequate functional α-crystallin is therefore critical for proper maintenance of lens transparency and refraction.

2. The βγ-Crystallins

The βγ-crystallins comprise the second major group of crystallins in human lenses. Both are mainly structural proteins whose high solubility and dramatic stability are well suited to the environment of lens fiber cells. Both β- and γ-crystallins are composed of two domains, although interdomain interactions and oligomeric states differ between the two (Bloemendal et al. 2004). Several different β- and γ-crystallins, which are homologous but contain many sequence variations amongst one another, are major contributors to lens transparency. They are, by and large, lens-specific with small amounts of βB2-crystallin expressed in the retina, brain and testis (Magabo et al. 2000).

Recent proteomic analyses identified γ-crystallins in the retina of diabetic mice, although the implications of this finding are unknown (Fort et al. 2009).

The γ-crystallins are monomeric proteins found in terminally differentiated lens fiber cells. In humans, there are seven genes encoding γA-F and γS-crystallin (*CRYGA-F; S*). *CRYGA-F* are located in a cluster on chromosome 2q33-36 (Shiloh et al. 1986) while *CRYGS* is spatially distinct, found on chromosome 3q26.3 (Wijnen et al. 1989). The major γ-crystallins expressed in the human lens are γC, γD, and γS, while γE and γF are pseudogenes (Brakenhoff et al. 1990). They are the final crystallins expressed in the developing lens. All γ-crystallins are composed of two homologous domains, an N-terminal domain (N-td) and a C-terminal domain (C-td) that arose from a gene duplication event (Shimeld et al. 2005). Each domain is constructed from eight β-strands that form two intercalated Greek Key motifs. The domains interact by way of well-conserved interface residues, suggesting that the domain interface plays a major role in the maintenance of protein structure.

a. γD-Crystallin

Human γD-crystallin (HγD-Crys) is one of the two major γ-crystallins found in the lens nucleus, comprising up to 8% of total soluble lens protein (Robinson et al. 2006). Its expression is upregulated during the last stages of fiber cell differentiation, following that of both the α- and β-crystallins. As one of the major structural proteins in the lens, it is important for formation of the polydisperse, yet regular arrangement of crystallins that results in lens transparency. It is particularly enriched in the oldest region of the lens, requiring this protein to be unusually long-lived.

HγD-Crys is a 20.6 kDa, 173 residue protein. Its crystal structure has been solved to 1.25 Å (Basak et al. 2003). As with other γ-crystallin structures, each Greek Key motif exchanges its third strand with the facing motif (Figure 1-4B). The protein is rich in aromatic residues, including several aromatic pairs, that make substantial contributions to its stability and folding (F. Kong, personal communication). Each domain contains a highly stabilizing tyrosine corner, in which the Tyr side chain is hydrogen bonded to the peptide backbone (Hemmingsen et al. 1994). Determination of the high resolution

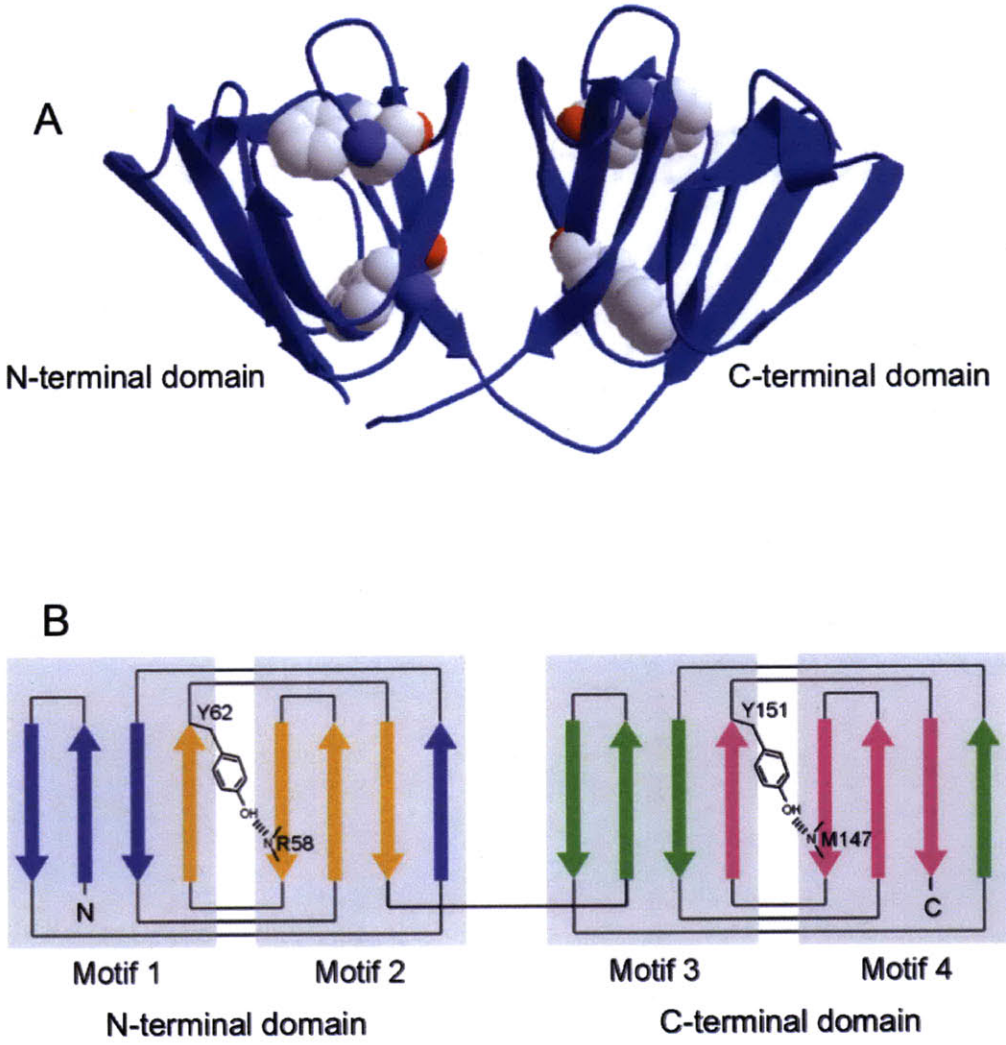

Figure 1-4: **(A)** Crystal structure of human γD-crystallin. PDB ID 1HK0. The four tryptophan residues are shown in space fill. **(B)** Topology diagram of HγD-Crys. Note the intercalated nature of the Greek Key motifs. The tyrosine corners are denoted as well. (See Introduction section F.1)

structure of HγD-Crys has enabled extensive biochemical and biophysical study of this protein.

HγD-Crys contains four highly conserved buried tryptophan residues, two in each domain (W42 and W68 in the N-td; W130 and W156 in the C-td; Figure 1-4A), and in the native state this protein exhibits anomalous Trp fluorescence quenching (Kosinski-Collins and King 2003). Extensive studies of this phenomenon have determined that one Trp (W42 and W130) in each domain is highly fluorescent and upon excitation, transfers energy to the second Trp residue (W68 and W156) in the same domain. The unique backbone conformation, in combination with specifically oriented water molecules in the vicinity of W68 and W156, allow fast electron transfer to the protein backbone (Chen et al. 2006). Fluorescence anisotropy demonstrated the rigid nature of the Trp environments, which suggests that the hydrophobic core of HγD-Crys is tightly packed (Chen et al. 2008). Upon protein unfolding, quenching is relieved due to loss of these stringent structural requirements. The large change in Trp fluorescence upon unfolding has been utilized in a range of studies, including those documented in this thesis, to elucidate determinants of folding and stability for HγD-Crys (Figure 1-5A).

The long lifetime of HγD-Crys in the lens requires superior stability. It can be recombinantly expressed in *E. coli* and purified from the soluble fraction of the cell lysate. It was resistant to denaturation in 8 M urea (Kosinski-Collins and King 2003) and had a melting temperature above 80°C (Flaugh et al. 2006). Equilibrium unfolding/refolding experiments determined a three-state *in vitro* unfolding pathway (Flaugh et al. 2005a) with the first transition at 2.2 M GdnHCl corresponding to unfolding of the N-td. The second transition, with a midpoint at 2.8 M GdnHCl, corresponds to unfolding of the C-td. These measurements yielded an apparent total ΔG° = 16.6 kcal/mol for the WT protein (Figure 1-5B) (Kosinski-Collins et al. 2004; Flaugh et al. 2005a). A three-state unfolding pathway implies the presence of a populated partially-folded intermediate. Experiments with triple Trp mutants showed that this intermediate,

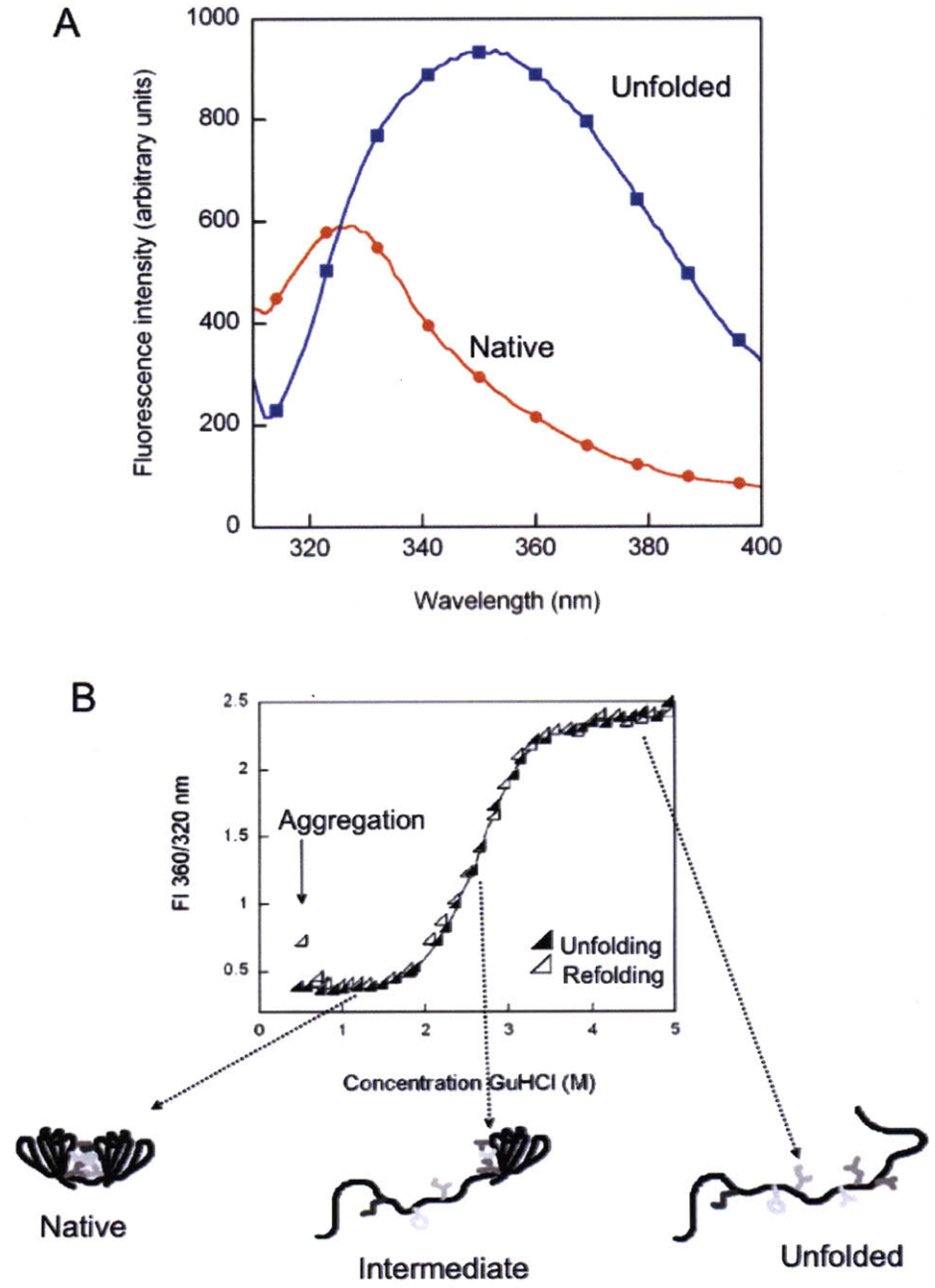

Figure 1-5: HγD-Crys Trp fluorescence and equilibrium unfolding pathway. **(A)** Trp emission fluorescence spectra for native and unfolded HγD-Crys. Native state fluorescence is quenched compared to the unfolded state. **(B)** Equilibrium unfolding/refolding of HγD-Crys highlights the population of a partially folded intermediate. Upon dilution from high GdnHCl concentrations an off-pathway aggregation reaction competes with productive refolding.

populated around 2.5 M GdnHCl, had a folded C-td and a fully unfolded N-td (Kosinski-Collins et al. 2004). Differential domain stability has been documented for other crystallins including bovine γB-crystallin. Although structurally homologous to HγD-Crys, the domain stabilities were reversed, with the N-td being more stable than the C-td. Likewise, the unfolding intermediate had a native N-td and a completely unfolded C-td (Rudolph et al. 1990; Mayr et al. 1997).

Kinetic stability is an equally, if not more important factor in the maintenance of HγD-Crys native tertiary structure for upwards of 80 years. Initial equilibrium unfolding/refolding experiments identified a hysteresis when the protein was incubated for six hours at 37°C. The hysteresis was more pronounced at 25°C, even after a 24-hour incubation period (Kosinski-Collins 2004; Kosinski-Collins et al. 2004; Mills-Henry 2007). This suggests a kinetic barrier to unfolding, possibly in the N-terminal domain. Mills-Henry used half-chevron plots to extrapolate the unfolding half-time of HγD-Crys in the absence of denaturant. The half-time for unfolding of the N-td was calculated to be 19 years, while that of the C-td (both in the context of the full-length protein) was a more modest 129 days (Mills-Henry 2007). This is an exceptionally long life, even in the dilute context of kinetic fluorescence experiments. A high activation energy for unfolding (24 kcal/mol) was also determined for bovine γF-crystallin, supporting the role of kinetic stability in the long-term maintenance of γ-crystallin structure (Das and Liang 1998). Excluded volume effects due to macromolecular crowding, which may also increase thermodynamic stability of the native state, probably serve to increase the effective lifetime of HγD-Crys and other crystallin proteins (Bloemendal et al. 2004).

The domain interface of HγD-Crys consists of a hydrophobic patch capped above and below by pairs of polar residues (Basak et al. 2003). Alanine mutagenesis showed that this hydrophobic cluster was important for both native state stability and folding of the N-td (Flaugh et al. 2005a). Substitution of the polar residue pairs with alanine destabilized the protein in a similar manner, specifically affecting the N-td (Flaugh et al. 2005b). One polar pair consists of two glutamine residues (Q54/Q143) and substitution of either or both with glutamate to model deamidation, one of the most common covalent damages to proteins of the aging lens (Wilmarth et al. 2006), lowered the kinetic barrier

to unfolding (Flaugh et al. 2006). The domain interface contributed to the high ΔG° by specifically stabilizing the N-td (Mills et al. 2007). A complete description of the folding pathway was given by Flaugh *et al.* (Flaugh et al. 2006). The authors proposed that folding begins with motif 4 in the C-td to form the interface Greek Key, and is followed by motif 3 to form the complete C-td. Motif 2 in the N-td is then formed using the interface as a template and motif 1 folds in the final stages.

Upon dilution from high denaturant concentrations, a robust aggregation reaction competes with productive refolding of HγD-Crys (Kosinski-Collins and King 2003). The aggregates, visualized by atomic force microscopy (AFM), were filamentous, although not amyloid in nature (Figure 1-7C). Subsequent analysis of this aggregation pathway by Acosta-Sampson and King found that the C-td is the likely region involved in the initiation of aggregation (Acosta-Sampson and King 2010) .

b. γC- and γS-Crystallins

Human γC-crystallin (HγC-Crys) is the other major γ-crystallin of the lens nucleus, totaling 12-16% of soluble protein (Robinson et al. 2006). It is 173 residues and 20.7 kDa, and 71% identical to HγD-Crys. Although the crystal structure of the human protein has not been determined, a structure for the homologous murine γC-crystallin is available (Purkiss et al. 2007). HγC-Crys is resistant to heat-induced denaturation and aggregation, and required temperatures above 60°C for protein aggregation and precipitation to occur (Fu and Liang 2001). Equilibrium unfolding/refolding at room temperature indicated unfolding transitions above 2 M GdnHCl and global analysis of absorbance, Trp fluorescence and circular dichroism data found that HγC-Crys also unfolded by way of a populated intermediate, with a total $\Delta G^{\circ} = 8.7$ kcal/mol (Fu and Liang 2002a). High thermodynamic stability is a shared property of HγD- and HγC-Crys.

On the contrary, HγC-Crys is much less soluble than its counterpart. Purkiss *et al.* suggest that this is at least in part due to the presence of a cysteine residue at position 79. Substitution of an arginine at this position, as found in HγD-Crys, resulted in a dramatic solubility increase, from < 1 mg/ml for WT HγC-Crys to 90 mg/ml for the C79R mutant (Purkiss et al. 2007). However, C79R was not the only substitution that increased

solubility, indicating that this position is not the sole determinant of differential solubility between these proteins. Regardless, it seems that HγC-Crys evolved under selective pressure for high stability rather than high solubility. This underscores the importance of maintaining a range of polydisperse crystallin proteins in the lens.

The third major γ-crystallin of the lens is human γS-crystallin (HγS-Crys). This protein is 177 amino acid residues in length and 20.7 kDa. Although evolutionarily more divergent that HγD and HγC, HγS-Crys maintains ~50% identity with both of them. No crystal structure exists for the full-length human protein, although an NMR solution structure of murine γS-crystallin and a crystal structure of the C-terminal domain from HγS-Crys support its high structural similarity to other γ-crystallins (Purkiss et al. 2002; Wu et al. 2005). This protein has a short N-terminal extension of four residues before the start of the first Greek Key motif. N- and C-terminal extensions are more commonly found in the β-crystallins (discussed in more detail below). In addition to these differences, HγS-Crys exhibits differential expression patterns from other γ-crystallins. It is highly expressed in the lens cortex as opposed to the lens nucleus and cDNA transcripts have been identified in 40-year-old human lenses (Wistow et al. 2002).

HγS-Crys stability, while overall great, is less than that of HγD-Crys. In equilibrium unfolding/refolding experiments, it reversibly unfolded through a cooperative two-state mechanism with a transition midpoint of 2.3 M GdnHCl (Mills et al. 2007). Its melting temperature was 74°C. Like HγD, the kinetic stability of HγS-Crys was measured by half-Chevron plot analysis. In contrast to equilibrium experiments, kinetic unfolding detected the presence of a populated unfolding intermediate, suggested to have an unfolded N-td and a folded C-td. Extrapolated half-times of unfolding for each domain in the context of the full-length protein were 1.6 years for the N-td and 2 days for the C-td (Mills-Henry 2007). Again, although the N-td is the first to unfold and is less stable in isolation, its high kinetic stability creates a significant barrier not necessarily expected from thermodynamic analysis alone. It is important to note the ~10-fold difference in unfolding half-times between HγD- and HγS-Crys. Because of the later expression of HγS-Crys in the adult lens cortex, the need for kinetic stability may not be quite as great as in the lens nucleus (Mills-Henry 2007). Therefore, selective pressure to maintain this feature was not as strong as for HγD-Crys.

c. The β-Crystallins

The β-crystallins are the third class of ubiquitous crystallin proteins found in the human lens. Like γ-crystallins, they are predominantly structural proteins, and their expression is upregulated during fiber cell differentiation. Upregulation occurs after that of the α-crystallins and before that of the γ-crystallins (Aarts et al. 1989). There are seven β-crystallin genes in the human genome and their products are categorized as either acidic (βA1, βA2, βA3 and βA4) or basic (βB1, βB2 and βB3) (Lampi et al. 1997). βA1 and βA3 are different proteins arising from different start codons in the same transcript (Hogg et al. 1986), with βA3 being larger. The βB1- and βB3-crystallins are expressed especially early and they are found in the lens nucleus, while βB2 is prominent throughout all lens fiber cells (Aarts et al. 1989; Lampi et al. 1998). The acidic β-crystallins are widely expressed in both the lens cortex and nucleus, although βA2-crystallin protein is not detected (Lampi et al. 1997; Lampi et al. 1998). Unlike the γ-crystallins, β-crystallins form a range of oligomers and separation of lens-derived crystallins by size exclusion chromatography identified two populations: the β_H fraction, composed of hexamers and octamers, is more prominent in the lens nucleus; and the β_L fraction, comprising smaller oligomers such as dimers and tetramers, dominates in the cortex (Zigler et al. 1980).

Crystal structures are available for three human β-crystallins: βA4, βB2 and a truncated form of βB1 (Figure 1-6) (Bax et al. 1990; Van Montfort et al. 2003; Chaikuad et al. 2010). β-Crystallins share their overall tertiary structure with the γ-crystallins but differ in important ways. First, all β-crystallins possess N-terminal extensions and the basic β-crystallins have C-terminal extensions as well. These extensions are flexible and do not contribute to the Greek Key motifs or participate in domain interface interactions. Second, the linker region connecting the two domains varies considerably from that of the γ-crystallins. While the γ-crystallin linker is flexible and allows for intramolecular domain pairing, the β-crystallin linker can remain extended so that intermolecular pairing is sterically allowed as well. This is clearly evident in the

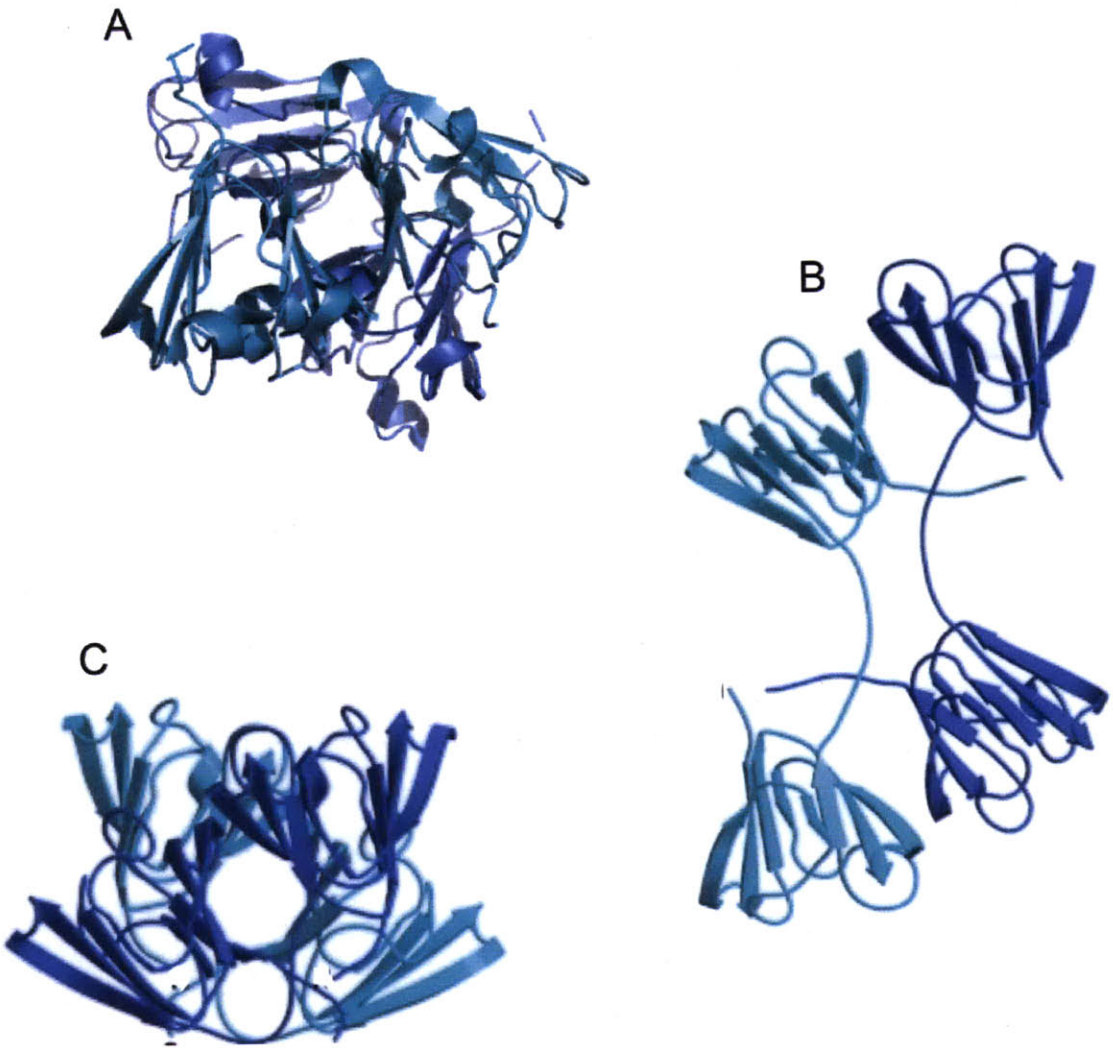

Figure 1-6: The β-crystallins form varied oligomers. **(A)** The crystal structure of βA4-crystallin is a dimer. Each monomer forms an intramolecular domain interface like that of HγD-Crys and the dimer forms from monomers packing against each other and rotating roughly 90° relative to one another. One monomer is blue and the other is teal. **(B)** The crystal structure of βB2-crystallin. In contrast to the previous example, this dimer is formed by domain swapping that generates intermolecular domain interfaces. One monomer is blue and the other is teal. **(C)** The crystal structure of βB1-crystallin is similar to that of βA4-crystallin. One monomer is blue and the other is teal.

structure of βB2-crystallin, which forms a dimer by domain swapping (Bax et al. 1990). In contrast, the crystal structure of truncated βB1-crystallin revealed a domain interface formed by intramolecular pairing as in the γ-crystallins and the dimer was formed by the pairing of monomers adjacent to one another (Van Montfort et al. 2003). Very recently, a structure for βA4-crystallin was deposited in the Protein Data Bank (PDB ID: 3lwk). This dimer is formed from two molecules with γ-crystallin-like bent linkers and an interface similar to that formed by βB1-crystallin (Chaikuad et al. 2010). Higher order oligomerization in the β-crystallins is not completely understood and *in vitro* conditions have not yet replicated the larger oligomers observed in the soluble β_H lens protein fraction (Bloemendal et al. 2004).

In general β-crystallins are less stable than the γ-crystallins. Dimeric rat βB2-crystallin can be completely unfolded in 5 M urea through a three-state mechanism and the populated intermediate is a partially unfolded monomer with an unfolded N-td and a native C-td (Wieligmann et al. 1999). Human βB2-crystallin equilibrium unfolding was described by a three-state transition with a total $\Delta G^{\circ} \cong 11.8$ kcal/mol (Fu and Liang 2002a). The acidic β-crystallins are well-known to hetero-oligomerize and it was shown that hetero-oligomerization of βA1 and βB1 enhanced stability (Bateman et al. 2003). This mechanism may be utilized within the crowded lens environment.

D. Cataract Disease

Cataract disease is the leading cause of blindness in the world, affecting over 22 million Americans age 40 and older (Prevent Blindness America 2008). Cataract is any opacification of the lens and in general is a disease directly related with aging. These opacities are the result of the scattering of light as it passes through the lens (Figure 1-7A,B). There are currently no treatments to prevent cataract or delay its onset. The only "cure" is surgical removal of the opaque lens and replacement with an artificial intraocular lens implant. The implant is placed inside the natural lens capsule, which is not removed during surgery. This procedure, although lauded by optometrists and ophthalmologists, is not without risk. In up to 40% of patients who have undergone cataract surgery, a secondary opacity develops known as posterior capsular opacification

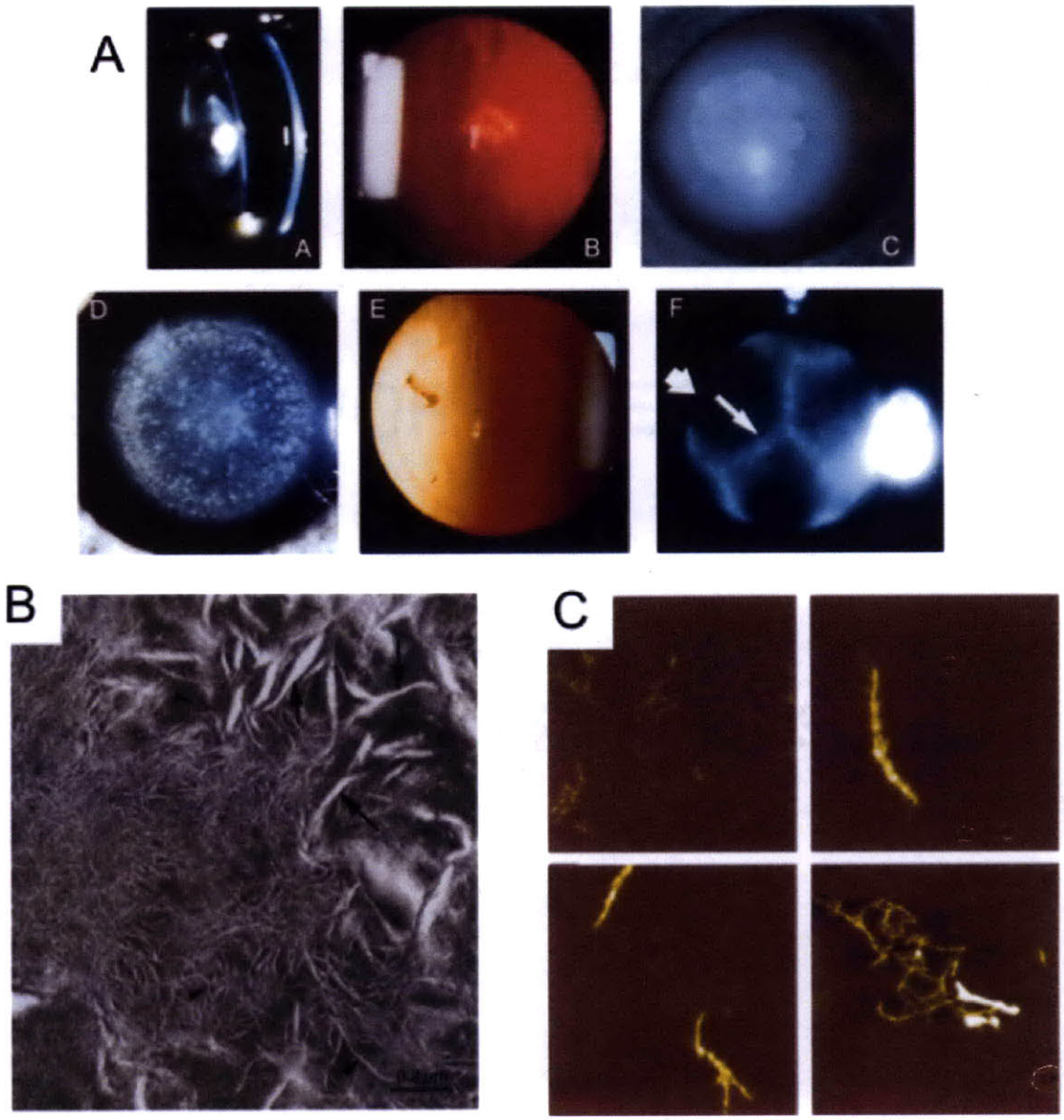

Figure 1-7: Gross cataract and protein aggregate phenotypes. **(A)** A variety of cataracts presented by patients afflicted with congenital cataracts. Reprinted with permission from Elsevier (Hejtmancik 2009). **(B)** Fibril-like structures observed in thin sections of the lens from the OXYS rat, a strain with increased oxidative stress. Reprinted with permission from Elsevier (Marsili *et al.* 2004). **(C)** Time course of AFM images of fibrillar HγD-Crys aggregates produced *in vitro* upon dilution from high concentrations of denaturant. Reprinted and modified with permission from Kosinski-Collins and King (2003).

(Wormstone 2002). This condition results from the ectopic growth of remaining lens epithelial cells on the posterior lens capsule, causing the capsule to wrinkle which, in turn, scatters light.

In the United States alone, an estimated $6.8 billion is spent each year on cataract surgery and all related medical expenses (Prevent Blindness America 2008). This figure will only grow as our population ages. In the developing world cataract presents even more of a problem. Surgery is not an option for many people due to the lack of accessible facilities and funds, an understanding of the condition, or a combination thereof. To compound this problem, cataract is more prevalent in certain regions of the developing world. In India for example, significantly more people develop cataracts at an earlier age than in the US. The INDEYE Feasibility Study, conducted in several villages in Northern India, found that 57% of individuals over age 50 were affected with cataract (n = 1260) (Murthy et al. 2007). An earlier study of South Indian populations agreed with these findings (Nirmalan et al. 2003). Although not directly life threatening, cataract disease has a major medical, economic and social impact on individuals, families and societies as a whole.

As discussed previously, lens transparency results from an overall constant refractive index through the lens. This is achieved by a combination of fiber cell packing, membrane compaction and extremely high concentrations of a polydisperse mixture of soluble, stable crystallin proteins. There are currently two main theories on how age-related cataract develops and both concern the loss of the constant refractive index through the visual axis of the lens. The first hinges on the solubility of the crystallins in their native state. Loss of solubility due to aberrant interactions of the native crystallins leads to separation into protein-rich and protein-poor regions within the lens (Benedek 1997). This phase separation disrupts the short-range order of the crystallins, resulting in pockets of varying refractive index and light scatter. The second theory treats cataract as a protein aggregation/deposition disease and is based on the stability of the crystallin proteins and their propensity to partially or fully unfold. The crystallins must maintain their three-dimensional structures for the lifetime of the individual despite continuous exposure to environmental stresses. Accumulation of partially unfolded, non-native molecules resulting from built up covalent damages can

lead to subsequent aggregation. This would also result in refractive index changes, light scatter and impaired vision. It should be noted that these two theories are not mutually exclusive.

It is important to distinguish the difference between protein aggregation and lowered protein solubility. Lowered solubility results in precipitation of protein while maintaining the native tertiary structure. This precipitation is reversible by diluting the protein to achieve lower overall concentrations. Protein aggregation, on the other hand, arises from the population of intermediates on the folding/unfolding pathway that participate in aberrant interactions leading to polymerization. Aggregation is the result of a specific process; it is kinetically controlled and irreversible (Speed et al. 1996; Betts and King 1999).

1. Age-Related Cataract

Greater than 50% of Americans over age 80 are affected with age-related cataract. Three main classes of the disease are described: (1) nuclear cataract is where the opacity presents in the center of the lens, where the oldest cells and oldest proteins are found; (2) cortical cataract is where the opacity is found in the outer regions of the lens, affecting cells and proteins that are young compared with those of the nucleus; and (3) posterior subcapsular cataract is an opacity at the back of the lens, just anterior to the lens capsule, where it often obstructs the visual axis.

The prevailing view on the cause of age-related cataract is that of a protein aggregation disease. In this model, the crystallin proteins are exposed to constant environmental stresses such as UV radiation, heat and oxidative species. In addition, proteomic analyses of lens proteins have identified several different covalent modifications, including deamidation, oxidation, glycation and truncation (Chiou et al. 1981; Lampi et al. 1998; Ma et al. 1998; Zhang et al. 2003; Hains and Truscott 2007; Hains and Truscott 2008; Hains and Truscott 2010). Protein destabilization due to the lifelong accumulation of damages may drive partial unfolding, population of intermediate conformations and exposure of heretofore buried hydrophobic residues. α-Crystallin, as the sole chaperone system of the mature lens fiber cells, binds to these residues with its

own hydrophobic regions, sequestering the intermediates from one another and reducing the concentration of aggregation-prone species. As the finite α-crystallin population is saturated with damaged, unfolded β- and γ-crystallins, it too can form aggregates large enough to scatter light and eventually become insoluble. In addition, without active α-crystallin, the remaining crystallins are no longer protected if they populate partially-unfolded intermediates and aggregation will continue unimpeded.

In support of this theory, proteomic studies have identified many sites of oxidation on the crystallins, including some sites that are clearly targeted in cataractous lenses (Hains and Truscott 2007; Hains and Truscott 2008). However, these studies alone do not indicate causation. The effects of oxidation have been studied *in vitro* using oxidized βB3-crystallin peptides and experiments showed that the presence of the oxidized peptide increased aggregation of both β- and γ-crystallins (Udupa and Sharma 2005a; Udupa and Sharma 2005b). Deamidation has been identified as one of the most prevalent covalent damages to the crystallins (Wilmarth et al. 2006). Deamidation results in the introduction of a negative charge either by transformation of glutamine to glutamate or by formation of the beta amino acid isoglutamine. Asparagine is also susceptible to deamidation and both Asn and Gln are modified in cataractous aggregates. Deamidation destabilized several β-crystallins as well as HγD-Crys, suggesting that it may contribute to protein unfolding and aggregation (Kim et al. 2002; Lampi et al. 2002; Flaugh et al. 2006; Lampi et al. 2006; Takata et al. 2007; Takata et al. 2008).

2. Congenital and Juvenile Cataract

Cataract disease is one of aging in the majority of cases. However, there are several well-documented cases of inherited cataract that either manifest as congenital—present at birth—or juvenile, usually developing within the first decade of life. These cataracts are generally classified as either syndromic or non-syndromic. Syndromic cataract is the development of the disease as part of a larger disorder, as in the X-linked Nance-Horan syndrome (Burdon et al. 2003). Non-syndromic cataract occurs in the absence of such a disorder and the cataract is the primary disease. Non-syndromic cataract is the focus of this section.

Mutations in crystallin genes account for a large percentage of non-syndromic early-onset cataract. After mapping and identification of the mutation, biochemical characterization is used to pinpoint the likely mechanism of cataract formation. Several mutations in the γ-crystallins have been characterized, including R14C, P23T, R36S, R58H and W156X in HγD-Crys. For the four substitutions, dramatic decreases in solubility are observed without major changes to the native structure of the protein (Kmoch et al. 2000; Pande et al. 2000; Pande et al. 2001; Evans et al. 2004; Pande et al. 2005; McManus et al. 2007; Jung et al. 2009; Pande et al. 2010). For both R36S and R58H, an increase in crystallization propensity is observed. In these cases, low solubility of the native state is the likely cause of lens opacity. For the truncation W156X, the final β-strand of motif 4 and its preceding loop region are removed. Given that HγD-Crys refolding likely begins with motif 4, this mutant is probably folding deficient and the aggregation pathway dominates. Experiments agree with this, and even purification from inclusion bodies yields very little protein (Talla et al. 2008).

Mutations in the other major γ-crystallins, as well as in the α- and β-crystallins are also associated with inherited cataract. The T5P substitution in HγC-Crys affected stability and crystallin-crystallin interactions (Fu and Liang 2002b; Fu and Liang 2003; Liu et al. 2008). HγS-Crys G18V lowered the transition midpoint of unfolding in GdnHCl and reduced its stability to heat denaturation (Ma et al. 2009). Several mutations, including Q155X, W151C and D128V in βB2 (Litt et al. 1997; Santhiya et al. 2004; Pauli et al. 2007); G220X in βB1 (Mackay et al. 2002); and numerous mutations that substitute out arginine residues in αA (Litt et al. 1998; Mackay et al. 2003; Hansen et al. 2007), segregate with the cataract phenotype. This list is not exhaustive but illustrates the detrimental effects that even single amino acid substitutions may have on lens structure and function.

The remaining identified mutations occured in a variety of protein-encoding genes expressed in the lens. Connexins 46 and 50 are two components of gap junctions and both missense and frameshift mutations have been associated with hereditary cataract in families (Pal et al. 2000; Berthoud et al. 2003; Minogue et al. 2005). Mutations in the integral membrane protein AQP0, a member of the aquaporin family of transporters, have also been linked to cataract development in humans. AQP0 is the most highly expressed

membrane protein in the lens, and two separate missense mutations in the gene have been shown to cause cataract by altering mutant AQP0 trafficking to the membrane, as well as interfering with normal transporter function when mutant subunits are incorporated at the membrane (Zampighi et al. 1989; Berry et al. 2000; Francis et al. 2000a; Francis et al. 2000b; Geyer et al. 2006). Due to the avascular nature of the lens tissue, gap junctions and aquaporins are important for intercellular communication and maintenance of lens homeostasis; loss of normal function could lead to imbalances that compromise lens function. The lens-specific beaded filament proteins filensin and CP49 are required for maintenance of the elongated structure of fiber cells and their ordered arrangement within the lens. Mutations in both proteins are associated with familial cataract (Conley et al. 2000; Jakobs et al. 2000; Ramachandran et al. 2007). Mutations in the genes of several different transcription and growth factors have also been associated with cataract development, including HSF4, FOXE3 and EYA1 (Azuma et al. 2000; Semina et al. 2001; Bu et al. 2002). However, cataract disease associated with growth factor mutations is generally syndromic in nature.

E. Cataract Questions and Answers: The Biological Context of This Thesis

While cataract is a major worldwide health problem that costs governments billions of dollars annually, its causes and prevention remain elusive. The critical question is: what changes in crystallin structure and stability cause cataract *in vivo*? And furthermore, can cases of congenital cataract serve as models for elucidation of the mechanisms of age-related cataract formation?

In terms of congenital cataract, a number of mutations resulting in single amino acid substitutions in the crystallins have been identified and characterized. These cases were examined in the preceding section, as well as in the Introduction to Chapter 2. The vast majority affected surface residues and experimental evidence suggested that changes in solubility cause the protein precipitation observed in these lenses. However, in crystallin proteins isolated from cataract patients, changes were not identified at these charged surface residues, and these congenital defects appear to be "special cases" that do not represent causation in age-related cataract. In addition, the experiments used to study

cataractous aggregates formed *in vivo* are, by requirement, endpoint characterizations. The numerous modifications identified by mass spectrometry cannot be deemed causative by these methods.

There remains the need to address how structure and stability changes affect protein aggregation and cataract formation. In particular, I am interested in the hydrophobic core of HγD-Crys and whether disruptive substitutions could result in aggregation such as that observed in cataractous lenses. This thesis aims to characterize a set of single amino acid substitutions in the hydrophobic core of HγD-Crys. The murine cataract phenotypes associated with these mutations were originally identified after ethylnitrosourea treatment and breeding, followed by phenotypic screening by slit-lamp examination (Favor 1983; Graw et al. 2002b; Graw et al. 2004). After confirmation of lens opacities, chromosomal mapping with microsatellite markers identified genomic regions that consistently segregated with the phenotype. These regions were known to contain γ-crystallin genes and further sequence analysis of these candidates identified base changes corresponding to the single amino acid substitutions: MγS-Crys F9S, MγD-Crys V76D, MγD-Crys I90F (Sinha et al. 2001; Graw et al. 2002b; Graw et al. 2004). Chapter 2 characterizes the biochemical properties of HγD-Crys containing each of the homologous amino acid substitutions. Chapter 3 continues to study two of the three mutant proteins in greater detail by analyzing their interactions with human αB-crystallin. Figure 1-8 shows the location of each mutation studied within the WT HγD-Crys three-dimensional structure.

These experiments are some of the first to analyze cataract-associated hydrophobic core mutations in HγD-Crys. We present results that identify a direct link between the cataract disease phenotype observed in mice and *in vitro* biochemical observations and measurements. We provide important information towards elucidating the mechanism of cataract formation and suggest that there may in fact be several different routes by which cataract develops. This is supported by the many different phenotypic manifestations of cataract disease.

The final section of this Introduction will review relevant principles of protein folding and stability followed by a discussion of mechanisms of misfolding and protein aggregation. Along with the preceding sections detailing crystallin structure and

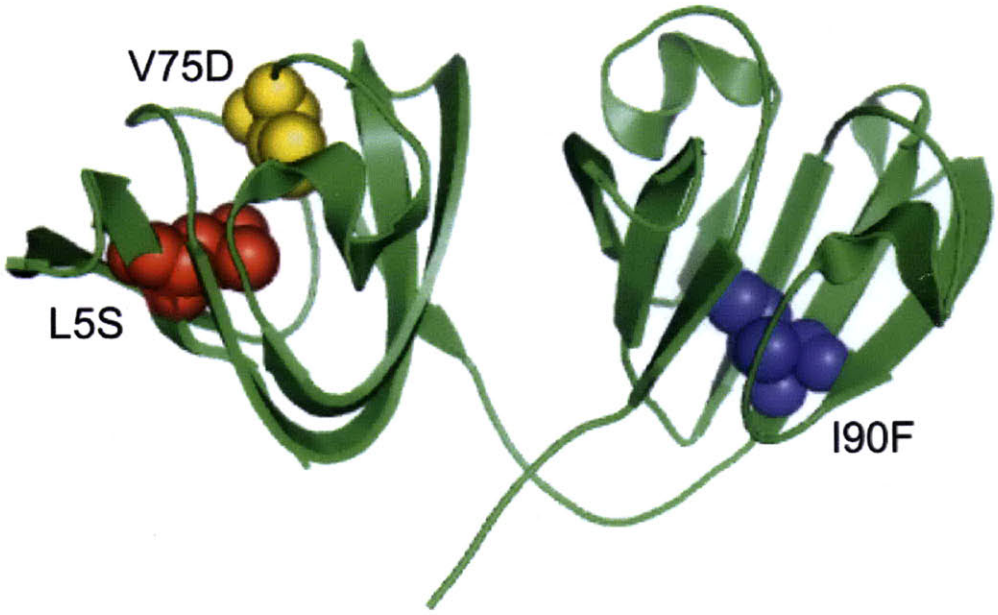

Figure 1-8: Murine congenital cataract amino acid substitutions created in HγD-Crys. These are the three mutations studied in Chapters 2 and 3. Side chains are depicted in spacefill. Note that all side chains are directed inwards and contribute to the hydrophobic core of HγD-Crys.

function, this will create the biochemical background in which the experiments of Chapters 2 and 3 are based.

F. Protein Folding, Misfolding and Aggregation

Proteins are composed of long chains of amino acids assembled *in vivo* on the ribosome. From this linear chain, they must fold to adopt their functionally active three-dimensional structure. Christian Anfinsen described the encoding of a protein's tertiary structure in the linear sequence of amino acid residues (Anfinsen 1973) and proposed that it contains all the information for folding. While true in many cases, a significant number of both prokaryotic and eukaryotic proteins require assistance in the form of various chaperones to achieve their native structure.

The native structure of a protein is classically viewed as its lowest energy state; however, there are naturally occurring examples in which this is not the case (Baker et al. 1992). Folding is driven foremost by the hydrophobic effect, which increases the entropy of the surrounding water molecules and buries hydrophobic side chains in the protein core where favorable van der Waals interactions occur. The native states of many proteins, especially those of mesophilic organisms, are just on the verge of stability and the native state is only slightly lower energy than the unfolded ensemble. This is advantageous for many reasons, such as the need for protein flexibility and breathing to accommodate protein-protein interactions and the requirement for fast, temporally controlled protein turnover as in proteins active in the cell cycle.

How proteins fold to achieve their native state on a biologically relevant timescale is one of the major long-standing questions in biology. Cyrus Levinthal first proposed the protein folding problem now known as Levinthal's Paradox (Levinthal 1968). In short, it states that if a polypeptide chain folded by sequentially sampling each possible amino acid conformation, it would take times longer than the age of the universe to reach its native state. However, it is well-known that many small proteins fold on a microsecond timescale (Burton et al. 1996; Mayor et al. 2000; Jager et al. 2001) and even large proteins requiring chaperone assistance fold within tens of seconds (Horwich and Fenton 2009). Instead, Levinthal proposed that these polypeptide chains fold by

following specific pathways that avoid the vast majority of possible conformations (Levinthal 1968). This is achieved through sites of nucleation, where small regions of the chain fold up into native or near-native conformations. This limits the conformational flexibility of the rest of the chain, allowing it to sample only a tiny subset of structures, driving folding into the native structure. These folding pathways are often visualized as folding funnels to emphasize that as folding progresses and energy is minimized, the number of available conformational states is dramatically reduced (Dill and Chan 1997). These funnels also emphasize the numerous local energy minima that actively folding chains encounter. Some represent obligate intermediate structures, while others are misfolded kinetic traps with deep energy minima.

1. β-Sheet Protein Folding

Folding of β-sheets is less understood than that of α-helices. The primary reason for this is that α-helices are formed by residues in close proximity to one another in both three-dimensional space and primary structure. A β-sheet, on the other hand, can be formed from strands that are distant in a protein's primary structure, with the intervening sequence forming other structural elements or flexible loop regions. Understanding the underlying mechanisms of β-sheet protein folding is an active area of research and significant progress has been made in the field.

Many small β-sheet proteins and domains fold through two-state mechanisms without populating detectable intermediates. Src homology domains from several proteins (Guijarro et al. 1998; Plaxco et al. 1998), tendamistat (Schonbrunner et al. 1997) and cold shock protein B (Schindler et al. 1995; Schindler and Schmid 1996) all folded without the population of intermediates and their transition states contained high proportions of buried residues. In contrast, folding intermediates were identified for larger β-sheet proteins including cellular retinoic acid binding protein 1 (CRABP 1) (Clark et al. 1996), intestinal fatty acid binding protein (Burns et al. 1998) and interleukin 1-β (Heidary et al. 1997).

One of the most important findings is that formation of β-turns, and in particular β-hairpins, are the likely nucleating events in the folding of β-sheets. A β-turn reverses

the direction of the polypeptide chain, therefore compacting it and contributing to the globular structure of the protein (Marcelino and Gierasch 2008). Synthesized sequences derived from naturally occurring turns formed stable conformations in water (Dyson et al. 1985) and this work paved the way for establishing the likelihood of turn formation. In the larger context of β-hairpin structures and full-length polypeptide chains, mutagenesis studies have shown that optimization of turns contributed to thermodynamic and kinetic stability, though often at the expense of function (Truhlar and Agard 2005; Jager et al. 2006). Studies on the folding of the P22 tailspike adhesin protein identified turn residues of the β-helix that, when mutated, adversely affected folding and led to chain aggregation (Villafane and King 1988). Peptide studies confirmed that these mutations reduced the propensity for turn formation, confirming the link between turn formation and productive protein folding reactions (Stroup and Gierasch 1990). Extensive studies of CRABP 1 identified two of seven turns that possessed structure outside of the context of the polypeptide chain (Rotondi and Gierasch 2003). Of these, turn IV seemed to nucleate folding while turn III folded later, forming passively alongside hydrophobic interactions as part of the overall stabilizing tertiary structure (Marcelino and Gierasch 2008). Therefore, specific β-turns may serve as nucleating sites for protein folding. Aside from turns, Φ-value analysis for folding of the third fibronectin domain of the human tenascin protein, an Ig-like Greek Key domain, identified a ring of four residues whose native-like structure was formed in the transition state (Hamill et al. 2000b). These residues are found in both β-sheets composing the sandwich domain and their high Φ-value suggests that they may form a folding nucleus.

The tyrosine corner is a highly conserved structural feature found almost exclusively in the Greek Key motif (Hemmingsen et al. 1994). It consists of a tyrosine residue near the end of a β-strand whose side chain hydroxyl forms a hydrogen bond with the Y – 4 residue. The Y – 4 (or in some cases Y – 3/Y – 5) residue is located in a different strand and creates a bridge between the two β-sheets (see Figure 1-4). This feature is thought to contribute not only to protein stability, but to serve as a folding nucleus as well (Hemmingsen et al. 1994). Thermodynamic and kinetic studies of a set of four Greek Key-containing domains found that while the tyrosine corner contributed to native state stability in all cases, chevron plot analysis concluded that this feature was

only important for folding in the two Ig domains analyzed (Hamill et al. 2000a). Interestingly, the tyrosine corner is not present in the NMR structure of MγS-Crys (Wu et al. 2005). If the corresponding tyrosine corner is not formed in HγS-Crys, this may partially explain its reduced stability in comparison to HγD-Crys.

2. Determinants of Protein Stability and the Effects of Mutations

It is widely accepted that a combination of non-covalent factors contribute to overall protein stability. These include hydrogen bonding, electrostatic interactions, the hydrophobic effect and van der Waals interactions (Rose and Wolfenden 1993; Jaenicke 1999). The prediction of contributors to protein stability and the *de novo* design of protein molecules is still a work in progress. Therefore, the findings and conclusions concerning protein stabilization by and large result from experiments based on mutagenesis and its corresponding effects, monitored by a variety of techniques.

The contribution of hydrogen bonding to native state protein stability is still a somewhat open question. In general, backbone or side chain hydrogen bonding should occur equally as well with another residue or with bulk water, suggesting that the formation of intramolecular hydrogen bonds do not contribute to native state stability (Rose and Wolfenden 1993). However, later studies found that the opposite is true, estimating hydrogen bonds to contribute -0.5 – -4.5 kcal/mol to protein stability (Dolgikh et al. 1981; Fersht et al. 1985). Using the example of RNAse T1, mutagenesis to eliminate hydrogen bonds calculated that each bond contributed about 1.3 kcal and that collectively, they contributed roughly equally to the hydrophobic effect in terms of stabilization (Shirley et al. 1992). Jaenicke proposed that the extensive hydrogen bonding between the β-strands of the γ-crystallins must contribute substantially to their overall high stability (Jaenicke 1994). It is supported then that there is an energy difference for amino acid residues forming hydrogen bonds with water versus another residue. One critical assumption of these experiments is that the mutation does not affect the folding or conformation in any other way aside from deletion of the interaction of interest. Additional induced structural changes would muddy this interpretation.

Electrostatic interactions are proposed to contribute only weakly to overall protein stability. Extensive mutagenesis studies with the model protein T4 lysozyme have shown that long-range electrostatic interactions contribute very little to stability (Dao-pin et al. 1991b). Single amino acid substitutions hypothesized to create surface salt bridges resulted in little or no stabilization and side chains of the non-native residues were quite mobile, indicating the absence of salt bridges at these positions (Sun et al. 1991). The same authors also introduced non-native His-Asp pairs to investigate the role of salt bridge formation on protein stabilization. Surprisingly, mutant proteins were less stable than wild-type T4 lysozyme due to backbone conformational strain. The authors concluded that the loss of conformational entropy upon salt bridge formation is not offset by the interaction, thus salt bridges may not contribute to stability in many cases. Of course, discrete salt bridges are found in proteins and the backbone conformation must "allow" for these interactions to occur without unfavorable strain (Sun et al. 1991). Electrostatic helix dipole interactions were also investigated and the introduction of a negative charge at the N-terminus of a helix in T4 lysozyme stabilized the protein in a pH dependent manner (Nicholson et al. 1991). Introduction of a charge into the hydrophobic core of T4 lysozyme increased protein mobility and decreased stability, although it was still folding-competent (Dao-pin et al. 1991a). Buried ionic charges are less common, but nevertheless play a role in many important biological processes. A shift in pK_a of buried charged residues is one method of stabilization (Karp et al. 2007; Isom et al. 2010).

The hydrophobic effect has generally been regarded as the major driving force of protein folding. The term "hydrophobic effect" refers to the tendency of a polypeptide chain in aqueous solution to bury its hydrophobic residues so they are shielded from bulk water. The loss of conformational entropy is offset by the increase in entropy of the water surrounding the protein. This results in the formation of a hydrophobic protein core consisting of residues whose packing rivals that of crystals of small organic molecules (Richards 1977). Therefore, the hydrophobic core is expected to contribute largely to protein stability through entropy increase and favorable van der Waals interactions. The major experimental approach to evaluate the role of the hydrophobic core is through the use of site-directed mutagenesis. Again, T4 lysozyme has been used as a model system in numerous studies. Mutations that resulted in repacking of the

hydrophobic core were mostly accommodated by small, local changes to the backbone (Baldwin et al. 1993). The substitution of core residues—using two mutants L133F and A129V—to fill internal cavities were presumed to increase stability. However, the bulky side chains introduced strain to the molecule and created unfavorable van der Waals contacts, resulting in marginal stability decreases (Karpusas et al. 1989). Just as filling cavities was assumed to be stabilizing, the creation of cavities was assumed to be destabilizing by reducing favorable van der Waals contacts. Virtually all cavity-creating mutations in the core of T4 lysozyme decreased stability, although structurally their effects varied; it seemed that as long as the residues surrounding the cavity were rigid and able to prevent collapse of the molecule, the cavity remained and was not accessible to solvent in the majority of cases (Eriksson et al. 1992; Xu et al. 1998). The Introduction to Chapter 2 describes additional experiments designed to study the effects of amino acid substitutions in a protein's hydrophobic core.

3. Protein Misfolding, Aggregation and Disease

Although fast two-state folding mechanisms have been identified for many small proteins less than 100 kDa, most larger proteins achieve their native conformation by navigating a rough folding landscape. They will encounter local energy minima, some of which represent on-pathway populated intermediates, while others are off-pathway. The energy wells of these off-pathway intermediates may be deep enough to form kinetic traps, where the activation energy is too great to return to the folding pathway that ends at the native state.

The predominant thought on protein misfolding is that a labile on-pathway folding intermediate must be in equilibrium with a transient misfolded intermediate structure. Under conditions that favor productive refolding to the native state, equilibrium vastly favors the on-pathway intermediate. However, a change in external (i.e. a change in physical or chemical environment) or internal (i.e. a genetic mutation resulting in an amino acid substitution or more dramatic change in protein primary structure) conditions may push this equilibrium towards the transient structure. Once populated, this

misfolded intermediate, which contains regions normally not exposed, may interact with other misfolded molecules forming large multimeric aggregates.

Protein folding gone awry *in vivo* results in the formation of intracellular inclusion bodies. In prokaryotes, these inclusion bodies are composed mainly of the specific misfolded protein, while in mammalian cells a host of other proteins including chaperones, proteasome components and cytoskeletal proteins are found in or associated with them (Kopito 2000). The polypeptide chains composing inclusion bodies represent a misfolded, aggregated state of the protein and disruption of inclusion bodies under strongly denaturing conditions yields folding competent material (Mitraki 1989). King and colleagues showed that upon mixing together phage P22 tailspike and coat proteins under conditions favoring aggregation, two separate reactions occurred, corresponding to the aggregation of each protein independent of the other (Speed et al. 1996). Experiments using fluorescence microscopy and FRET demonstrated that inclusion bodies, as well as dispersed protein aggregates, were composed of specific chains and there were no interactions between two unrelated aggregation-prone chains *in vitro* or *in vivo* (Rajan et al. 2001).

If aggregation arises by way of a misfolded intermediate structure, interest is directed to the nature of this intermediate and its relation to both the native and aggregated states. A number of aggregation pathways are related to human disease and their mechanisms of protein aggregation are of great medical interest. Several examples of protein aggregation and related diseases are presented in further detail in the following subsections.

a. The Amyloidoses and Cross-β Structure Formation

Amyloid fibrils are identified by several characteristic features. They display an x-ray diffraction pattern consistent with a fibrillar cross-β structure, in which the β-strands run perpendicular to the fibril axis (Figure 1-9A, B) (Nelson et al. 2005). They bind the fluorescent dyes Thioflavin T (ThT) and Congo Red (CR), and CR exhibits a distinct "apple green" birefringence under cross-polarized light when bound to amyloid. For the most part, they form long straight, unbranched fibrils up to 10 nm wide. Fibrils

are composed of several protofilaments that exhibit a twisted morphology when viewed by TEM. The core amyloid fibril structure is extremely stable, being both detergent and protease resistant. A wide array of proteins form amyloid fibrils under specific partially denaturing conditions, suggesting that the molecular structure of the fibrils may be generic and accessible to the majority of polypeptide chains given the proper set of conditions (Dobson 2003).

A number of human diseases are intimately associated with the presence of amyloid fibers. Alzheimer's disease (AD) and the Aβ protein fragment is probably the most well-known, and others include Huntington's disease and the associated Huntingtin protein; the transmissible spongiform encephalopathy, Creutzfeldt-Jakob disease caused by the human prion protein; and the transthyretin-associated amyloidoses. This list is by no means exhaustive.

In these diseases, the proteins or protein fragments of interest are found either in intracellular inclusion bodies, as in Huntington's disease, or as extracellular protein deposits, as in the plaques observed in the brains of AD patients. When initially identified, these large aggregates were assumed to be cytotoxic. However, more recent evidence suggested that smaller oligomers, the species that act as nuclei for aggregation *in vitro*, may in fact be the toxic species and that the larger aggregates may form as a sort of defense mechanism (Kitamura and Kubota 2010). If the small oligomeric species are the toxic form of these amyloidogenic proteins, understanding the transition to the aggregation-prone conformation is critical to halting these initial steps. Unfortunately, for many disease-associated proteins, these steps are not well-understood. Progress made with some proteins however, will surely uncover experimental methods applicable to other cases.

Transthyretin (TTR) is a secreted human protein present in the serum and cerebrospinal fluid. Wild-type TTR is associated with senile systemic amyloidosis, while a range of mutant TTR proteins containing single amino acid substitutions are associated with familial amyloid cardiomyopathy and polyneuropathy and central nervous system selective amyloidosis (Connelly et al. 2010). TTR is a tetramer containing two binding sites for the hormone thyroxine. Each monomeric subunit is composed of an eight-stranded β-barrel and a single short helix and tetramers are composed of two dimers

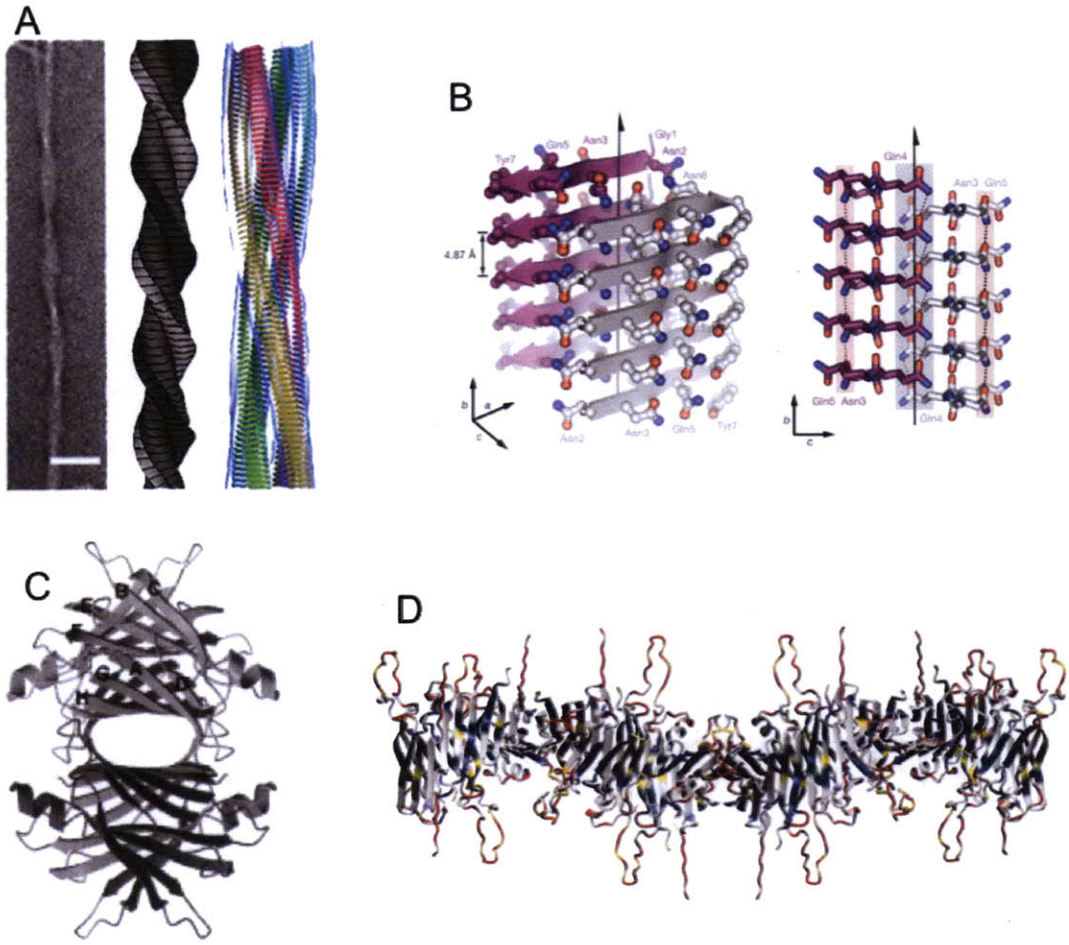

Figure 1-9: Amyloid structural models. **(A)** α-Synuclein amyloid fibrils exhibit classic structure. On the left is an electron micrograph. The fibrils are built up from twisted protofilaments. Reprinted and modified with permission from Jiminez *et al.* (2002) © by the National Academy of Sciences. **(B)** The high resolution cross-β structure of an amyloid fibril. Reprinted by permission from MacMillan Publishers Ltd: Nature, Nelson *et al.* (2005). **(C)** The native tetrameric structure of transthyretin. Reprinted with permission from Elsevier (Damas and Saraiva 2000). **(D)** A model of amyloid fibril formation by full length transthyretin. A portion of each molecule participates in the β-sheet amyloid structure while certain loops remain outside of the core structure (Olofsson *et al.* 2004).

(Figure 1-9C) (Hamilton et al. 1993). Disease-associated mutant TTR tetramers were destabilized under physiological conditions, leading to tetramer dissociation (Colon and Kelly 1992). The tetramer dissociation equilibrium was linked to monomer unfolding, leading to the population of a partially unfolded aggregation-prone conformation that formed amyloid fibrils (Jiang et al. 2001). WT TTR also underwent structural changes leading to amyloid formation at increased temperature (Chung et al. 2001; Ferrao-Gonzales et al. 2003). Small molecule binding at the thyroxine binding sites resulted in stabilization of the native tetramer, creating a larger kinetic barrier to dissociation and subsequent monomer unfolding and aggregation (Hammarstrom et al. 2003). The aggregation-prone partially unfolded conformation is not known with certainty, although studies implicate altered conformations of β-strands C and D and their connecting loop at the outer edges of the dimeric units; rearrangement of these strands may expose hydrophobic regions (Figure 1-9D) (Kelly and Lansbury 1994; Serpell et al. 1996; Olofsson et al. 2004).

In contrast to aggregation of a full-length protein, the amyloid-forming species in AD is formed by cleavage of the amyloid precursor protein to yield the 40 or 42 residue Aβ peptide. The normal function of the membrane-bound precursor protein is unknown, but cleavage on the extracellular side by β-secretase and on the intracellular side by γ-secretase results in the aggregation-prone species (Buchet and Pikula 2000). Both Aβ40 and Aβ42 are amyloidogenic although Aβ42 formed fibrils faster *in vitro* (Jarrett et al. 1993). Aβ amyloid fiber formation exhibits classic nucleation-growth kinetics (Jarrett et al. 1993), as in the initial stages of hemoglobin S aggregation (Ferrone et al. 1985). Seeding with pre-formed fibrillar material altered the aggregation kinetics, diminishing the lag phase associated with the nucleation step (Harper and Lansbury 1997). This indicates that formation of the oligomeric nucleus is the rate-limiting step in aggregation.

b. Domain Swapping

Another method of polymerization, termed three dimensional domain swapping, involves the exchange of partial or entire protein domains. At one time domain swapping was only defined for proteins that populated both monomeric and dimeric or higher order

structures; however, the definition has loosened and includes proteins exhibiting reciprocal exchange of regions, even if a monomeric equivalent has not been observed. The key feature of domain swapped subunits for which monomeric structures are known, is the maintenance of the native-like structural contacts observed in the monomeric state, except involving intermolecular interactions. As more structures are solved, the number of proteins exhibiting domain swapping is increasing, and this mechanism is observed in α-helical, β-sheet and mixed α/β proteins (Gronenborn 2009).

Some proteins, including select crystallins, exhibit domain swapping in their native state. βB2-crystallin is a domain swapped dimer (Bax et al. 1990). Its structure is similar to that of HγD-Crys (Basak et al. 2003), except the intramolecular domain interface of HγD-Crys is replaced by an intermolecular interface in βB2. The N-td:C-td interface is maintained, although between two different molecules and the difference between HγD-Crys and βB2 lies in the conformation of the linker; it is bent in the former but extended in the latter. This type of difference is common among domain swapped species, in that all interactions are native-like in both monomer and oligomer, except for the flexible hinge loop regions, which enable the swap (Figure 1-10A*1,2*) (Gronenborn 2009). Others, like mutant versions of the B1 domain of streptococcal protein G, form varied oligomeric states including dimeric and tetrameric assemblies that exhibit different modes of domain swapping (Kirsten Frank et al. 2002; Byeon et al. 2003).

The examples above illustrate closed domain swapping, in which oligomers of specific sizes are formed. Open-ended or runaway domain swapping can also occur, resulting in the formation of large polymeric species, as in some protein deposition diseases (Figure 1-10A*3*). Unfortunately, the direct structural evidence for runaway domain swapping is hard to come by. In most cases, closed-ended domain swapped structures demonstrate the assumed general mechanism of polymerization and indirect biochemical evidence is used to support the topologically identical swap in the aggregated or polymerized state (also see the discussion of loop-sheet insertion in the following section). Human cystatin C, a monomeric cysteine protease inhibitor composed of a five-stranded β-sheet and a long helix that rests across the width of the sheet, formed domain swapped dimers under destabilizing conditions such as low pH and increased temperature. A disease variant of this protein, L68Q, is associated with

hereditary cystatin C amyloid angiopathy, a disease that causes cerebral hemorrhage in individuals during early adulthood (Olafsson and Grubb 2000). Unlike the WT protein, the disease variant dimerized at physiological temperature and with increased kinetics at 40°C (Abrahamson and Grubb 1994). A crystal structure of the WT domain swapped dimer features exchange of the major helices and extension of a β-strand from each subunit so that they bridge the β-sheets of each monomer (Figure 1-10B) (Janowski et al. 2001). Although the crystal structure forms a closed domain swap, the same general mechanism is hypothesized during polymer formation. The introduction of engineered disulfide bonds designed to stabilize the monomer and prevent domain swapping did not disrupt native protein function but abolished dimerization and dramatically reduced amyloid formation at low pH (Nilsson et al. 2004).

The human prion protein (PrP^{C}) undergoes a structural transition to the infectious amyloidogenic PrP^{Sc} in the transmissible encephalopathies. A crystal structure of the domain swapped PrP protein exhibits extensive exchange of helical regions, the formation of novel intersubunit disulfide bonds and formation of a novel β-sheet structure in the hinge loop mediating exchange (Knaus et al. 2001). Seeded oligomerization was demonstrated using reduction-oxidation altered hamster PrP; this treated protein exhibited a cross-β-like x-ray diffraction pattern and upon mixing with PrP^{C}, was able to convert the normal protein into an oligomerized form (Lee and Eisenberg 2003). The oligomerization is thought to proceed through an open-ended domain swap, at least partially-mediated by intersubunit disulfide bonds like those identified in the dimeric crystal structure. An alternative proposal for the conformation of polymerized PrP^{Sc}, which has more β-sheet content, postulates the formation of a left-handed β-helix by a portion of the protein which mediates trimer formation (Govaerts et al. 2004). In this model, the intramolecular disulfide bond is maintained in a helical region not participating in formation of the β-helix. Later studies using electron paramagnetic resonance demonstrated that the C-terminal helical region undergoes dramatic structural rearrangement to form a region of high β-sheet content (Cobb et al. 2007; Cobb et al. 2008), which is in line with the proposed structure of Govaerts *et al.* (2004). (Compare the structures shown in Figure 1-10C and 1-10D.)

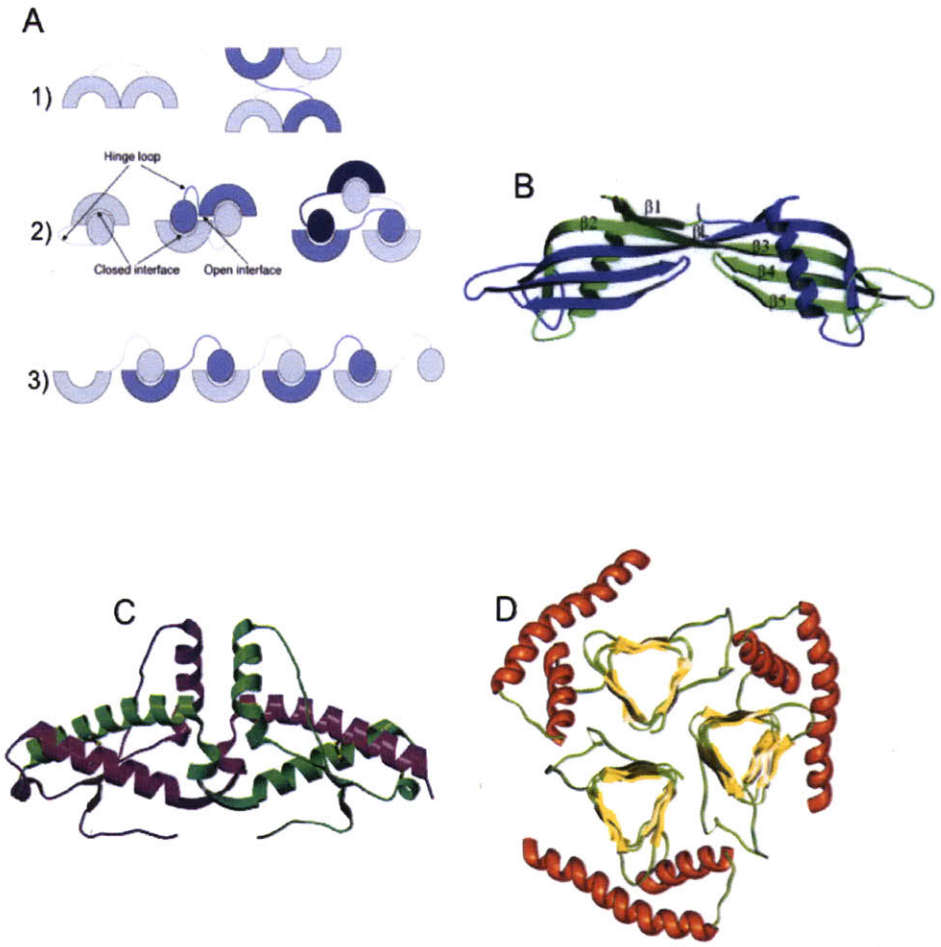

Figure 1-10: Domain swapping and aggregate formation. **(A)** Schematic diagrams of domain swapping mechanisms. *1)* and *2)* are examples of closed domain swaps, where all interacting interfaces are satisfied. *3)* is an example of open-ended domain swapping, where an interface is always exposed and addition to the end exposes a new face. Reprinted with permission from Elsevier (Gronenborn 2008). **(B)** The closed domain swapped crystal structure of cystatin C. One monomer chain is colored blue and the other is colored green. β-Strands 1 and 2 are swapped and β2 is extended to form a long strand across both molecules. Reprinted with permission from Janowski *et al.* (2001). **(C)** The closed domain swapped crystal structure of human PrP protein. One monomer is colored green and the other is colored purple. An open domain swap involving the same helical regions is the proposed mechanism of aggregate formation. Reprinted by permission from MacMillan Publishers Ltd.: Nature Structural Biology, Knaus *et al.* (2001). **(D)** A second potential model for the aggregation of human PrP. This model postulates the formation of a β-helical region (yellow) in each monomer and this region trimerizes. Trimers are proposed to stack on top of one another through favorable polar backbone interactions in the β-helices. Reprinted and modified with permission from Govaerts *et al.* (2004) © by the National Academy of Sciences.

Although these studies provide evidence for the crystallographic dimers as viable models for open-ended domain swapping, actual structures of PrP^{Sc} and other aggregating proteins involved in deposition diseases are still elusive.

c. The Serpinopathies and Loop-Sheet Insertion

The serpinopathies are a class of diseases caused by polymerization and subsequent loss of function of serine protease inhibitor proteins known as the serpins. The serpins act as suicide inhibitors, irreversibly inhibiting their target proteins. All serpin proteins share at least 30% sequence homology with α_1-antitrypsin. The overall tertiary structure contains three β-sheets (A-C), several helices and a mobile reactive loop that is critical for function (Figure 1-11A) (Lomas and Carrell 2002). The normal function of α_1-antitrypsin is the inhibition of elastase, a protease present in the lungs that cleaves elastin. Mutations in α_1-antitrypsin result in improper trafficking of the protein from the liver to the lungs. Uninhibited elastase cleaves elastin, destroying the flexible nature of the lung tissue, leading to premature emphysema. In addition, mutant α_1-antitrypsin that is unable to leave the liver builds up in the endoplasmic reticulum of hepatocytes, forming polymerized protein inclusions that impair liver function (Lomas and Carrell 2002).

Knowledge of the structure of α_1-antitrypsin is critical for understanding the function of WT and mutant versions of the protein. The WT protein functions by exposing a stretch of amino acids in the reactive loop that acts as a decoy substrate of the protease target (Lomas and Carrell 2002). When the protease binds to the decoy, α_1-antitrypsin undergoes a dramatic structural rearrangement. The reactive loop swings from the top to the bottom of the molecule, carrying the protease with it and inactivating it in the process (Huntington et al. 2000). The structural change is stabilized by insertion of the reactive loop into the middle of β-sheet A, expanding the sheet width by one strand (Figure 1-11A, compare left and right structures) (Huntington et al. 2000). The inactive protease-serpin complex is then degraded.

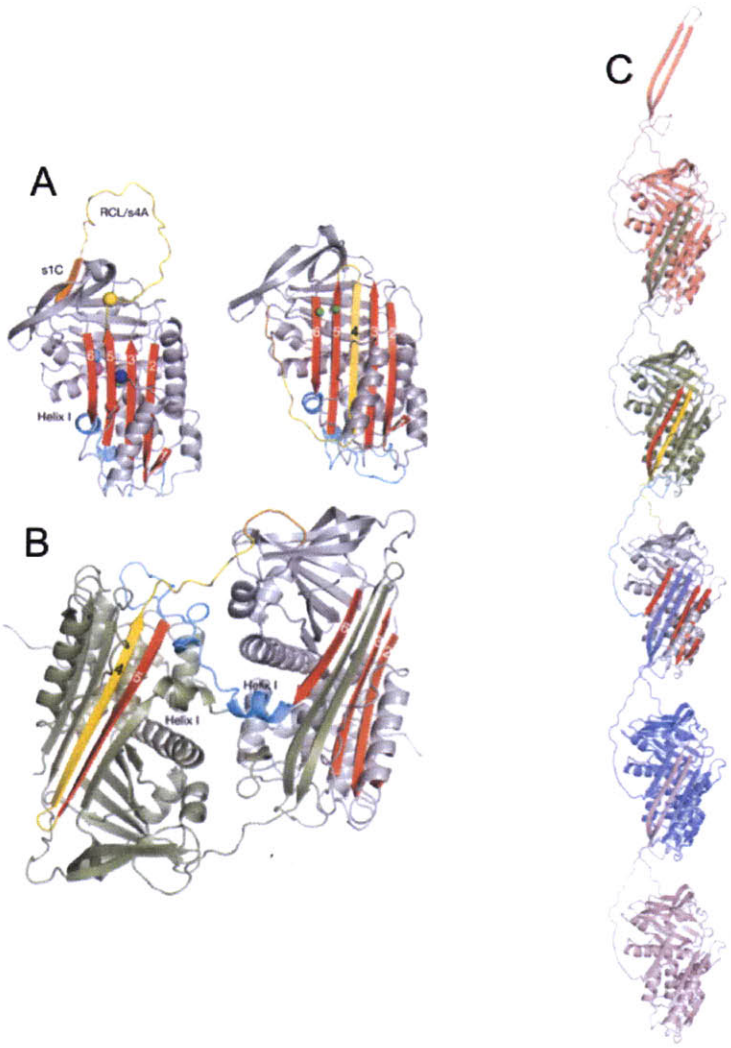

Figure 1-11: The serpins and loop-sheet insertion. **(A)** The reactive (*left*) and latent (*right*) structures of α_1-antitrypsin. The mobile reactive loop is shown in yellow and β-sheet A is shown in red. The latent structure depicts the insertion of the reactive loop into sheet A. **(B)** The dimeric crystal structure of α_1-antitrypsin exhibits the extended loop-sheet insertion. β-Sheets 4 and 5 are exchanged. The monomer on the right is shown as in (A) and the second monomer is shown in green. **(C)** The model for α_1-antitrypsin polymerization by extended loop-sheet insertion. Yamasaki *et al.* refer to this mechanism as domain swapping. Figures adapted from Yamasaki *et al.* (2008).

This mechanism is termed "loop-sheet insertion" and it is critical for proper function of the serpins. However, mutations in several regions of α_1-antitrypsin, including residues in or proximal to the reactive loop and β-sheet A, make the protein susceptible to inappropriate structural rearrangements. The Z variant of α_1-antitrypsin contains an amino acid substitution, E342K, at the base of the reactive loop near β-sheet A. The Z variant was found to polymerize *in vitro* upon incubation at physiological temperature. Incubation in the presence of a synthetic peptide derived from the reactive loop of antithrombin inhibited polymerization completely, due to peptide binding in the expanded β-sheet where the reactive loop would erroneously insert (Lomas et al. 1992). This finding suggests that polymerization occurs by way of domain swapping; the mobile reactive loop from one molecule inserts into the expanded β-sheet of a second molecule, leaving the sheet from the first molecule open. More recent x-ray crystallographic evidence found that a larger loop-sheet insertion event formed a dimeric species with two adjacent β-strands exchanged between molecules, including the strand originating from the reactive loop (Figure 1-11B) (Yamasaki et al. 2008). Using a combination of modeling and biochemical data, Yamasaki *et al.* showed that the polymerized serpin molecule appeared to exchange a greater β-sheet region than previously thought, undergoing larger structural changes to accomplish this (Figure 1-11C). Hydrogen/deuterium exchange experiments supported the insertion of the reactive loop into β-sheet A and in addition suggested that β-strand 1C and helix F have altered conformations in the polymerized form due to their reduced accessibilities for exchange under those conditions (Tsutsui et al. 2008).

d. Native State Polymerization

Unlike the previous examples, native state polymerization occurs without partial unfolding and population of an aggregation-prone intermediate species. Instead, aggregates are formed through interactions of the natively folded protein. The most well-characterized example of this is polymerization of the sickle cell hemoglobin (HbS) variant with the amino acid substitution E6V (Eaton and Hofrichter 1990). This

substitution places a hydrophobic valine residue on the surface of the protein. Under oxygenated conditions, such as in arterial blood, there is no effect on protein conformation. However, under low oxygen conditions like those present in venous blood, the protein undergoes conformational changes associated with the loss of oxygen from the hemes. This change exposes a hydrophobic pocket to which the exposed valine at position 6 can bind. The dimeric nature of hemoglobin necessarily means that each functional unit contains two hydrophobic patches at the location of E6V and two hydrophobic pockets that are exposed under deoxygenated conditions. This enables polymer formation because hydrophobic patches and pockets will continually be exposed (Figure 1-12A) (Eaton and Hofrichter 1990).

Extensive studies of hemoglobin aggregation kinetics elucidated a double nucleation-growth mechanism (Figure 1-12B), exemplified by a lag phase during which nucleation occurs (Ferrone et al. 1985). After the lag phase, rapid growth by extension of polymers is observed and a second growth phase is initiated by formation of new nuclei on existing polymers (Ferrone et al. 1985). Incomplete disintegration of HbS polymers upon exposure to oxygen results in a seeding-like mechanism, so that growth of polymers occurs more rapidly after successive rounds of deoxygenated conditions. This results in the extensive polymerization observed in the red blood cells of patients afflicted with sickle cell disease (Eaton and Hofrichter 1990).

In contrast to many of the cases described in the previous subsections, the native state polymerization of HbS is well-characterized and the relationship between the biophysical and biochemical effects of the mutation and the observed clinical phenotype is quite clear. Unfortunately, for aggregation mechanisms involving misfolded or transiently populated conformers, the elucidation of structure, as well as defining the relationship between the *in vitro* observations and the *in vivo* phenotype is less clear cut.

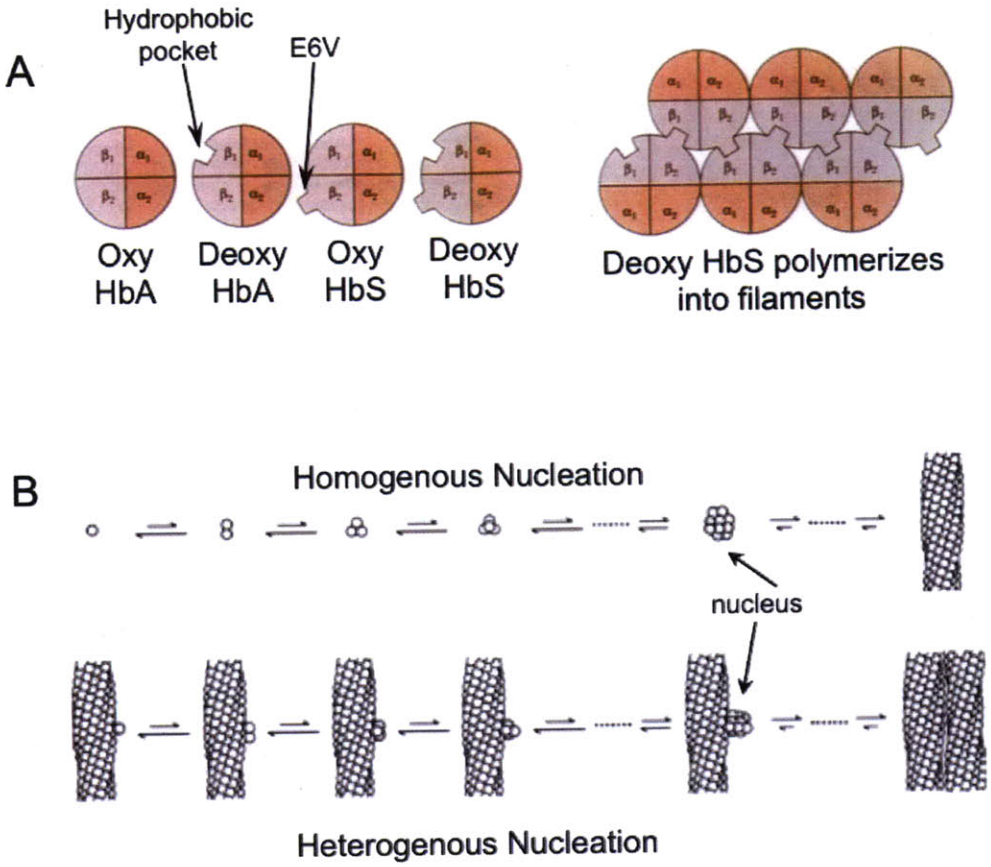

Figure 1-12: Native state polymerization of HbS. **(A)** Both WT and mutant Hb proteins expose a hydrophobic pocket in the deoxygenated state. Only HbS, which contains the amino acid substitution E6V, has a hydrophobic residue on its surface, which can interact with the native hydrophobic pocket. Figure generously provided by Dr. Kelly Knee. **(B)** Hb polymerizes by a double-nucleation mechanism. In the first stage, the rate-limiting step is formation of the nucleus of polymerization. Once formed, fibrils grow quickly. A second stage of nucleation occurs along the length of existing polymers. Reprinted with permission from Elsevier (Ferrone *et al.* 1985).

CHAPTER 2:

HYDROPHOBIC CORE MUTATIONS ASSOCIATED WITH CATARACT DEVELOPMENT IN MICE DESTABILIZE HUMAN γD-CRYSTALLIN*·

*· This research was originally published in the Journal of Biological Chemistry. Kate L. Moreau and Jonathan King. 2009. Hydrophobic Core Mutations Associated with Cataract Development in Mice Destabilize Human γD-Crystallin. *J. Biol. Chem.* 284(48): 33285-33295. © The American Society for Biochemistry and Molecular Biology

A. Abstract

The human eye lens is composed of fiber cells packed with crystallins up to 450 mg/ml. Human γD-crystallin is a monomeric, two-domain protein of the lens central nucleus. Both domains of this long-lived protein have double Greek key β-sheet folds with well-packed hydrophobic cores. Three mutations resulting in amino acid substitutions in the γ-crystallin buried cores—two in the N-terminal domain (N-td), and one in the C-terminal domain (C-td)—cause early-onset cataract in mice, presumably an aggregated state of the mutant crystallins. It has not been possible to identify the aggregating precursor within lens tissues. To compare *in vivo* cataract-forming phenotypes with *in vitro* unfolding and aggregation of γ-crystallins, mouse mutant substitutions were introduced into HγD-Crys. The mutant proteins L5S, V75D and I90F were expressed and purified from *E. coli*. WT HγD-Crys unfolds *in vitro* through a three-state pathway, exhibiting an intermediate with the N-td unfolded, and the C-td native-like. L5S and V75D in the N-td also displayed three-state unfolding transitions, with the first transition, unfolding of the N-td, shifted to significantly lower denaturant concentrations. I90F destabilized the C-td, shifting the overall unfolding transition to lower denaturant concentrations. During thermal denaturation, the mutant proteins exhibited lowered thermal stability compared with WT. Kinetic unfolding experiments showed that the N-td's of L5S and V75D unfolded faster than WT. I90F was globally destabilized and unfolded more rapidly. These results support models of cataract formation in which generation of partially unfolded species are precursors to the aggregated cataractous states responsible for light scattering.

B. Introduction

The human lens is a tissue composed of onion-like layers of fiber cells. The lens core, or nucleus, is formed *in utero* and is composed of primary fiber cells. These cells are enucleated and devoid of all organelles, presumably to assist in maintaining transparency to visible light. During an individual's lifetime, lens epithelial cells, found in a single layer on the anterior portion of the lens, differentiate to become secondary fiber cells that surround the lens nucleus in layers, thus forming the lens outer cortex. Secondary fiber cells maintain their organelles and some level of protein synthesis and turnover.

The primary fiber cells of the lens have no protein synthesis or turnover. Thus proteins translated *in utero* must maintain their native structure and remain soluble throughout the lifetime of the individual. The α, β, and γ-crystallins together account for 90% of lens proteins, present in concentrations of up to 450 mg/ml (Fagerholm et al. 1981; Siezen et al. 1988; Slingsby and Clout 1999). α-Crystallin provides both structural and chaperone functions in the lens, while the β- and γ-crystallins appear to function solely as structural proteins (Horwitz 1992; Boyle and Takemoto 1994; Jaenicke and Slingsby 2001). The continuous exposure of these proteins to environmental stresses such as UV light and oxidizing agents leads to the build-up of covalent damages (Hoenders and Bloemendal 1983; Hanson et al. 1998; Hanson et al. 2000). This can result in loss of native conformation and the generation of partially unfolded species that participate in aberrant protein-protein interactions. The resulting protein aggregation is likely to be a major pathway to cataract.

According to the World Health Organization, cataract is the leading cause of blindness worldwide. Age-related cataract (ARC) affects at least 50% of people in the United States over age 80 (Prevent Blindness America 2008). Comparison of cataractous lenses with normal lenses identifies some significant differences between the two. The most obvious difference is the increase in accumulation of high-molecular weight (HMW) aggregates. Proteins isolated from cataractous lenses were found to be highly oxidized at cysteine and methionine residues (Truscott and Augusteyn 1977a; Truscott and Augusteyn 1977b). Additional covalent modifications have been identified in aged

lenses in general, including truncations (Takemoto and Emmons 1991; Ajaz et al. 1997; Zhang et al. 2003), deamidation (Hanson et al. 1998; Lampi et al. 1998; Ma et al. 1998; Hanson et al. 2000), glycation of lysine residues (Chiou et al. 1981), and oxidation of tryptophan (Hains and Truscott 2007). It is unclear whether these modifications, particularly the extensive oxidation, initiate the aggregation process, or whether they are later effects, due to the trapping of partially unfolded species in the aggregate that are susceptible to damage. It is very plausible that accumulation of these various modifications destabilize lens crystallins, leading to their partial unfolding and exposure of hydrophobic core regions. Intermolecular interactions between these exposed regions could lead to aggregate formation, for example through a domain-swapping mechanism.

Since primary lens fiber cells lack nuclei and are terminally differentiated, they have not been propagated in tissue culture. In addition, studies of the initiation and growth of cataract within the intact lens have been very limited. As a result, it has not been possible to directly identify the state of crystallin precursors to cataract within lens fiber cells or the intact lens. We have attempted to circumvent this by examining the effects of mutations that cause cataracts in mice on the properties of human crystallin proteins *in vitro*.

Human γD-crystallin (HγD-Crys) is a monomeric, two-domain protein whose structure has been determined at 1.25 Å (Basak et al. 2003), revealing two structurally homologous domains each consisting of intercalated double Greek Key motifs. HγD-Crys is one of the most abundant γ-crystallins found in the lens (Lampi et al. 1997). It is primarily located in the central lens nucleus, the oldest region of the lens, and is therefore one of the longest-lived proteins in that tissue, as well as the entire human body. The two domains of HγD-Crys are connected by a short linker and interact through a set of hydrophobic interdomain contacts (Flaugh et al. 2005a). Systematic studies of the unfolding and refolding of HγD-Crys have identified a partially-folded intermediate with the N-terminal domain (N-td) unfolded and the C-terminal domain (C-td) folded (Kosinski-Collins et al. 2004; Flaugh et al. 2005a).

Rare mutations associated with juvenile-onset cataracts have been identified in the human γ-crystallin genes. Those identified in HγD-Crys primarily affect charged surface residues, including R14C, R36S, R58H, and E107A (Heon et al. 1999; Stephan et al.

1999; Kmoch et al. 2000; Messina-Baas et al. 2006); the non-surface mutation P23T has also been identified in families with inherited cataract (Santhiya et al. 2002; Nandrot et al. 2003; Burdon et al. 2004). Truncations of human γ-crystallins also result in inherited, early-onset cataract in some cases (Santhiya et al. 2002; Hansen et al. 2007). Previous studies with surface residue mutations have revealed that thiol-induced aggregation occurs in the case of R14C (Pande et al. 2000), while drastic decreases in solubility lead to crystallization of R36S and R58H mutant proteins (Pande et al. 2001). The P23T protein had reduced solubility (Evans et al. 2004; Pande et al. 2005)—though the thermodynamic stability was not affected—and structural studies at the atomic level revealed the altered conformation of an adjacent histidine residue (Jung et al. 2009). The human γC-crystallin (HγC-Crys) T5P and R168W mutant proteins and human γS-crystallin (HγS-Crys) G18V are three more amino acid substitutions affecting γ-crystallins that are associated with cataract formation (Heon et al. 1999; Sun et al. 2005).

The crystallins are characterized by two classes of hydrophobic buried cores: the predominantly hydrophobic side chains within the β-sheets of the Greek Key motifs; and the buried residues at the interface of the duplicated domains. Substitution of any of the six residues forming the hydrophobic domain interface of HγD-Crys resulted in a sharp destabilization of the native state and increased population of a partially-folded intermediate with an unfolded N-td and folded C-td (Flaugh et al. 2005a). Human families carrying mutations at sites in the tightly packed hydrophobic core of these proteins have not yet been reported. However, hydrophobic core mutations have been identified in murine crystallin genes (Sinha et al. 2001; Graw et al. 2002a; Graw et al. 2002b; Graw et al. 2004). Murine γD-crystallin (MγD-Crys) and HγD-Crys are closely related proteins of the same length with 83% sequence identity and 91% sequence similarity. Murine γS-crystallin (MγS-Crys) is more distantly related to HγD-Crys, as the vertebrate γS-crystallin lineage is believed to have diverged from other γ-crystallins earlier (Wistow et al. 2005). Even considering this more distant relationship, MγS-Crys and HγD-Crys share 50% sequence identity and 70% sequence similarity.

Integrity of the hydrophobic core is generally vital for maintenance of a protein's tertiary structure. Studies on the N-terminal domain of the λ repressor showed that a wide range of amino acid substitutions in the protein core altered both structure and function

(Lim et al. 1992). In particular, substitution of hydrophobic core residues with polar or charged residues resulted in large thermodynamic destabilizations *in vitro*. Dramatic decreases in biological activity were also observed, indicating that the structure was perturbed *in vivo* as well (Lim et al. 1992). In the case of SNase, the introduction of buried charges in the hydrophobic core was less disruptive due to local conformational changes that helped to stabilize the charges (Denisov et al. 2004). A complete set of alanine substitutions in the P22 Arc repressor protein identified many destabilizing mutations. Five key residues, when substituted, resulted in polypeptide chains that did not appear to fold or adopt the native dimeric structure of the Arc repressor (Milla et al. 1994). Four of these five residues have hydrophobic side chains. In the 13-rung, parallel β-helix P22 tailspike adhesin, substitution with alanine of each of 140 residues in the elongated buried core resulted in folding defects for more than 100 of the mutant proteins (Simkovsky and King 2006).

The importance of the hydrophobic core has also been illustrated in the opposite sense, by stabilizing proteins through the introduction of hydrophobic residues. The concurrent substitution of three charged residues (Arg31, Glu36, and Arg40) with the hydrophobic residues Met31, Tyr36, and Leu40 (MYL) in the Arc repressor resulted in a mutant protein that refolded with an apparent rate constant ~150-fold faster than the wild-type protein (Waldburger et al. 1996). Investigations on the hydrophobic core of T4 lysozyme found that compensatory "size-switch" mutations destabilized the protein to a lesser extent than expected for additive effects (Baldwin et al. 1996). X-ray crystal structures of these mutants showed that the surrounding residues shifted to some extent to help accommodate the altered side chains. Hydrophobic protein cores appear to be quite sensitive to substitutions and maintenance of ideal packing and geometries contribute greatly to protein stability.

The three amino acid substitutions, F9S in MγS-Crys (Everett et al. 1994; Sinha et al. 1998; Sinha et al. 2001), and V76D (Graw et al. 2002b) and I90F (Graw et al. 2004) in MγD-Crys, are associated with congenital or early-onset cataract in mice. Sinha et al. (Sinha et al. 2001) previously identified the F9S substitution in MγS-Crys as causative for the murine *Opj* cataract phenotype (Favor 1983; Favor 1984). Opacities, which increased in severity over time, were observed in the lenses of both *Opj/+* and *Opj/Opj*

mice, though the phenotypes of the homozygotes were more severe. As a function of temperature *in vitro*, the F9S mutant displayed a loss of secondary structure and increased propensity for aggregation, both at lower temperatures than wild type (Sinha et al. 2001). Wang et al. (Wang et al. 2007) found that lenses from mice homozygous for the V76D mutant allele contained intranuclear γ-crystallin protein aggregates and that the water-soluble γ-crystallin fraction of lens proteins was diminished. In transfection studies, the V76D mutant protein aggregated in both the nuclei and cytosol of cultured lens epithelial cells.

To further explore the effects of mutations to residues found in the hydrophobic core of HγD-Crys, we prepared a set of three HγD-Crys proteins carrying the murine amino acid replacements. All proteins were expressed in *E. coli* and purified to study their overall conformation and thermodynamic and kinetic stabilities. Their significant destabilization highlights the importance of the tightly packed hydrophobic core of the γ-crystallins and sheds light on the possible mechanisms of congenital cataract formation associated with these mutations.

C. Experimental Procedures

1. Mutagenesis, Expression, and Purification of Recombinant HγD-Crys

Constructs containing each of the three mutations, L5S, V75D, and I90F, were made by site-directed mutagenesis. Mutant primers (IDT-DNA) were used to amplify the HγD-Crys gene in the pQE.1 plasmid (Qiagen), which contains an N-terminal His_6 tag. Mutations were confirmed by sequencing of the entire gene (Massachusetts General Hospital).

Wild-type HγD-Crys and mutant proteins V75D and I90F were expressed as previously described (Kosinski-Collins et al. 2004). The mutant protein L5S was found in inclusion bodies in the insoluble portion of the cell lysate when expressed at physiological temperature. Overnight expression at 17°C yielded a greater amount of natively folded protein. Cells were pelleted, resuspended in lysis buffer (50 mM NaPi, 300 mM NaCl, 15 mM imidazole, pH 8.0) and stored at -80°C.

Cells were lysed by ultrasonication and insoluble cell debris was pelleted by centrifugation at 13,000 rpm for 45 minutes using an SS-34 rotor. Supernatants were filtered and applied to an Ni-NTA column using an AKTA Purifier FPLC system (GE Healthcare). Protein was eluted using a linear gradient of increasing imidazole. Fractions containing the protein of interest were pooled and dialyzed three times against 10 mM ammonium acetate, pH 7.0.

2. Circular dichroism spectroscopy

CD spectra of the wild-type and mutant proteins were obtained using an AVIV model 202 CD spectrometer (Lakewood, NJ). Protein samples were prepared at a concentration of 100 μg/ml in 10 mM NaPi pH 7.0. Spectra were collected from 260-195 nm in a 1 mm quartz cuvette held at 37°C. Spectra were buffer-corrected and mean residue ellipticity was calculated.

3. Fluorescence emission spectroscopy

Tryptophan fluorescence spectra of all proteins was measured using an Hitachi F-4500 fluorimeter. Samples contained protein at a concentration of 10 μg/ml in 100 mM NaPi, 1 mM EDTA, 5 mM DTT, pH 7.0 and 5.5 M guanidinium hydrochloride (GdnHCl) for unfolded samples. An excitation wavelength of 295 nm was used to selectively excite tryptophan residues and emission spectra were recorded from 310-400 nm and corrected for buffer signal.

4. Equilibrium unfolding/refolding

Equilibrium unfolding and refolding experiments were performed at 37°C and pH 7.0 as previously described (Flaugh et al. 2006). The unfolding and refolding data were fit to a two-state (Greene and Pace 1974) or three-state model (Clark et al. 1993) using the curve-fitting feature of the Kaleidagraph software package (Synergy Software). The increases in fluorescence of the refolding curves at low GdnHCl were due to light

scattering resulting from protein aggregation of a partially-folded intermediate into high molecular weight complexes. These points were not included in curve-fitting analysis. Transition midpoints, ΔG° and *m*-values were calculated for all transitions. Averages and standard deviations were calculated from three trials.

5. Thermal denaturation

Thermal denaturation experiments were performed using an AVIV model 202 CD spectrometer. Temperature was monitored and raised with an internal Peltier thermo-electric controller. Samples were prepared as described above except a 10 mm screw-top quartz cuvette was used to prevent evaporation of buffer at high temperatures. Changes in ellipticity at 218 nm were monitored every 1°C from 25-90°C. Sample temperature was allowed to equilibrate for 1 min before ellipticity was measured over a 3-s averaging time. Melting temperatures were determined by calculating the midpoints of transitions. Reported values are averages of three trials.

6. Unfolding kinetics

All kinetic unfolding experiments were carried out at 18°C. Experiments were performed by diluting wild-type and mutant proteins into 5.5 M and 3.5 M GdnHCl, respectively, buffered with 100 mM NaPi, 1 mM EDTA, 5 mM DTT, pH 7.0. Fluorescence emission at 350 nm was monitored over time using an Hitachi F-4500 fluorimeter with an excitation wavelength of 295 nm. Unfolding samples contained protein at a final concentration of 10 μg/ml. Kinetic unfolding data were fit with single or double exponentials and residuals were calculated using the curve-fitting feature of Kaleidagraph. Best fits were chosen by agreement of calculated and observed parameters and a random distribution of residuals. Experiments were performed in triplicate for each protein and parameters were averaged.

7. Refolding and Aggregation Turbidity Measurements

All protein samples at an initial concentration of 2 mg/ml were unfolded at 37°C for at least 36 hours in buffer (100 mM NaPi, 1 mM EDTA, 5 mM DTT, pH 7.0) containing various concentrations of GdnHCl. Unfolded protein was placed in a quartz cuvette and diluted 20-fold with the appropriate buffer/GdnHCl solution to achieve a final protein concentration of 0.1 mg/ml and a final GdnHCl concentration of 0.17-0.18 M. The sample was immediately mixed after dilution by inverting the cuvette five times. It was then placed in a Cary 50 UV/Vis spectrophotometer and the solution turbidity was measured by the apparent absorbance at 350 nm for 20 minutes. All protein and buffer solutions were kept in a 37°C water bath during the experiments and the cuvette temperature was maintained at 37°C using a single cell Peltier controller. All experiments for each protein were performed in triplicate. The refractive indices of the diluted solutions were measured to confirm that all samples contained the same final concentration of GdnHCl.

D. Results

1. Protein Purification and Structural Characterization

To determine how these mutations, which have been linked to early-onset cataract in mice, affect HγD-Crys three human proteins were made: V75D, I90F and L5S. (Numbering of residues is based on that of the wild-type HγD crystal structure, PDB ID: 1HK0.) The residues V75 and I90 are conserved and occur at identical positions in mouse and human γD-crystallins. The mutant alleles encoding V75D and I90F were constructed by site-specific mutagenesis of the human cDNA sequence cloned into the vector pQE1. The third mutation, encoding L5S, was constructed in a similar manner to the above-mentioned mutations; however, this amino acid substitution was based on the cataract-associated F9S mutation in MγS-Crys (Sinha et al. 2001). MγS-Crys has a four residue N-terminal extension not found in mouse or human γD-crystallins. The homologous position in HγD-Crys to MγS-Crys F9S, based on protein sequence

alignment, is L5; thus the nucleotides corresponding to this residue were changed to mimic this third mutation. Although this mutation is based on one described in MγS-Crys, this region in the first β-strand of the first Greek Key motif appears to be important in other crystallins as well. The T5P substitution in HγC-Crys resulted in congenital cataract (Heon et al. 1999) and *in vitro* studies have found that the mutant protein had an altered conformation and lowered thermal stability (Fu and Liang 2003).

All proteins were expressed in *E. coli* with N-terminal His_6 tags. When expressed at 37°C, L5S was found in aggregates in the insoluble portion of the cell lysate. This indicates that this mutation affected the *in vivo* folding of the protein at physiological temperature. The L5S mutant protein was then expressed at 17°C and a greater portion was found in the soluble fraction of the cell lysate. These results are in line with observations by Sinha et al. (Sinha et al. 2001), who observed thermal aggregation of the murine mutant protein F9S at temperatures as low as 46°C. V75D and I90F proteins were expressed and soluble at 37°C, indicating that these mutations did not affect the initial *in vivo* folding to the same extent as L5S. Both wild-type and mutant proteins were purified by Ni-NTA affinity chromatography.

CD and fluorescence spectroscopy were used to compare the overall structures of the mutant proteins with that of wild-type HγD-Crys. These experiments distinguished any gross changes in secondary and tertiary structure among the mutant and wild-type proteins. The far-UV CD (Figure 2-1) spectrum of wild-type HγD-Crys agreed with previous results (Flaugh et al. 2006). The spectrum displayed a minimum at 218 nm, indicative of high β-sheet content, and a small shoulder around 208 nm. The three mutant proteins displayed CD spectra with minima at 218 nm of similar intensity to wild type. L5S and I90F showed slight differences in the region around 208 nm, while V75D was indistinguishable from wild type in this region.

Tryptophan fluorescence was used to probe the overall tertiary structure of wild-type HγD-Crys and the three mutants. HγD-Crys has 4 buried tryptophan residues, arranged symmetrically between the two domains. It also contains 14 tyrosine residues, and an excitation wavelength of 295 nm was used to selectively excite the tryptophans. Trp fluorescence is strongly quenched in the native state of HγD-Crys compared to the unfolded state (Chen et al. 2006). Therefore, Trp fluorescence can be used as a sensitive

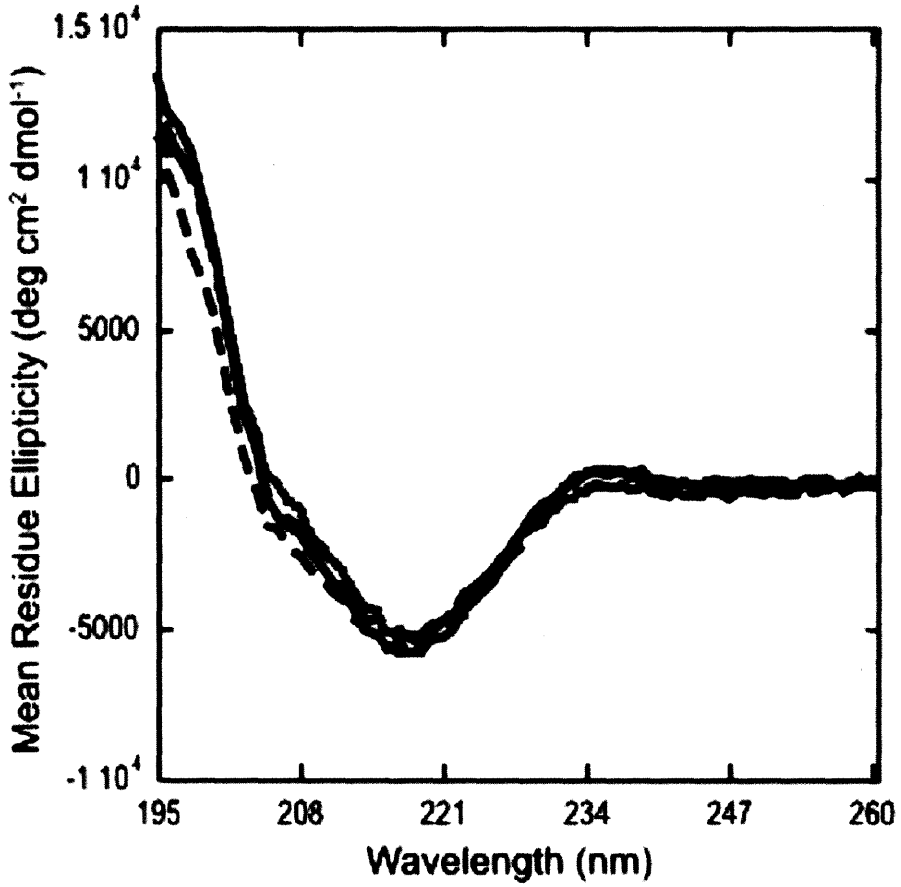

Figure 2-1: Far-UV CD spectra of wild-type HγD-Crys (solid black line) and mutant proteins L5S (short dashed line), V75D (long dashed line), I90F (dotted line). All proteins were present at 100 μg/ml in 10 mM NaPi, pH 7.0. Spectra were collected at 37°C.

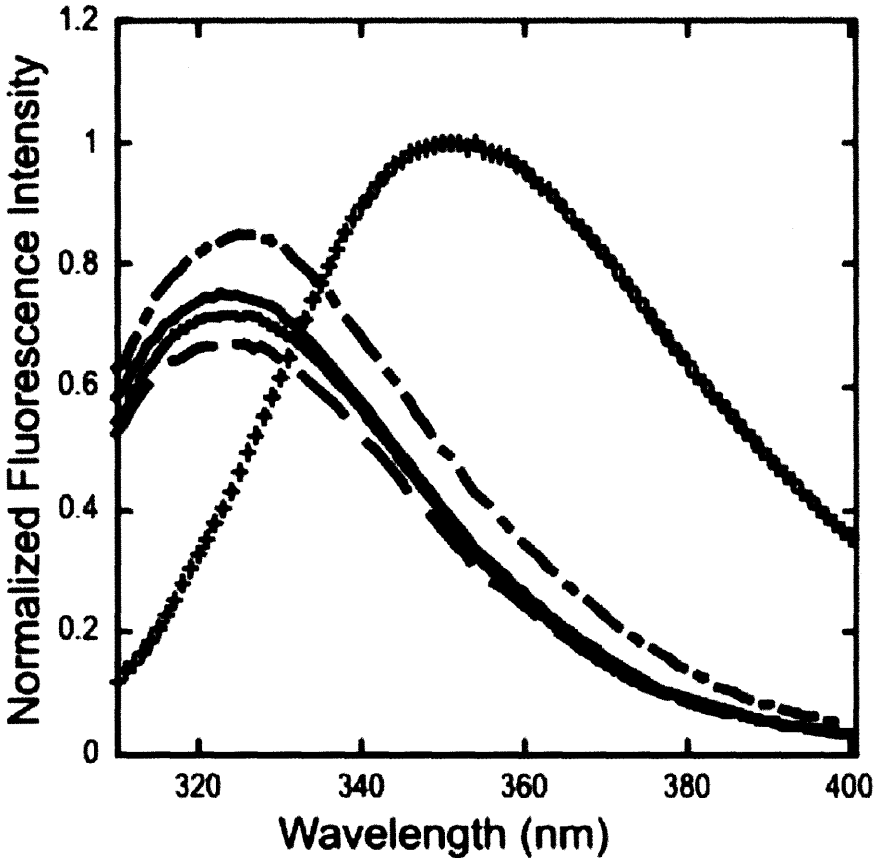

Figure 2-2: Fluorescence spectra of native wild-type HγD-Crys (solid black line) and mutant proteins L5S (long dashed line), V75D (short dashed line), and I90F (dotted line). Normalized tryptophan fluorescence spectra of native wild-type protein and mutants is shown with fluorescence spectra of unfolded wild-type HγD-Crys (+) for comparison. Data was normalized to account for slight variations in concentrations. Spectra were collected at 37°C. Protein solutions contained 100 mM NaPi, 1 mM EDTA, 5 mM DTT, pH 7.0, with 5.5 M GdnHCl for the unfolded samples.

indicator of tertiary structure for this protein. For the quenching to be maintained in mutant proteins, the tertiary structure of the native state cannot be greatly altered from that of WT. Otherwise, loss of quenching would be expected, due to the change in geometries of both the backbone and water molecules.

In agreement with previous experiments, native wild-type HγD-Crys had an emission maximum at about 326 nm (Figure 2-2) (Kosinski-Collins et al. 2004). HγD-Crys unfolded in 5.5 M GdnHCl had a shifted emission maximum at 350 nm which increased in intensity due to the loss of fluorescence quenching and energy transfer that is present in the native state (Kosinski-Collins et al. 2004; Chen et al. 2006). Native L5S and I90F proteins both had fluorescence maxima at about 326 nm (Figure 2-2). The peak fluorescence intensity of the native L5S protein was about 10% less than that of wild type, while that of I90F was very similar. Native V75D protein had a fluorescence maximum at 327 nm, and the peak fluorescence was about 13% greater that than of wild-type HγD-Crys (Figure 2-2). These differences could be due to slight variations in solution conditions, or they may have been caused by slight structural perturbations around the Trp side chains. Quenching of native state Trp fluorescence was observed for all mutants, further indicating that their structure was similar to that of WT.

2. Equilibrium Unfolding and Refolding of Wild-type and Mutant Human γD-Crystallins

Previously, equilibrium unfolding/refolding experiments were used to analyze the thermodynamic stability of wild-type HγD-Crys under physiological conditions (37°C, pH 7.0) (Flaugh et al. 2005a; Flaugh et al. 2005b; Flaugh et al. 2006). These experiments utilized guanidinium hydrochloride (GdnHCl) as the denaturing agent due to the fact that wild-type HγD-Crys does not fully unfold in up to 8 M urea (Kosinski-Collins and King 2003). Tryptophan fluorescence was used to probe the conformation of proteins and changes in fluorescence intensities at 360 nm and 320 nm were used for data analysis. Previous experiments found that the unfolding/refolding curves were best fit by a three-state model, which indicated the existence of a populated, partially-folded intermediate with an unfolded N-td and a native-like C-td (Flaugh et al. 2005a). The first transition

representing the unfolding of the N-td, had a midpoint of 2.2 M GdnHCl. The second transition, representing the unfolding of the C-td, had its midpoint at 2.8 M GdnHCl (Table 2-1). Wild-type HγD-Crys chains aggregated upon refolding into buffer by dilution. Evidence for this aggregation was the distinct increase in scattering by the refolding samples at GdnHCl concentrations below 1 M.

Note that although the y-axes in Figure 2-3 describing equilibrium experiments are labeled as fluorescence intensity, the rise of the refolding curves at low GdnHCl concentrations is due to the right-angle light scattering by the aggregated chains. AFM images of these aggregated species can be seen in Kosinski-Collins and King, 2003 (Kosinski-Collins and King 2003). Though the right-angle scattering interferes with the fluorescence emission spectra of the aggregated species, a distinct red-shift was still evident. This suggests that the chains in the aggregates are misfolded. Higher GdnHCl concentrations inhibit this off-pathway aggregation.

Thermodynamic stabilities of the three mutant proteins L5S, V75D, I90F and WT HγD-Crys were analyzed by the same methods described above. Fluorescence data for all the mutants were analyzed by changes in the fluorescence intensity at 360 nm. The data are shown as the ratio of fluorescence intensities at 360/320 nm for clarity. Parameters calculated for both sets of data agreed within the standard deviation of the experiments.

The L5S substitution is in the first β-strand of the N-td of the protein. Similar to wild type, the data were fit by a three-state model and the presence of a folding intermediate was indicated by a prominent plateau in the range of 1 to 2.3 M GdnHCl (Figure 2-3, Table 2-1). The first transition had a midpoint of ~0.72 M GdnHCl and an apparent ΔG^0_{N-I} of 3.1 kcal · mol^{-1}. The N-td is extremely destabilized compared to wild type, consistent with the location of the substitution. The midpoint of the second transition was ~2.9 M GdnHCl and the apparent ΔG^0_{I-U} was 9.0 kcal · mol^{-1}. These values are very similar to those calculated for wild-type HγD-Crys. Thus, it appears that this substitution does not affect the stability of the C-td. Like the wild-type protein, L5S appeared to aggregate upon refolding into buffer as evidenced by the increase in fluorescence due to scattering from these refolding samples (Figure 2-3). Unlike WT,

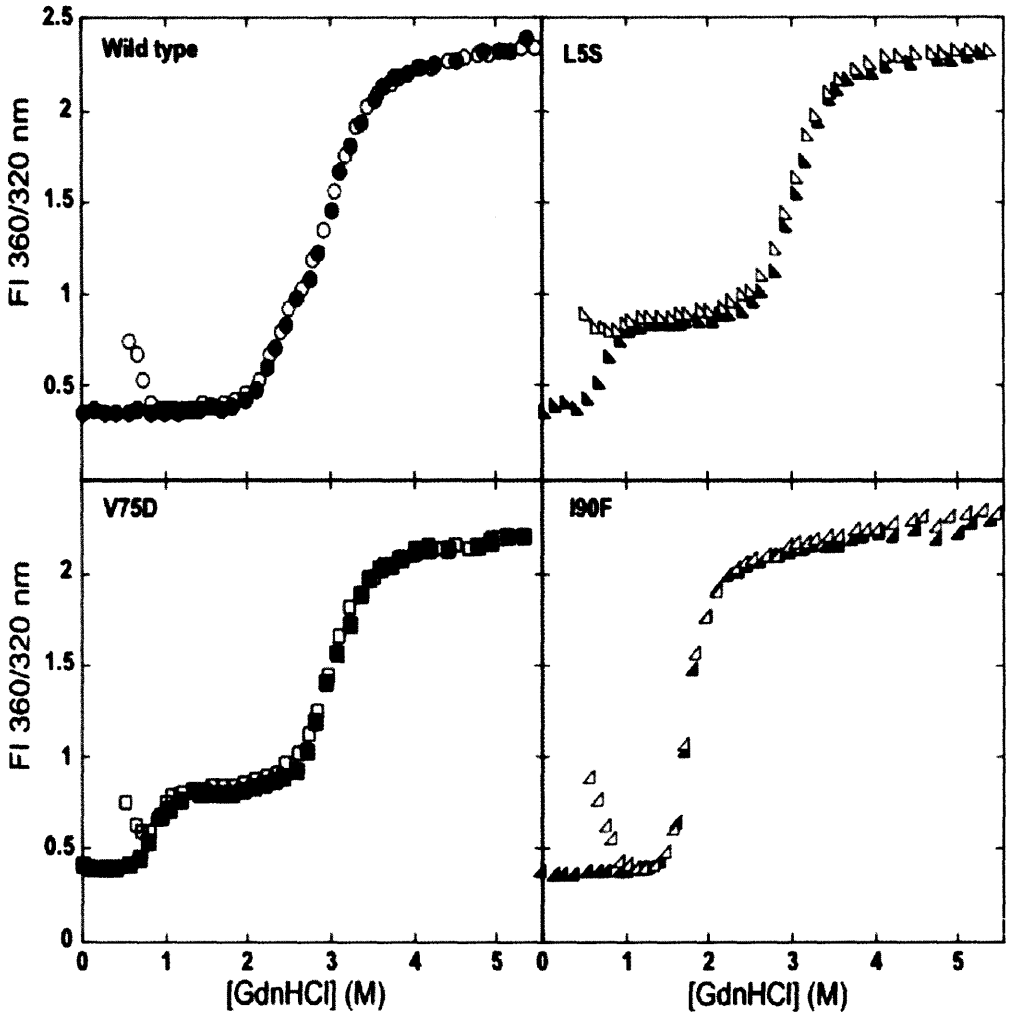

Figure 2-3: Equilibrium unfolding (solid symbols) and refolding (open symbols) of wild-type HγD-Crys (●) and mutant proteins L5S (◣), V75D (■), and I90F (◢). All proteins were present at 10 μg/ml in 100 mM NaPi, 1 mM EDTA, 5 mM DTT, pH 7.0 and GdnHCl from 0 to 5.5 M. Measurements were collected at 37°C. The ratio of fluorescence intensities at 360/320 nm is shown for visual clarity. Note that the increased fluorescence of the refolding curve at low GdnHCl concentrations represents light scattering due to aggregation and is not increased fluorescence intensity. All calculations were performed using single wavelength fluorescence emission data at 360 nm.

this mutant protein was too destabilized to refold to a native-like conformation over the range of conditions present in these experiments.

The V75D substitution is located in the loop region between the fifth and sixth β-strands of the protein's N-td. The unfolding/refolding transitions of the V75D protein were quite similar to those of L5S and were also fit by a three-state model (Figure 2-3, Table 2-1). The first transition had a midpoint at 0.81 M GdnHCl and an apparent ΔG^0_{N-I} of 2.9 kcal · mol^{-1}. The second transition had a midpoint at 2.9 M GdnHCl and an apparent ΔG^0_{I-U} of 9.0 kcal · mol^{-1}. Like L5S, the V75D mutant had a dramatically destabilized N-td, consistent with the location of the amino acid substitution. The C-td was unaffected by this substitution and had a stability equal to that of wild-type HγD-Crys. The V75D protein also displayed aggregation behavior similar to that of L5S.

Unlike the previous two proteins, I90F was mutated at the start of the first β-strand in the C-td of the protein. Instead of the three-state transitions observed for wild-type, L5S and V75D proteins, the unfolding/refolding data for I90F was fit by a two-state model (Figure 2-3, Table 2-1). This suggests that there is not a significantly populated intermediate in this transition. In agreement with this, the transition regions of the unfolding/refolding curves were clearly steeper than either transition region for the wild type, L5S and V75D proteins. The midpoint of this single transition was at 1.7 M GdnHCl. This is lower than the midpoints of either transition for wild-type HγD-Crys. The apparent ΔG^0_{N-U} for I90F was 9.4 kcal · mol^{-1}. In a similar fashion to wild type, this mutant refolded to a native-like state at GdnHCl concentrations above 1 M, but aggregated when diluted into buffer.

3. Thermal Unfolding of Wild-type and Mutant Human γD-Crystallins

Thermal unfolding employing a low ionic strength buffer was used as a second measure of stability of wild-type HγD-Crys and the three mutant crystallins. These experiments used a circular dichroism spectrophotometer to monitor changes in ellipticity at 218 nm from 25 to 90°C. At high temperatures all proteins aggregated as shown by the clouding and opacification of all samples. With increasing temperature the spectra

Table 2-1. Equilibrium unfolding/refolding parameters for wild-type and mutant proteins at pH 7.0

Protein	Equilibrium Transition 1			Equilibrium Transition 2			Transitions 1 and 2
	C_m [a]	Apparent *m* value[b]	Apparent $\Delta G^0_{N\text{-}I}$ [c]	C_m [a]	Apparent *m* value[b]	Apparent $\Delta G^0_{I\text{-}U}$ [c]	$\Delta\Delta G_{N\text{-}U}$ [d]
Wild type[e]	2.2 ± 0.1	3.6 ± 0.1	7.7 ± 0.2	2.8 ± 0.1	3.1 ± 0.4	8.9 ±1.3	-
L5S	0.7 ± 0.1	4.4 ± 0.2	3.1 ± 0.2	2.9 ± 0.1	3.1 ± 0.2	9.0 ± 0.4	4.6
V75D	0.8 ± 0.1	3.6 ± 1.1	2.9 ± 0.9	2.9 ± 0.1	3.0 ± 0.4	8.7 ± 1.1	5.0
I90F	1.7 ± 0.1	5.5 ± 1.2	9.4 ± 2.1	-	-	-	7.2

[a] Transition midpoints in units of M GdnHCl.
[b] Apparent *m* values in units of kcal·mol^{-1}·M^{-1}.
[c] Free energy of unfolding in the absence of GdnHCl in units of kcal·mol^{-1}.
[d] $\Delta\Delta G_{N\text{-}U} = (\Delta G^0_{N\text{-}I(\text{wild type})} + \Delta G^0_{I\text{-}U(\text{wild type})}) - (\Delta G^0_{N\text{-}I(\text{mutant})} + \Delta G^0_{I\text{-}U(\text{mutant})})$ in units of kcal·mol^{-1}.
[e] Parameters of wild type are from Flaugh *et al.* (2005).

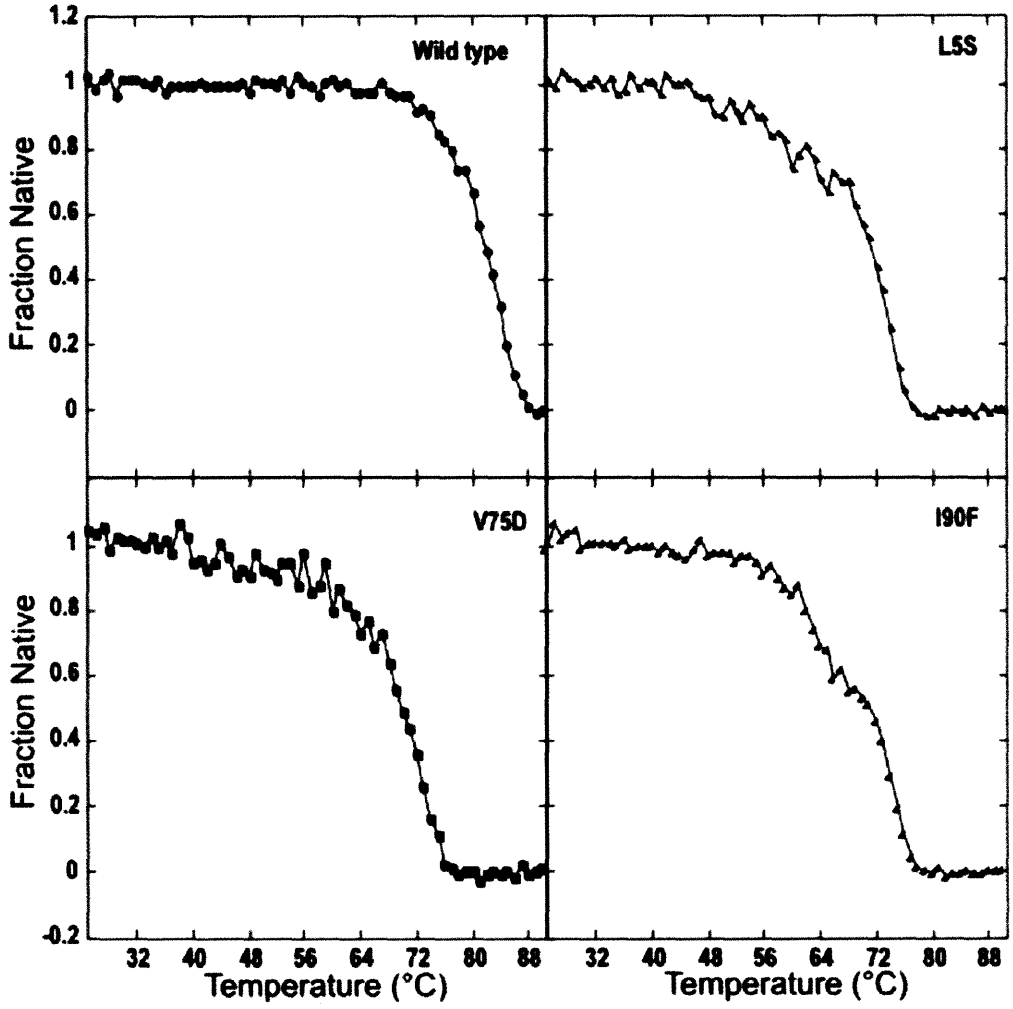

Figure 2-4: Thermal unfolding of wild-type HγD-Crys and mutant proteins. Unfolding was monitored by the change in ellipticity at 218 nm with increasing temperature. All proteins were present at 100 μg/ml in 10 mM NaPi, pH 7.0. Symbols used are: wild-type HγD-Crys (●), L5S (◣), V75D (■), and I90F (◢).

Table 2-2. Thermal unfolding parameters of wild-type and mutant proteins at pH 7.0

Protein	Thermal Unfolding Transitions	
	T_{m1}[a]	T_{m2}[a]
Wild type[b]	83.8 ± 1.3	-
L5S	57.4 ± 2.8	73.0 ± 0.2
V75D	71.7 ± 0.2	-
I90F	64.2 ± 0.5	74.8 ± 0.4

[a] Midpoints of melting transitions monitored by CD in units of °C.

[b] Thermal unfolding data of wild type are from Flaugh *et al.* (2006).

exhibited reduced ellipticity of the 218 peak, representing loss of β-sheet structure and accumulation of both partially-folded and aggregated species.

Confirming previous results (Flaugh et al. 2006), the thermal denaturation of wild-type HγD-Crys was fit by a two-state model without an obvious stable intermediate (Figure 2-4). The melting temperature was 83.8°C (Table 2-2). The thermal unfolding of the mutant protein V75D appeared overall to be two-state, but with a gradual decrease in negative ellipticity from 40 to 50°C. The melting temperature of this mutant was 71.7 °C (Figure 2-4, Table 2-2). In contrast, the thermal unfolding of the L5S and I90F proteins were best fit by three-state models. The first transition in the unfolding of L5S had a shallower slope with a midpoint at 57.4°C. The second transition was much steeper with a midpoint at 73.0°C (Figure 2-4, Table 2-2). These results follow a similar pattern to those observed for the F9S MγS-Crys mutant compared to wild-type MγS-Crys (Sinha et al. 2001). Thermal unfolding of the mutant I90F had a much flatter native baseline and a small plateau in the transition region corresponding to ~50% of the protein population existing in the native state. This indicates a populated intermediate on the unfolding pathway. The midpoint of the first transition was at 64.2°C, and that of the second transition was 74.8°C (Figure 2-4, Table 2-2).

4. Kinetic Unfolding of Wild-type and Mutant Human γD-Crystallins

To evaluate the effects of these mutations on the unfolding kinetics of HγD-Crys, we performed kinetic unfolding experiments by monitoring the increase in tryptophan fluorescence intensity at 350 nm over time when native protein was diluted into high concentrations of GdnHCl. All three mutant proteins unfolded very rapidly. To obtain unfolding rate constants, experimental conditions were altered to slow unfolding reactions. The three mutant proteins were rapidly diluted into 3.5 M GdnHCl, pH 7.0, at 18°C. Wild-type HγD-Crys does not completely unfold under these conditions, so it was diluted into 5.5 M GdnHCl, pH 7.0, at 18°C. These two sets of conditions enabled the measurement of unfolding rate constants and the calculation of unfolding half-times. Although rates may be not directly comparable, the use of 3.5 M GdnHCl emphasizes the destabilization induced by these mutations.

At 18°C in 5.5 M GdnHCl, pH 7.0, the kinetic unfolding transitions of wild-type HγD-Crys (Figure 2-5) were best fit by two exponentials. This suggests the presence of one unfolding intermediate, consistent with observations from equilibrium unfolding/refolding experiments. The unfolding transitions had $t_{1/2}$ values of 403 s and 3531 s for the two phases, respectively (Table 2-3). These values were in agreement with previous results for HγD-Crys unfolding at 18°C from Mills-Henry (Mills-Henry 2007). Flaugh et al. (Flaugh et al. 2006) measured the kinetic unfolding transitions in 5.0 M GdnHCl, pH 7.0, at 37°C . Their data were best fit by three exponentials with $t_{1/2}$ values of 0.79, 33, and 200 s for the three phases, respectively (Flaugh et al. 2006). It may be that this first transition was not discernible under the conditions employed here.

Kinetic unfolding rates of the mutant proteins were measured in a similar manner using the lower denaturant concentration of 3.5 M GdnHCl. The temperature and pH were maintained as for the wild-type protein. The kinetic unfolding transitions for the two mutant crystallins L5S and V75D were very similar (Figure 2-5). They both exhibited an extremely rapid increase in fluorescence, which then reached a plateau over the course of three hours. This plateau did not correspond to the fully unfolded protein but to ~40% of the chain existing in the unfolded state. The final fluorescence emission spectra of the unfolding samples were similar to the spectra for partially unfolded samples in equilibrium unfolding experiments (data not shown). This was consistent with the previous observation that neither wild-type HγD-Crys nor its isolated C-td unfolded completely in 3.5 M GdnHCl, pH 7.0, at 18°C (Mills-Henry 2007). Therefore, the rapid initial increases in fluorescence observed for both proteins most likely corresponded to the unfolding of the highly destabilized N-td, while the C-td remained folded. The observed unfolding transitions for L5S and V75D were fit by single exponentials, with $t_{1/2}$ values of 2.5 and 2.0 s, respectively (Table 2-3). In contrast, the mutant protein I90F unfolded completely under the same denaturant and temperature conditions utilized for the N-td mutants. The kinetic unfolding transition exhibited a rather rapid, steady rise in fluorescence (Figure 2-5). This transition was best fit by a single exponential with a $t_{1/2}$ value of 338 s (Table 2-3). The final fluorescence emission spectra of the sample confirmed that the protein was completely unfolded.

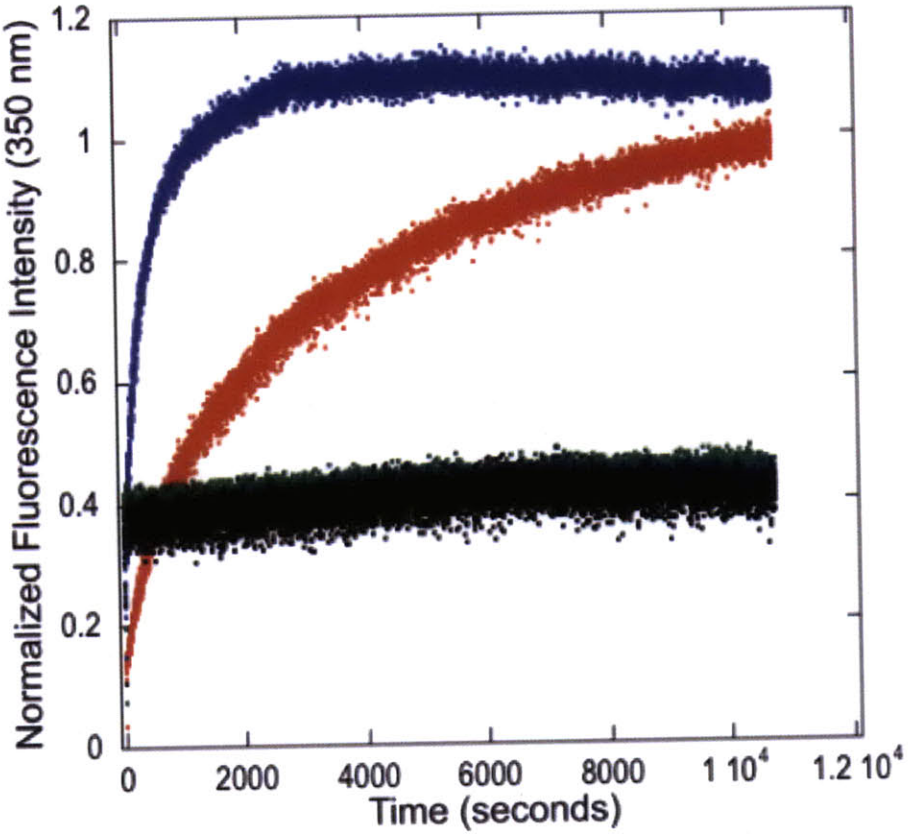

Figure 2-5: Kinetic unfolding of wild-type HγD-Crys (red) and mutant proteins L5S (green), V75D (black), and I90F (blue). All experiments were carried out at 18°C at a final protein concentration of 10 μg/ml. Wild-type HγD-Crys was unfolded in 5.5 M GdnHCl while all mutants were unfolded in 3.5 M GdnHCl to better measure kinetic parameters. All GdnHCl solutions were buffered with 100 mM NaPi, 1 mM EDTA, 5 mM DTT, pH 7.0. The increase in fluorescence at 350 nm was used to monitor unfolding of the proteins. Fluorescence data was normalized for comparison. L5S and V75D are not completely unfolded at 3.5 M GdnHCl. (See text for details.)

Table 2-3. Kinetic unfolding parameters of wild-type and mutant proteins at pH 7.0 and 18°C

Protein	Kinetic Unfolding Transition 1		Kinetic Unfolding Transition 2	
	k_{ul} [a]	$t_{1/2}$ [b]	k_{ul} [a]	$t_{1/2}$ [b]
Wild type	0.0017 ± 0.00017	403 ± 39	0.0002 ± 0.000029	3531 ± 502
L5S	0.32 ± 0.14	2.5 ± 1	-	-
V75S	0.32 ± 0.065	2.0 ± 0.4	-	-
I90F	0.0021 ± 0.00016	338 ± 28	-	-

[a] Kinetic rate constants in units of s^{-1}.
[b] Half-times in units of seconds.

5. Refolding and Aggregation of Partially Unfolded Wild-type and Mutant HγD-Crys

Both mutant proteins containing N-td amino acid substitutions, L5S and V75D, populated partially-folded intermediates over a wide range of denaturant concentrations. The C-td mutant protein, I90F, did not appear to populate such an intermediate in the experiments described here. To determine whether the partially-folded intermediates populated by the L5S and V75D proteins were aggregation-prone, proteins were partially unfolded in 0.2, 2, and 4 M GdnHCl at a concentration of 2 mg/ml under equilibrium conditions at 37°C. The unfolding solutions at equilibrium were then diluted 20-fold to a final protein concentration of 100 μg/ml in ~0.2 M GdnHCl. These are conditions under which the mutant proteins were previously observed to aggregate when refolded from fully denatured state, represented here by the samples incubated in 4 M GdnHCl. Changes in the absorbance of the solution at 350 nm were monitored, with increasing absorbance indicating the formation of light scattering aggregates.

Both L5S and V75D proteins followed very similar aggregation patterns (Figure 2-6). Aggregation upon dilution was only observed for samples that were fully denatured in 4 M GdnHCl. Partially unfolded samples that populated the observed folding intermediate did not form light scattering aggregates upon dilution. These results were similar to those obtained with the negative control samples. Wild-type HγD-Crys incubated under the same sets of conditions was only observed to aggregate when diluted out of 4 M GdnHCl, conditions under which the protein is fully unfolded. The N-td of the wild-type protein is only just beginning to unfold in 2 M GdnHCl and no light scattering was seen when diluted from this condition.

The mutant protein I90F was treated somewhat differently because no obvious folding intermediate was observable in equilibrium unfolding/refolding experiments. 2 mg/ml protein samples were incubated at 37°C in 0.2, 1.7, and 4.0 M GdnHCl until equilibrium was reached. 1.7 M GdnHCl was chosen as an intermediate concentration because this is the unfolding transition midpoint determined from GdnHCl-induced equilibrium unfolding/refolding experiments. Interestingly, during initial unfolding of the protein, the sample incubated in 1.7 M GdnHCl began to aggregate (Figure 2-7). The aggregate was visible by eye and the protein solution appeared cloudy. This was the only

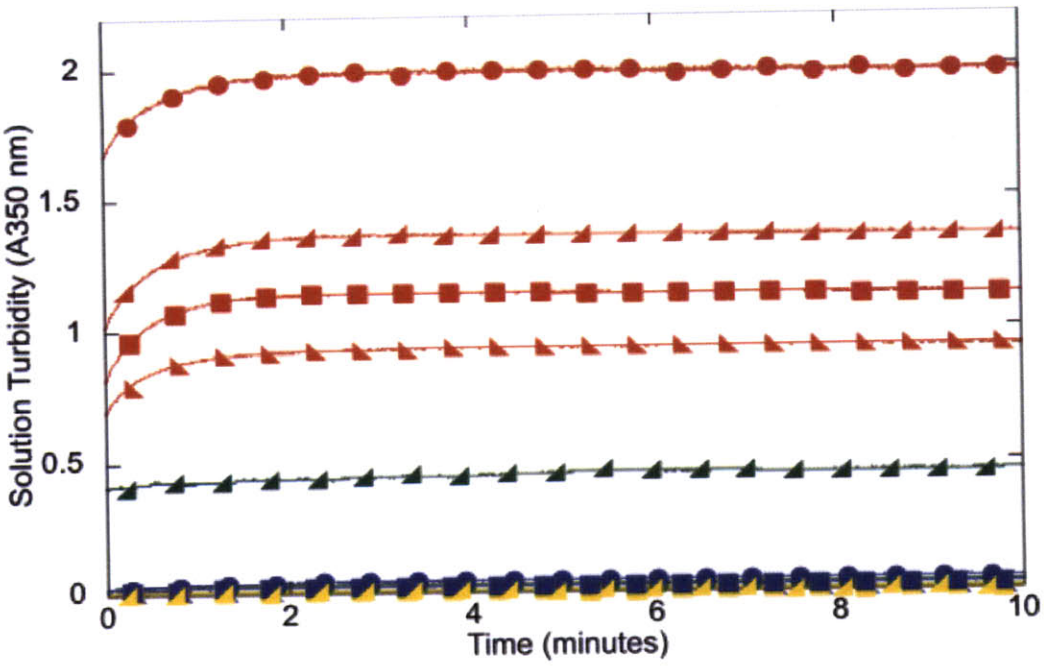

Figure 2-6: Refolding aggregation of wild-type HγD-Crys (●) and mutant proteins L5S (◣), V75D (■), and I90F (◢). All samples were incubated at 37°C overnight at given concentrations of GdnHCl, indicated by the color of the points/lines: 4.0 M (red); 2.0 M (blue); 1.7 M (green); 0.2 M (yellow). Protein samples were diluted with the appropriate buffer to a final denaturant concentration of ~0.2 M GdnHCl. Aggregation was monitored by measuring changes in absorbance at 350 nm over time.

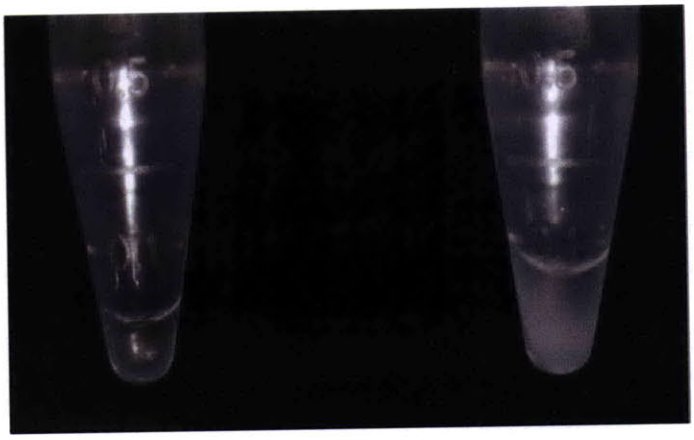

Figure 2-7: Upon incubation of I90F (2 mg/ml) at 37°C in 1.7 M GdnHCl, cloudy aggregates, visible by eye, formed that adhered to the sides of the microcentrifuge tube. On the right, the aggregated I90F sample is shown. On the left, wild-type HγD-Crys incubated under the same conditions is shown. No aggregation was visible for the WT sample and the solution turbidity was essentially zero over the course of the experiment.

sample among all proteins and denaturant concentrations for which this was observed. Because an obvious folding intermediate was not detectable by other methods, it is difficult to speculate on the mechanism of aggregation. When diluted 20-fold, the aggregates remained intact and significant scatter was observed (Figure 2-6). The level of scatter remained constant over the entire length of the experiment; there was no initial increase as observed for the fully unfolded samples that were diluted to induce aggregation. As expected, the fully unfolded I90F protein aggregated upon dilution with buffer in a manner similar to all other fully unfolded (4.0 M GdnHCl) samples (Figure 2-6).

E. Discussion

As a result of the physical integrity of the lens, it has been difficult to study cataract formation in the native environment. Thus direct evidence linking the aggregation reactions documented *in vitro*, with cataract formation *in situ*, has been lacking. We have attempted to bridge this gap by characterizing the effects of mouse crystallin cataract-causing mutations on human lens crystallins.

For a number of protein aggregation diseases, partially unfolded chains are thought to be the precursors in the aggregation reactions (Dobson 2004). The γ-crystallins appear to have an extremely rigid three-dimensional structure with tight side chain packing (Chen et al. 2008). The three cataract-associated mutations were chosen to investigate the effects of mutation on the tightly packed hydrophobic core of HγD-Crys. All three mutations investigated dramatically destabilized HγD-Crys in equilibrium unfolding/refolding experiments. Overall ΔG^0 values were decreased by 4.6 kcal/mol and 5.0 kcal/mol for L5S and V75D mutant crystallins, respectively. For I90F, the ΔG^0 value decreased by 7.2 kcal/mol in comparison to wild-type HγD-Crys. The site of the substitution was directly related to the domain destabilization. For the two N-td mutants, L5S and V75D, only the stability of the N-td was affected, in that its unfolding transition midpoint was lowered. The C-td unfolding transition midpoint was not affected in either case. For the I90F substitution, which is found in the C-td, a steep two-state transition was observed with no discernible intermediates. This indicates that both domains are

destabilized and the entire protein is globally unfolding without significantly populated intermediates. Previous work showed that HγD-Crys folds through a three-state pathway with the C-td folding first, followed by the N-td (Kosinski-Collins et al. 2004). Destabilization of the C-td may result in global protein destabilization because the domain interface, which is known to play a role in HγD-Crys stability (Flaugh et al. 2005a), may not be in its native conformation.

Wild-type HγD-Crys is resistant to thermal denaturation; its melting temperature is ~83°C. The three amino acid replacements lowered the melting temperatures, and the melting curves for all mutant proteins indicated population of partially unfolded intermediates. However, because these data are based on CD measurements of overall secondary structure, decreases in melting temperature and appearance of possible intermediates cannot be attributed to specific regions of the protein's three-dimensional structure. This is in contrast to the tryptophan fluorescence unfolding data, which reports on the regions of the protein surrounding the buried tryptophans.

In kinetic experiments, all three mutant proteins unfolded faster than wild-type HγD-Crys. Previously, it was shown that wild-type HγD-Crys requires 1 hour in 5.5 M GdnHCl at 37°C to unfold completely (Flaugh et al. 2006). Under these conditions, all three mutant proteins unfolded within the dead time of the experiment (~1 second). Experimental conditions were altered to 3.5 M GdnHCl and 18°C to slow unfolding and enable observation of the unfolding transition(s) by changes in tryptophan fluorescence. Under these altered conditions, the wild-type protein will not fully unfold. This fact alone attests to the dramatic destabilizing effects of these substitutions on HγD-Crys.

Similar to the results of the equilibrium unfolding/refolding experiments, the location of the mutation corresponded with the observed kinetic destabilization. For both N-td substitutions L5S and V75D, the single kinetic transition observed for each mutant protein most likely corresponded to the unfolding of the N-td. Under the altered experimental conditions, neither of these proteins fully unfolded, which was consistent with previous observations that neither wild-type HγD-Crys nor its isolated C-td fully unfold under these milder conditions (Mills-Henry 2007). Our results further support the observation that mutations in the N-td, even at different locations within the domain, appear to solely affect that domain's stability. Mills-Henry and colleagues (Mills-Henry

2007) found that the extrapolated *in vitro* unfolding half-time of wild-type HγD-Crys in the absence of denaturant was ~19 years. This number is likely greatly reduced for all of the mutants investigated here. A hysteresis was observed in previous equilibrium unfolding/refolding experiments, particularly for the unfolding of the N-td of full length HγD-Crys (Kosinski-Collins and King 2003). It was concluded that the domain interface contributed substantially to the kinetic stability of the protein. The large destabilization of the N-td for both the L5S and V75D proteins disrupts the interactions at the domain interface and this may contribute to an overall destabilization of the protein. Further kinetic analysis could address this issue.

In contrast, the C-td mutant I90F completely unfolded through a single observable kinetic transition, most likely the simultaneous unfolding of both domains. In agreement with equilibrium data, the disruption of the C-td by I90F resulted in destabilization of the entire protein. The N-td cannot remain folded if the C-td is unfolded in the full-length protein. However, Mills et al. showed that the isolated N-terminal domains of HγD- and HγS-Crys fold into distinct structures that exhibit the fluorescence quenching characteristic of the γ-crystallins and tryptophan fluorescence spectra similar to the full-length proteins (Mills et al. 2007). Therefore, the N-td of HγD-Crys in isolation is capable of folding. Nonetheless, in the context of the full-length protein, the C-td must be fully folded with its domain interface contacts available for proper folding of the N-td. The simplest model to explain these data is that the interface formed by the C-td is used as a template for folding of the N-td.

The effects of these mutations on the kinetic and thermodynamic stabilities of HγD-Crys are in line with studies of other proteins as described in the introduction (Lim et al. 1992; Milla et al. 1994; Denisov et al. 2004; Flaugh et al. 2005a; Simkovsky and King 2006). The introduction of a charged side chain into the protein core with the V75D substitution was extremely destabilizing and a slight increase in native state fluorescence measurements indicate possible local perturbations in structure, particularly around the Trp residues in the N-td. The L5S substitution also introduces a polar residue into the core, and most likely creates a cavity due to the introduction of a much smaller side chain. (The volume of the leucine side chain is 166.7 $Å^3$, while the volume of the serine side chain is 89 $Å^3$.) This could be very destabilizing due to the loss of favorable

van der Waals interactions. Filling of cavities in the hydrophobic protein core has been shown to be stabilizing in some cases (Ishikawa et al. 1993). The experimental results presented here for L5S support and complement the work previously discussed (Sinha et al. 2001). The destabilization resulting from the substitution of phenylalanine for isoleucine at position 90 is likely due to the introduction of a large bulky aromatic residue. Although this substitution retains the hydrophobic nature of the side chain, the increase in volume may introduce strain or disrupt other favorable interactions that are stabilizing the protein structure.

In contrast to the surface substitutions linked to congenital and early-onset cataract, the effect of these mutations is destabilization of the native state of HγD-Crys. The mutant proteins also unfolded significantly faster under less denaturing conditions than wild type. This implies that their unfolding half-life in non-denaturing conditions may also be significantly shortened. Lens proteins are synthesized early in life and there is no protein turnover after birth in the central, innermost regions of the lens. The accumulation in the lens of partially or fully unfolded crystallins at extremely high concentrations may saturate the finite α-crystallin population, which is the only mechanism present in the lens nucleus for binding and sequestering partially unfolded or misfolded proteins.

1. Aggregation of HγD-Crys requires partial unfolding of C-terminal domain

For proteins with duplicated domains, the simplest pathway to polymerization would be a domain-swap mechanism (Liu and Eisenberg 2002).This type of interaction is naturally occurring for βB2-crystallin (Bax et al. 1990) whose crystal structure was found to be a dimer. Aggregation by a domain swap mechanism has not yet been observed for the crystallins, but has been documented for cystatin C (Wahlbom et al. 2007). Models of aggregation by domain swapping have been hypothesized for the human prion protein (Knaus et al. 2001) and β2-microglobulin (Eakin et al. 2004) based on a wide range of structural analysis.

Contrary to the simplest form of the domain-swap hypothesis, the partially folded intermediates investigated here did not form aggregates under these experimental

conditions. For all proteins, both wild-type and mutant, it seems that at least partial unfolding of the C-td was necessary for aggregation to occur. This hints at a possible β-strand insertion mechanism of aggregation, where at least one β-strand from one molecule of HγD-Crys is inserted into the domain of a second molecule. This may be somewhat similar to the β-sheet expansion modeled for serpin polymerization (Yamasaki et al. 2008). (Yamasaki *et al.* refer to this mechanism of polymerization as domain swapping. For our discussion of the crystallins, we have used domain swapping to refer to the exchange of the entire N-terminal or C-terminal domains.) The aggregation of the mutant protein I90F even at intermediate GdnHCl concentrations emphasizes the strength of the intermolecular interactions occurring in these polymeric species.

The cloudiness and precipitation observed for this sample was most likely not a result of phase separation. Pande et al. (Pande et al. 2005) showed that phase separation occurs for the inherited cataract mutant P23T HγD-Crys. P23T separated into two phases, one consisting of monomers and the other consisting of clusters of protein that precipitated out of solution. It was demonstrated that this phase change occurred without changes in protein structure, and furthermore, that this mutant does not have altered thermal stability compared with WT. In contrast, I90F had decreased stability and the observed aggregation only occurred when the protein was subjected to partially denaturing conditions. The protein remained soluble under native conditions.

Both bovine and human γ-crystallins have been shown to form amyloid fibrils under partially denaturing, acidic conditions (Meehan et al. 2004; Papanikolopoulou et al. 2008). Fibrillar structures have been observed by thin section transmission electron microscopy in both the *Opj/Opj* mouse lens (Sinha et al. 2001) and the OXYS rat lens (Marsili et al. 2004), from a strain that generates excessive reactive oxygen species. Though the *Opj* and OXYS phenotypes lead to cataract, they may affect lens development as well as lens opacity and function. Due to the high β-sheet content of the γ-crystallins, there may be underlying similarities between their mechanisms of amyloid formation and the aggregation pathways observed in both our and the aforementioned studies. The molecular basis of γ-crystallin aggregation is an area that warrants further investigation.

The correlation between the cataract phenotype of the single amino acid substitutions in the mouse crystallins and the *in vitro* thermodynamic and kinetic destabilization of the purified human mutant proteins supports models of cataract formation following from protein conformational change and aggregation.

CHAPTER 3

DIFFERENTIAL INTERACTIONS OF HUMAN αB-CRYSTALLIN WITH HUMAN γD-CRYSTALLIN CONGENITAL CATARACT MUTANTS

A. Introduction

As presented in Chapter 2, γD-crystallin is one of the three major γ-crystallins found in the human ocular lens. It is specifically found at high concentrations in the lens nucleus, which is formed *in utero* during early developmental stages. As such, this protein must maintain its native structure and solubility over the lifetime of the individual, sometimes into the ninth decade. Numerous genetic mutations have been associated with the γ-crystallin genes in cases of hereditary and congenital cataract in both humans and mice (Hejtmancik 2008). Chapter 2 characterized the biochemical and biophysical effects of three individual mutations identified in cataract-afflicted mice that altered the hydrophobic core of HγD-Crys.

Understanding the molecular mechanism of the aggregation of γ-crystallins is essential for uncovering the mechanisms of cataract formation and development of prophylactics. AFM was used to image growing aggregates formed upon dilution of unfolded HγD-Crys into buffer and this showed that while fiber-like, they are not amyloid in nature (Kosinski-Collins and King 2003). Additional studies of this aggregation pathway found that the C-td of the protein must be partially unfolded and solvent-exposed for aggregation to proceed (Acosta-Sampson and King 2010). Molecular dynamics simulations have further defined regions of the C-td that likely serve as nuclei for aggregation (Das et al. 2010).

Animal models of cataract have identified genes essential for proper lens clarity and function, and imaging of sectioned cataractous lenses provide additional information about the structure of aggregates once formed. For the mutant γ-crystallins addressed here, these studies have shed light on the behavior of these proteins in a cellular context. In the case of V75D, originally identified as V76D in MγD-Crys, mice expressing the mutant γD gene displayed cataract and abnormal lens histology, including aggregates composed of γ-crystallins in cells of the lens nucleus (Graw et al. 2002b). A dramatic decrease in the water-soluble fraction of γ-crystallins was observed for (V76D/V76D) homozygotes and in lens epithelial cell cultures, V76D mutant protein formed aggregates localized to both the nucleus and cytoplasm (Wang et al. 2007). The murine version of the I90F substitution caused a milder cataract phenotype visualized by slit-lamp but

further characterization of the mutant protein is not documented (Graw et al. 2004). Unfortunately, terminally differentiated primary lens fiber cells cannot be maintained in cell culture, limiting studies to lens epithelial cells or non-lens cells, where γ-crystallins are not normally found at high levels.

The γ-crystallins, as well as α- and β-crystallins, form amyloid fibrils *in vitro* and in certain cases *in vivo*. In the case of human γ-crystallins, full-length WT HγD-Crys as well as its isolated N- and C-terminal domains formed distinct amyloid fibrils at pH 3 and 37°C (Papanikolopoulou et al. 2008). HγC-Crys also formed amyloid fibrils at pH 3 in a concentration and temperature dependent manner (Wang et al. 2010). Murine γB^{nop}, truncated after the 144th amino acid, formed intracellular inclusions that bound CR and exhibited the birefringence and fluorescence associated with binding to amyloid fibrils (Sandilands et al. 2002). The truncated protein also formed fibrils *in vitro*. F9S MγS-Crys, which was described in the Introduction of Chapter 2, was also shown to form ThT-binding fibrils when incubated in low concentrations of GdnHCl (Lee et al. 2010). WT recombinant αA and αB and the R120G αB mutant, which is associated with cataract and desmin-related myopathy, all readily formed amyloid fibrils under mildly denaturing conditions and neutral pH (Meehan et al. 2007). Bovine α-, β- and γ-crystallins formed fibrils at pH 2.0 and α-crystallin formed ThT-binding fibrils at pH 7.4 and elevated temperature (Meehan et al. 2004).

α-Crystallin was shown by Horwitz in 1992 to have a strong molecular chaperone activity, suppressing the thermal aggregation of the bovine β_L-crystallin and γ-crystallin fractions of soluble lens protein (Horwitz 1992). It also suppressed aggregation of a range of other proteins including insulin, α-lactalbumin, apolipoprotein C-II, citrate synthase and alcohol dehydrogenase (Horwitz 1992; Farahbakhsh et al. 1995; Lindner et al. 1997; Reddy et al. 2000; Hatters et al. 2001; Rajaraman et al. 2001). With respect to its physiological substrates in the lens, Finet and colleagues (Michiel et al. 2010) have shown that α-crystallin suppressed thermal aggregation of WT and deamidated human βB2-crystallin, although suppression of the latter was not as efficient. Similar findings with human βB1-crystallin showed that α-crystallin did not suppress aggregation of deamidated and truncated mutants to the same levels as WT βB1, but higher

concentrations of chaperone did improve suppression (Lampi et al. 2002). Complex formation between α-crystallin and its physiological substrates was also measured without inducing thermal aggregation. Both αA and αB bound destabilized mutant versions of β-crystallins when incubated together, and binding was correlated with the population of an unfolding intermediate of mutant βB2-crystallin (Sathish et al. 2004; McHaourab et al. 2007)

In the case of cataract-causing mutations in the γ-crystallins, interactions with α-crystallin are important for understanding molecular mechanisms. The truncation mutant murine γB^{nop}, mentioned above, formed a complex with α-crystallin upon *in vitro* mixing (Sandilands et al. 2002). In comparisons of mice whose lenses expressed either WT or V76D MγD-Crys, 2-D gel electrophoresis showed little change in α-crystallin partitioning between the water-soluble and insoluble lens fractions, indicating little or no interaction of α-crystallin with this mutant protein (Wang et al. 2007). I4F MγB-Crys, another murine mutant crystallin, formed complexes with bovine α-crystallin *in vitro* upon heating to 45°C and SEC analysis of water-soluble lens extract identified a complex peak between murine α-crystallin and γ-crystallin, presumably the I4F mutant (Liu et al. 2005). For murine and bovine crystallins, differential interactions are found between α-crystallin and mutant γ-crystallins.

In Chapter 2, I discussed the possibility that cataract formation represented the destabilization and subsequent misfolding of γ-crystallins, but the possibility remains that it is also due to the failure of α-crystallin to rescue the destabilized HγD-Crys chains from their aggregation pathway. Chapter 3 focuses on WT and two of the previously characterized mutant γD-crystallins, V75D and I90F, and their interactions with wild-type human αB. These two mutants represent substitutions in the hydrophobic cores of each double Greek Key domain. A variety of aggregation pathways are studied including: (1) the aggregation pathway that competes with productive refolding; (2) aggregation that results from destabilization of the native state *in the absence* of denaturant; (3) the amyloid fibril-forming pathway that dominates under specific solution conditions. Similarities and differences among mutant and WT protein behavior and

their interactions with αB are highlighted and discussed, with particular attention to their relevance to mechanisms of cataract formation.

B. Materials and Methods

1. Cloning, Protein Expression and Purification

Plasmids containing WT and mutant HγD-Crys proteins V75D and I90F were prepared as described in Chapter 2. Plasmids were transformed into *E. coli* M15 [pREP4] cells (Qiagen). Cultures were grown in LB media and protein expression was induced by addition of 1 mM IPTG. His-tagged WT and mutant HγD-Crys proteins were purified as described in Chapter 2.

Human αB was expressed and purified following the protocols of Acosta-Sampson and King (Acosta-Sampson and King 2010). The αB gene in vector pAED4 was transformed into *E.coli* BL21 (DE3) cells and protein expression was induced by the addition of 1 mM IPTG at 18°C. Expression continued at this temperature for 18-20 hours. Cells were pelleted by centrifugation, resuspended in anion exchange lysis buffer (buffer A: 50 mM Tris, pH 8.5) and stored at -80°C. Cells were thawed at 16°C, lysed using lysozyme (3 mg/ml of lysate) for 30 minutes at room temperature with gentle rocking. The lysate was then treated with DNAse (0.005 mg/ml of lysate) and deoxycholic acid (0.5 mg/ml of lysate) for 20 minutes on ice to degrade DNA and further disrupt the cell membranes, respectively. This was followed by ultrasonication on ice and centrifugation to pellet cell debris. The supernatant was decanted and polyethylenimine was added to a final concentration of 0.12 % to precipitate the remaining nucleic acids. The supernatant was incubated for 10 minutes on ice and the precipitate was pelleted by centrifugation. The cleared lysate was filtered through 0.2 μm membrane, spiked with 1 ml of anion exchange elution buffer (buffer B: 50 mM Tris, 1 M NaCl, pH 8.5) and loaded onto a Hi-Prep 16/10 Q Sepharose FF column attached to an AKTA Purifier FPLC system (GE Healthcare). αB elutes in the flow-through at this step and the corresponding fractions were collected and dialyzed against lysis buffer for 3 hours at 4 °C. The sample was then split in two, each half was diluted to 50 ml with lysis

buffer and reloaded onto the anion exchange column. After sample loading, the column was washed with 3 CV of lysis buffer, then 2 CV of 2% buffer B, followed by 0.3 CV of 7% buffer B. αB was then eluted with a 7-30% linear gradient of buffer B over 6 CV. The fractions of interest were electrophoresed through 14 % SDS-PAGE gels and fractions containing αB were pooled and concentrated. The concentrated fractions were further purified by SEC using a Superose 6 10/300 GL column (GE Healthcare). For a typical prep, 4-6 SEC runs were performed, with 0.5 ml loaded onto the column for each run. Fractions were collected, electrophoresed through 14 % SDS-PAGE gels to check purity and finally combined and stored in SEC buffer (50 mM NaPi, 150 mM NaCl, pH 7.0). Protein purity was evaluated to be at least 90% by SDS-PAGE. Each batch of purified αB was tested for chaperone activity by performing aggregation suppression assays with WT HγD-Crys as described below.

Protein concentrations were determined by UV absorbance of the unfolded proteins at 280 nm using the following extinction coefficients: 42,860 M^{-1} cm^{-1} (WT, V75D and I90F HγD-Crys) and 13,980 M^{-1} cm^{-1} (αB). Extinction coefficients were calculated using the ExPASy ProtParam tool (Gasteiger et al. 2005).

2. *Aggregation and Aggregation Suppression Assays*

Aggregation and aggregation suppression assays were based on the protocols of Acosta-Sampson and King (Acosta-Sampson and King 2010). WT and mutant HγD-Crys proteins at 1 mg/ml were unfolded by incubating overnight at 37°C in 5 M GdnHCl, 100 mM NaPi, 1 mM EDTA, 5 mM DTT, pH 7.0. Unfolded protein was placed in a quartz cuvette and diluted 10-fold with refolding buffer (100 mM NaPi, 1 mM EDTA, 5 mM DTT, pH 7.0) to achieve final concentrations of 0.1 mg/ml HγD and 0.5 M GdnHCl. Samples were mixed by rapidly pipetting 12 times after the addition of buffer. Solution turbidity (apparent absorbance at 350 nm or OD_{350}) was measured continuously for 20 minutes, beginning immediately after sample mixing. Aggregation suppression assays were performed in the same manner, with the addition of αB in the refolding buffer at a final concentration of 0.5 mg/ml. A Cary 50 UV-visible spectrophotometer was used to record turbidity. Cuvette temperature was maintained at 37°C using a single cell Peltier

controller and all protein and buffer solutions were maintained at 37°C during the experiments. Experiments with each protein were performed at least six times.

After recording turbidity, samples from both aggregation and suppression assays were removed from the cuvette and incubated overnight at 37°C before SEC. Samples were then filtered through a 0.2 μm membrane, applied to a Superose 6 10/300 GL column and αB:γD complexes were separated from free αB and any native HγD. Aggregation samples that did not contain αB were also applied to the column for comparison. All chromatography was performed at 4°C.

3. Native Mixing and Interaction Assay

Each of the HγD proteins, WT, V75D and I90F, were mixed with αB in a 1:1 ratio at concentrations of 1 mg/ml in SEC buffer. Samples were then incubated in a 37°C warm room with constant rotation for up to 28 days. At days 0, 14, 21 and 28, samples were removed, filtered through a 0.2 μm membrane, and applied to a Superose 6 10/300 GL column. Fractions were collected every 0.5 ml and SDS-PAGE samples were prepared immediately following separation for further analysis. Separated samples were assessed for formation of αB:γD complexes, as well as decreases in free αB and free HγD-Crys peaks. Control samples were prepared containing either αB only or the individual HγD proteins, each at 1 mg/ml, and treated identically to experimental mixtures. Experimental mixing samples were prepared and analyzed at least in triplicate and controls were prepared and analyzed in duplicate or triplicate.

0.5 ml SEC fractions collected from native interaction sample separations were electrophoresed through 14% SDS-PAGE gels and proteins were transferred onto 0.2 μm pore size PVDF membranes. Sets of identical membranes were probed with primary monoclonal antibodies for αB and HγD-Crys (Santa Cruz Biotechnology). Alkaline phosphatase-conjugated secondary antibodies were used with detection by the Immun-Blot colorimetric assay (Bio-Rad).

4. pH Dependence of Trp Fluorescence and Tertiary Structure

The effects of pH on the tertiary structures of WT and mutant HγD-Crys were analyzed using intrinsic Trp fluorescence. Trp fluorescence was monitored from pH 3-7. The buffers utilized were: 100 mM NaPi, pH 7.0; 100 mM NaPi, pH 6.0; 100 mM NaOAc/HOAc, pH 5.0; 100 mM NaOAc/HOAc, pH 4.0; 100 mM NaOAc/HOAc, pH 3.0. Proportions of buffer components were calculated using the Henderson-Hasselbach equation. αB tertiary structure was also probed by Trp fluorescence at pH 7 and pH 3. All proteins were incubated for 5 hours at 37°C in the appropriate buffers and Trp fluorescence measurements were recorded at 37°C. Measurements were performed at least in triplicate. All spectrofluorimeter parameters were as described in Chapter 2.

5. HγD-Crys Fibril Formation and Inhibition of Fibril Formation by HαB-Crys at pH 3

The HγD-Crys proteins, WT, V75D and I90F, were concentrated to 6.1, 4.2 and 7.7 mg/ml, respectively. αB was concentrated to 13 mg/ml. All proteins were concentrated using Amicon Ultra 10kDa MWCO centrifugal concentrators. Low pH buffer (100 mM NaOAc/HOAc, 100 mM NaCl, pH 3.0) was prepared based on the Henderson-Hasselbach equation, using 98 mM HOAc and 2 mM NaOAc, and HOAc was used to make final pH adjustments. All fibril-forming reactions were conducted at 37°C in a dry heat block.

For fibril formation reactions (not containing αB), buffer was pre-warmed to 37°C for 15 minutes and then the appropriate volume of protein was added to achieve a final concentration of 1 mg/ml HγD for both WT and mutants. The solutions were mixed briefly by inverting the microcentrifuge tube several times and then incubated at 37°C for three hours. Samples were also prepared containing αB in addition to WT and mutant HγD-Crys to assess the ability of αB to inhibit fibril formation. Concentrated αB was pre-warmed at 37°C for 15 minutes and added in a 1:1 (αB:γD) ratio for a final concentration of 1 mg/ml. Samples containing αB in addition to HγD-Crys were incubated for 3 hours at 37°C. Sample volumes were generally 400 – 600 µl. The amyloid-binding fluorescent dye Thioflavin T (ThT) was used to monitor fibril formation as described below.

6. Thioflavin T Fluorescence assay

A working solution of 25 μM ThT in 50 mM NaPi, pH 7.0, was prepared from a 2 mM ThT stock solution in water. The working solution was freshly prepared and filtered through a 0.2 μm membrane each day. The 2 mM ThT stock solution, when protected from light and stored at room temperature, was functional for up to two months. For the ThT fluorescence assays, 8 μl of the low pH protein solutions described above were removed at various time points and immediately mixed with 392 μl of the ThT working solution. For all experimental samples, ThT samples were removed at the following times: 0, 1, 2, 5, 15, 30, 45, 60, 90, 120, 150 and 180 minutes. ThT samples of pH 7 controls were generally collected at 0 and 180 minutes unless otherwise noted. Samples of αB alone at pH 3 were collected at 0, 60, 120 and 180 minutes. ThT fluorescence was measured on a Hitachi F-4500 spectrofluorimeter. Instrument parameters were set as follows: the excitation wavelength was 444 nm and fluorescence emission was measured from 470 – 570 nm, the scan speed was 240 nm/min, the excitation bandwidth was 5 nm, the emission bandwidth was 10 nm, and the photomultiplier tube voltage was 950. An increase in fluorescence emission intensity at 485 nm was indicative of ThT binding to amyloid-like structures with high β-sheet content.

7. Endpoint Solution Turbidity Measurements

In addition to ThT fluorescence, solution turbidity was measured to assess the formation of light-scattering aggregates after the three-hour incubation time. A Cary-50 UV-visible spectrophotometer was used for all measurements. For all samples not containing αB, as well as pH 3 samples with the chaperone protein, absorbance was measured at 280, 350 and 600 nm. Turbidity measurements at 350 nm are reported here.

C. Results

1. Wild-type and Mutant HγD-Crys Proteins Aggregated to Similar Extents

Kosinski-Collins and King observed the aggregation of WT HγD-Crys when rapidly diluted from the unfolded state in 5.5 M GdnHCl to buffer with residual denaturant concentrations below 1 M GdnHCl (Kosinski-Collins and King 2003). This aggregation pathway is in kinetic competition with the productive refolding pathway of the protein. The aggregating polypeptide chains–visualized by atomic force microscopy–first formed small globular assemblies and then filamentous structures that grew longer and associated with each other over time (Kosinski-Collins and King 2003). The aggregation-prone intermediate species appears to have a fully unfolded N-td and a partially unfolded or otherwise destabilized C-td (Acosta-Sampson and King 2010). The C-td contains the initial aggregation-prone regions although it appears that the N-td participates in later stages of the aggregation reaction (Acosta-Sampson, personal communication).

Acosta-Sampson and King have extensively studied the aggregation of WT HγD-Crys and found that at least partial destabilization of the C-td is required for *in vitro* aggregation upon dilution from denaturant. In particular, it was shown that partial unfolding and population of the stable intermediate at 2.49 M GdnHCl did not result in appreciable aggregation upon dilution to 0.5 M GdnHCl (Acosta-Sampson and King 2010). Instead, increased initial GdnHCl concentrations were required. A similar requirement for partial C-td unfolding was observed for the mutant proteins L5S, V75D and I90F in order for aggregation to occur (Moreau and King 2009).

To evaluate the partitioning of protein between the aggregation and productive refolding pathways, we performed aggregation assays for WT, V75D and I90F HγD-Crys. All proteins were fully denatured in 5 M GdnHCl at 37°C and then diluted with buffer to induce aggregation. The final GdnHCl concentration was 0.5 M and the final protein concentration was 0.1 mg/ml for all samples. Solution turbidity was monitored by recording the apparent absorbance at 350 nm due to light scattering (OD_{350}) by the growing aggregates. Changes in OD_{350} were essentially the same for WT and both mutant HγD-Crys proteins (Figure 3-1). The OD_{350} increased very quickly over the first 2 minutes of the aggregation reaction, where it plateaued for the remainder of the experiment. OD measurements peaked and plateaued at about 1 AU for both the WT and

mutant proteins. The overall change in OD, or ΔA, was 0.31 for WT HγD-Crys, 0.36 for V75D, and 0.35 for I90F (Table 3-1). The fast aggregation reaction was kinetically favored over refolding of HγD-Crys to the native monomer. The aggregation sample was filtered through a 0.2 μm membrane and chromatographed over a Superose 6 SEC column and very little native protein was recovered at the expected 19 ml elution volume (Figure 3-3). Noticeably, there was an absence of soluble aggregate in the void volume at 7.5 ml, indicating that the aggregated species was too large to pass through the filter and did not enter the column matrix.

2. αB Suppressed the Aggregation of WT and Mutant HγD-Crys to Similar Extents

Acosta-Sampson and King have studied the suppression of aggregation of three of the abundant γ-crystallins present in the human lens and found that αB interacted with the three γ-crystallins differentially (Acosta-Sampson and King 2010). Although the mutant γD-crystallins discussed here appeared to aggregate through a similar pathway—attested to by their similar aggregation kinetics and overall levels of aggregation—it is possible that the passive chaperone αB could interact with one or both of the mutants in a different manner than with WT, resulting in a change in aggregation kinetics or overall suppression levels. To this end, aggregation suppression experiments were performed in a manner identical to the previously described aggregation assay, with the addition of a 5-fold excess of αB in the refolding buffer.

Under these conditions, αB suppressed the aggregation of both WT and mutant HγD-Crys to similar extents (Figure 3-2). The maximum OD_{350} for both WT and V75D HγD was 0.27 AU, while that of I90F was just slightly higher at 0.31 AU. There was a very slow increase in solution turbidity over the course of the experiment. The ΔA values were similar at 0.06-0.07 for all three proteins in the presence of the chaperone (Table 3-1). Based on maximum OD_{350} values, in the presence of αB, aggregation of WT HγD-Crys was suppressed by 72%. In comparison, V75D aggregation was suppressed by 73%

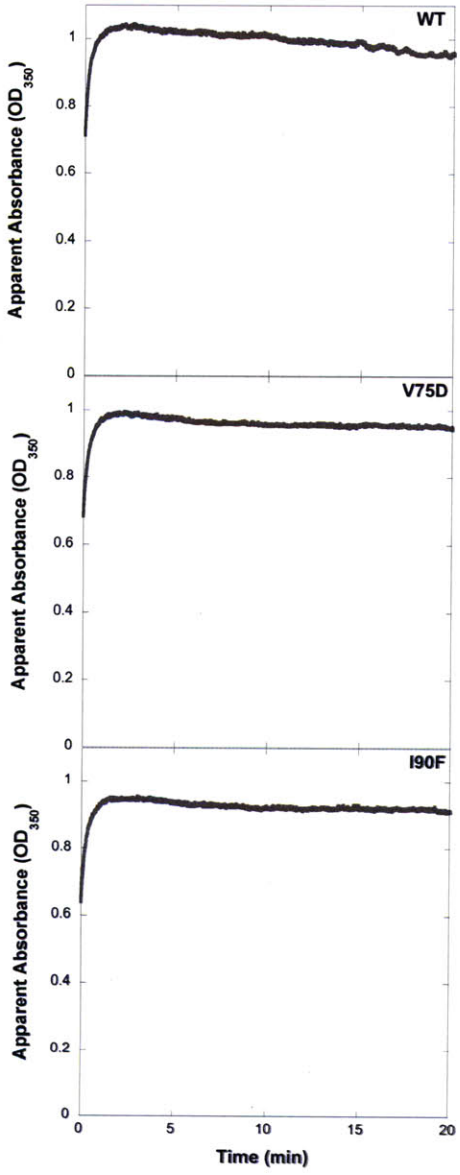

Figure 3-1: Aggregation reactions for WT, V75D, and I90F HγD-Crys. The apparent absorbance (OD_{350}) was monitored for 20 minutes to follow the formation of large light-scattering aggregates upon rapid dilution of HγD-Crys protein out of 5 M GdnHCl.

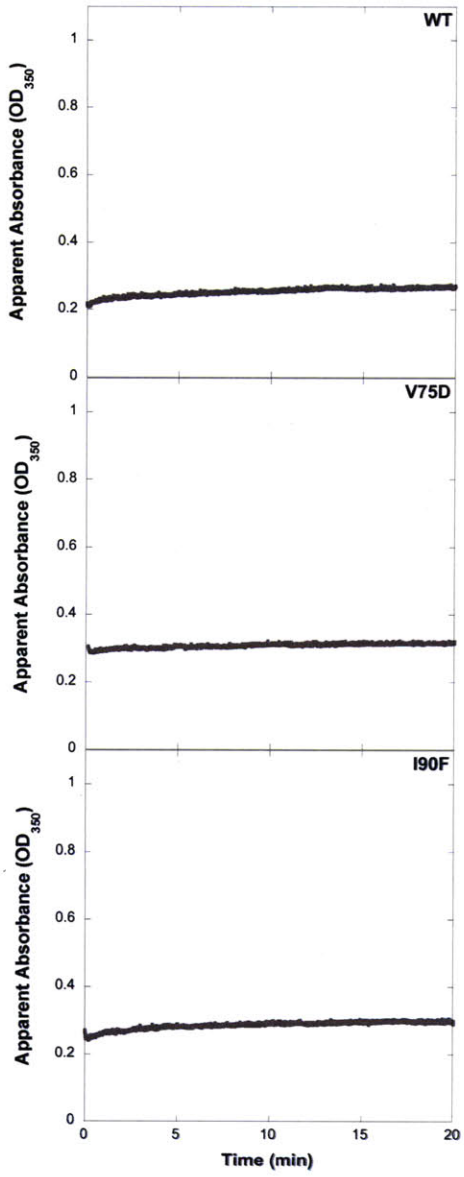

Figure 3-2: Aggregation suppression reactions for WT, V75D, and I90F HγD-Crys. The apparent absorbance (OD_{350}) was monitored for 20 minutes to follow the formation of large light-scattering aggregates upon rapid dilution of HγD-Crys protein out of 5 M GdnHCl in the presence of a 5-fold excess of αB.

Table 3-1: Solution Turbidity Measurements for WT and Mutant HγD-Crys in the Absence and Presence of αB.

	ΔA [a,b]		Maximum OD_{350} [a]	
Protein	- HαB	+ HαB	- HαB	+ HαB
WT	0.31 ± 0.05	0.06 ± 0.01	0.94 ± 0.1	0.27 ± 0.06
V75D	0.36 ± 0.04	0.06 ± 0.01	1.0 ± 0.05	0.27 ± 0.08
I90F	0.35 ± 0.05	0.07 ± 0.01	1.1 ± 0.1	0.31 ± 0.04

[a] Units are Absorbance Units (AU) and means ± standard deviations are given.
[b] ΔA = maximum OD_{350} − minimum OD_{350}

and I90F aggregation was suppressed by 70%. These levels are all within one standard deviation of each other (Figure 3-4).

Analysis of these suppression reactions by SEC resulted in separation of two distinct peaks (Figure 3-3). The first peak eluted in the void volume and was composed of long-lived complexes of αB and HγD-Crys. The second major peak corresponded to excess free chaperone and eluted in a broader peak around 13 ml. The native γD peak at about 19 ml was minor in the case of WT HγD-Crys and negligible in for both mutant proteins. This result is not surprising, in that a small amount of WT protein was shown to refold upon dilution from denaturant (Kosinski-Collins and King 2003; Flaugh 2006). The even smaller peaks present for both mutant proteins probably reflect the fact that the native state is more destabilized than WT under these conditions and the already small proportion of molecules that proceed down the productive folding pathway are further diminished for the mutants.

3. αB Interacted Differentially with Mutant HγD-Crys Proteins Initially in Their Native State

The aggregation suppression reactions described above were conducted with HγD-Crys initially unfolded in 5 M GdnHCl. The reactions under investigation were the *in vitro* refolding pathway and the competing *in vitro* aggregation pathway. WT, V75D and I90F HγD-Crys were recombinantly expressed and purified from the soluble portion of *E. coli* lysate, indicating that these proteins folded and achieved their native state within the cellular milieu. Therefore, it is important to study possible aggregation pathways in the opposite direction, in which a protein is initially in its native state and unfolds over time, populating conformations that may be aggregation-prone. If these proteins are aggregation-prone upon long-term incubation, does αB interact with them by recognizing exposed hydrophobic regions?

To address this question, purified HγD-Crys proteins were incubated for 28 days at 37°C in the absence or presence of the chaperone αB. For the mixtures, proteins were present in a 1:1 ratio at 1 mg/ml. SEC was performed at times 0, 14, 21, and 28 days to determine whether protein was lost to aggregation and if αB formed complexes with the

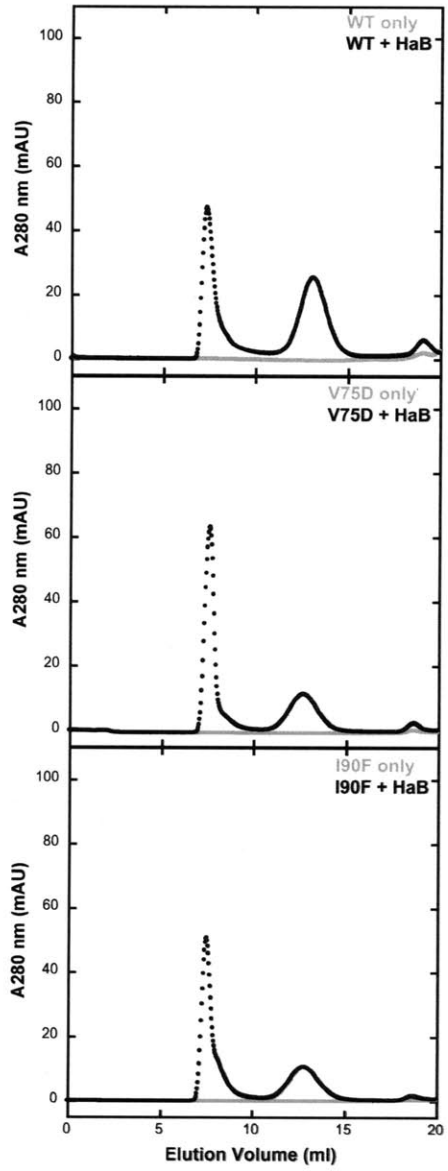

Figure 3-3: Size exclusion chromatography of aggregation samples (gray) and aggregation suppression samples (black) containing a 5-fold excess of αB. All samples were filtered through a 0.2 μm membrane before loading on a Superose 6 column.

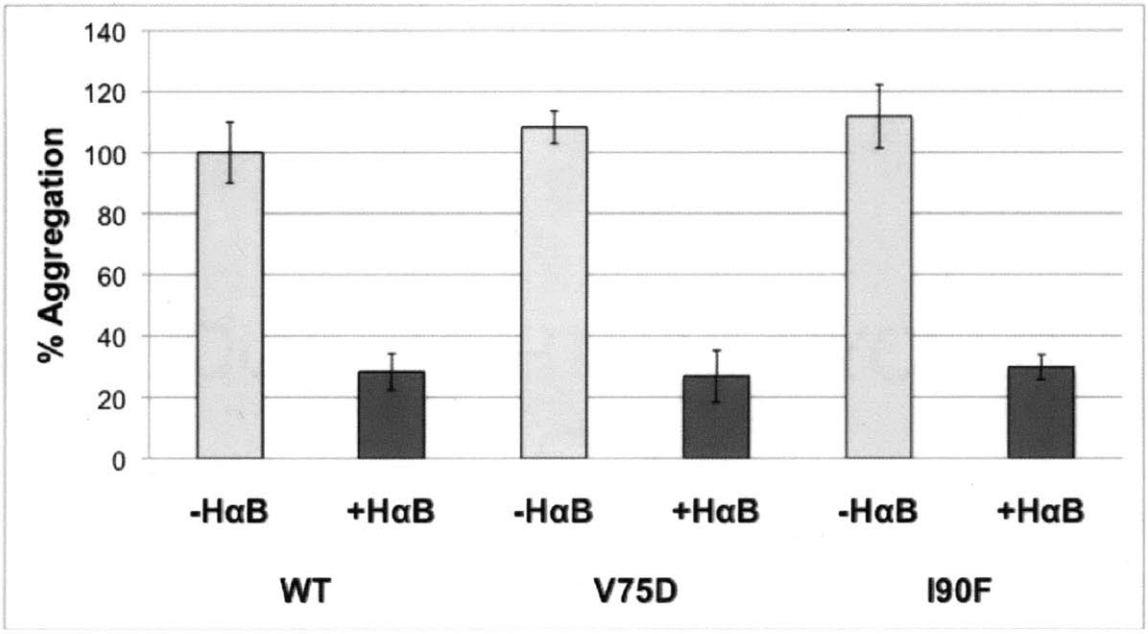

Figure 3-4: % Aggregation of WT and mutant HγD-Crys in the absence and presence of the αB chaperone protein. Aggregation levels in the absence of αB are normalized to that of WT HγD-Crys in the absence of chaperone protein. Levels in the presence of chaperone protein (+HαB) are calculated as percentages of each protein's total aggregation (-HαB). All percentages are calculated from maximum OD_{350} values. Error bars represent one standard deviation from the mean.

WT or mutant proteins. As in the previous assays, samples were filtered through a 0.2 μm membrane before loading onto the SEC column and large aggregates were not detected with this method. As controls, each protein, WT, V75D and I90F, was incubated by itself, as was αB.

In control samples not containing the chaperone, the levels of both WT and mutant HγD proteins decreased over time, as shown by the decreased peak size in later SEC traces (Figure 3-5). However, the amplitude of the decrease was not the same for all proteins. WT HγD-Crys had the smallest change in protein levels over the course of the experiment. In the case of V75D, almost all protein was lost to aggregation after 14 days of incubation at 37°C and aggregates were visible to the naked eye in the sample tube. The recovery of I90F was intermediate; more protein was lost to aggregation than for WT but a much greater proportion of protein remained in comparison to V75D. αB was unaffected by the prolonged incubation, which was expected for a protein that is upregulated in response to stress.

For samples containing both HγD-Crys and αB, there were several possible outcomes. αB might interact with either mutant HγD, inhibiting further protein aggregation? Or it could contribute to the aggregates, as α-crystallin is often identified as a component of the water-insoluble protein deposits removed from cataractous lenses (Chen et al. 1997; Hanson et al. 2000; Harrington et al. 2007; Hains and Truscott 2008). For the mixture of WT HγD with αB, no complexes were formed between the two proteins as shown by SEC (Figure 3-6). The αB peak remained unchanged over the course of the experiment while the HγD peak became somewhat smaller in height and broadened slightly. In the case of V75D, the presence of αB from the beginning of the incubation appeared to have no affect on its aggregation (Figure 3-6). Like the control samples, virtually all of the protein was lost after 14 days of incubation at 37°C and aggregates were visible to the naked eye. Complexes between αB and V75D were not present in SEC separations and the levels of αB did not decrease, indicating that it was not incorporated into large aggregates. Based on these results, V75D appears to aggregate through an intermediate not recognized by αB. This could account for its cataractogenic phenotype in the mouse.

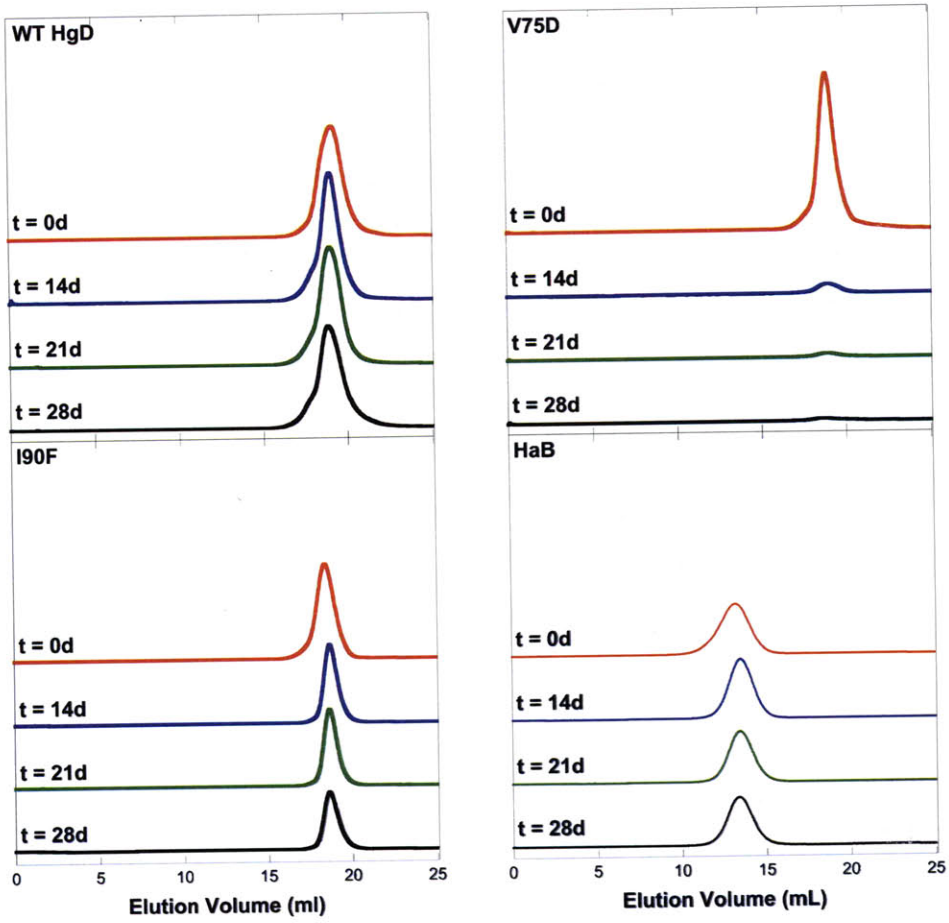

Figure 3-5: SEC traces of single protein controls for native mixing experiments. Separate samples were prepared for each time point in SEC buffer. In all cases proteins were at a concentration of 1 mg/ml.

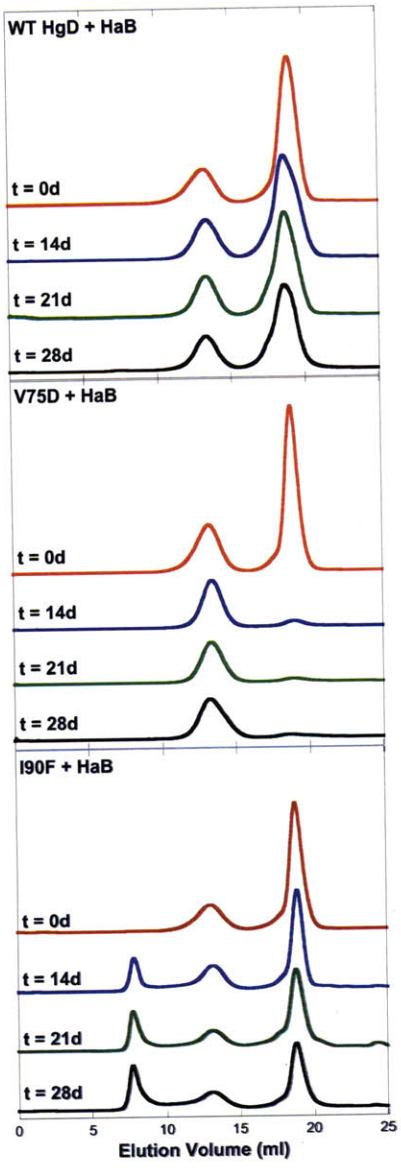

Figure 3-6: SEC traces of native protein mixtures. Separate samples were prepared for each time point in SEC buffer. Times given are in days. In all cases proteins were at a concentration of 1 mg/ml.

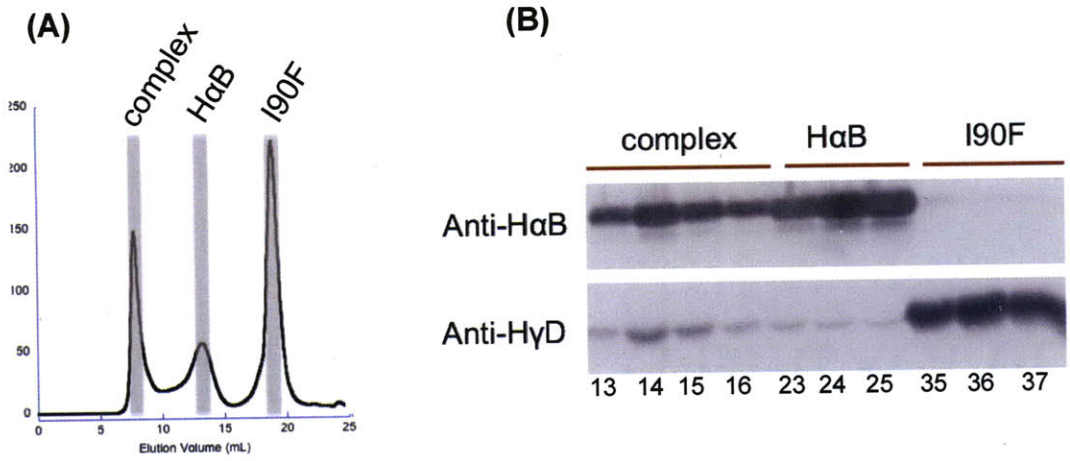

Figure 3-7: Western Blot analysis of I90F + αB native mixing experiment. **(A)** SEC trace of the I90F + αB mixture after a 27 day incubation at 37°C. The shaded areas represent the fractions from each peak that were analyzed by Western Blot. **(B)** Two Western Blots were performed on identical sets of samples. The upper panel detected the presence of αB and the lower panel detected I90F HγD-Crys. Numbers along the bottom are SEC fractions. Fractions 13-16 comprised the complex peak; fractions 23-25 comprised the αB peak; fractions 35-37 comprised the I90F peak.

In the final case of I90F with αB, a third result was observed. After 14 days of incubation at 37°C, samples separated by SEC contained large complexes that eluted in the void volume (Figure 3-6). Peaks were still present for both uncomplexed αB and I90F, although growth of the complex peak in the void volume was observed with a concomitant decrease in both of the single protein peaks over time.

To verify that the complex peak contained both αB and I90F, Western blots were performed using monoclonal antibodies for αB and WT HγD. Samples from SEC fractions corresponding to the three major peaks of the I90F + αB mixture (t = 27 days) were electrophoresed through 14% SDS-PAGE gels and proteins were transferred to PVDF membranes in the presence of SDS. One membrane was probed with αB monoclonal antibodies and the other was probed with HγD monoclonal antibodies. Samples from the uncomplexed αB and I90F peaks served as internal controls for antibody performance. Four fractions (13-16) from the complex peak were analyzed and all four contained both αB and I90F proteins. From the I90F:αB complex peak, fractions 14 and 15 were most abundant in I90F (Figure 3-7). This confirmed that the long-lived complex eluting in the void volume contained both α- and γ-crystallin proteins.

4. αB Slowed Fibrillation Kinetics of WT and Mutant HγD-Crys Proteins

αB interacted differentially with WT and mutant HγD proteins depending on which aggregation pathway was followed and what aggregation-prone intermediates were formed. Due to the high β-sheet content of the γ-crystallins and the fibrillar structures sometimes observed in the cataractous lenses of animals (Figure 1-7) (Marsili et al. 2004), it was plausible to examine the aggregation of these mutant crystallins under conditions that favor amyloid-like fibril formation. As described in the Introduction to this chapter, several crystallin proteins have been shown to form amyloid fibrils, both *in vivo* and *in vitro* under a variety of experimental conditions. In addition, αB was shown to inhibit amyloid formation by a number of proteins including α-synuclein, κ-casein and

β2-microglobulin (Raman et al. 2005; Rekas et al. 2007; Waudby et al. 2010). Numerous groups have studied the interactions of α-crystallin with several forms of Aβ peptide although results are currently somewhat conflicting (Kudva et al. 1997; Stege et al. 1999; Liang 2000; Wilhelmus et al. 2006). Do the mutants V75D and I90F form fibrils, and furthermore, could αB suppress their formation?

Wang et al. studied the formation of amyloid fibrils by HγC-Crys at pH 3 in an acetate-based buffer system (Wang et al. 2010). These experiments provided a jumping off point to study the fibrillation of WT HγD-Crys and the two mutant proteins V75D and I90F. Slight changes were made to increase the buffering capacity of the system at pH 3 and the final buffer composition was 100 mM acetate (98 mM HOAc/2 mM NaOAc), 100 mM NaCl, pH 3.0. This buffer alteration was necessary to reduce dilution effects upon addition of protein, specifically V75D, which did not reach high concentrations as readily as WT or I90F HγD-Crys.

HγC-Crys readily formed amyloid fibrils that bound the fluorescent dye ThT, an indicator of amyloid fibril formation (Wang et al. 2010). Analogous experiments were performed with WT, V75D, and I90F HγD-Crys. Protein was concentrated and then diluted into the buffer described above to achieve a final protein concentration of 1 mg/ml. Samples were removed at several time points over the course of three hours and mixed with ThT. Changes in ThT fluorescence were monitored over time and increases in fluorescence were indicative of fibril formation.

In the absence of the chaperone αB, all HγD-Crys proteins formed ThT-binding fibrils over the course of three hours (Figure 3-8). The slowest increase in ThT fluorescence was observed for WT HγD-Crys. ThT binding to V75D was faster than for WT HγD-Crys. The curve had a slight sigmoidal shape with a very short lower baseline. I90F formed ThT-binding fibrils the fastest, indicated by the rapid rise in ThT fluorescence. It should also be noted that the

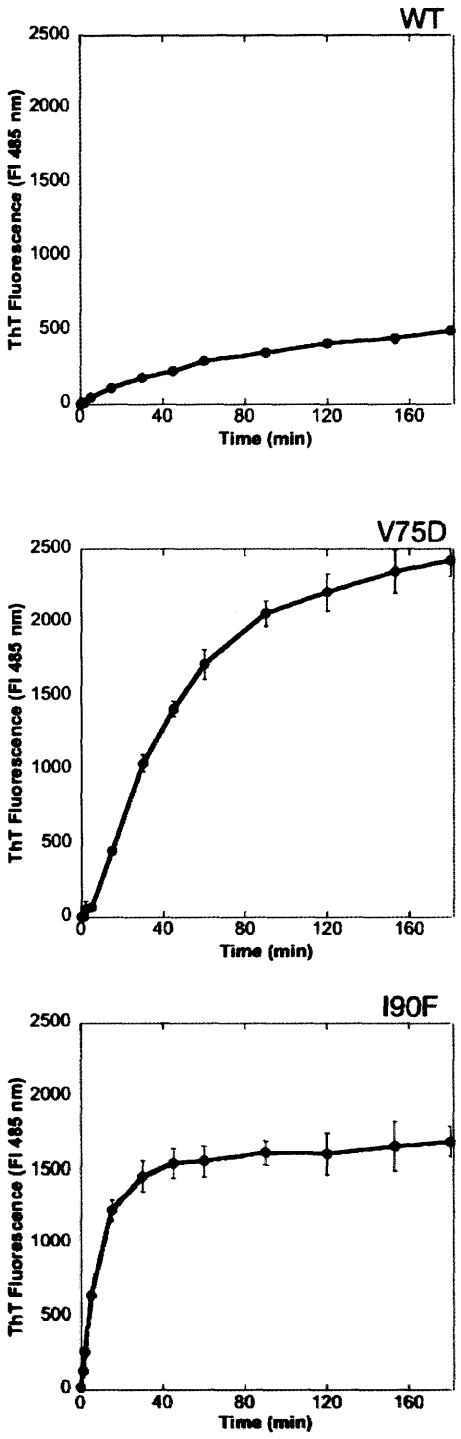

Figure 3-8: Fluorescence increase at 485 nm indicative of ThT binding for WT, V75D, and I90F incubated at 37°C for three hours. Data points are shown with connecting lines in black. Error bars represent one standard deviation.

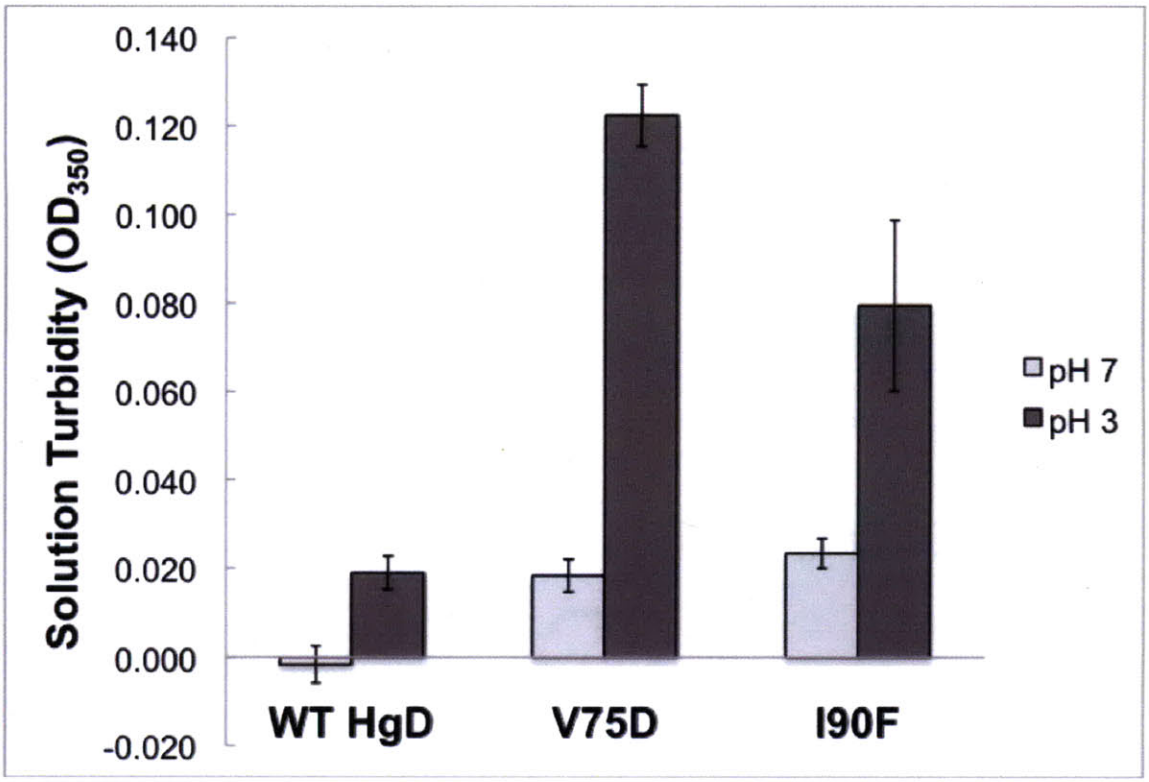

Figure 3-9: Endpoint turbidity measurements for HγD-Crys proteins incubated at pH 3 for three hours. The average of three trials is shown and error bars represent one standard deviation from the mean. The turbidity measurements of identical samples incubated at pH 7 are shown for comparison.

final ThT fluorescence levels were not equal among the three proteins. WT HγD-Crys had the lowest level with an average ThT fluorescence maximum of 495 a.u., followed by I90F with an average fluorescence maximum of 1696 a.u. V75D reached the highest levels at 2426 a.u. It is not clear as to why there is a discrepancy among these values, although it could be related to either the total fibrils formed or the presence of higher-order structures that form as the reaction continues. The ability of ThT to remain bound or continue to bind fibrils may be altered in the latter case.

At the end of the three-hour incubation, endpoint solution turbidity measurements were recorded. As previously described, turbidity was measured as the OD_{350}, which results from light scattering by the aggregated species. Turbidity levels mirrored maximum ThT fluorescence levels with WT HγD-Crys having the lowest, an OD_{350} of 0.02 AU. I90F followed with an OD_{350} of 0.08 AU, and V75D had the highest turbidity with an OD_{350} of 0.12 AU. For comparison, protein samples were incubated at pH 7 and turbidity measurements were recorded. In all cases, the turbidity of the pH 7 samples was lower than for the fibril-containing samples (Figure 3-9).

Following these initial measurements, samples were prepared again, this time containing αB. The chaperone was added to the reaction buffer at a final concentration of 1 mg/ml for a 1:1 γD:αB ratio. Samples were incubated as previously described and aliquots were removed for the ThT assay. Despite the presence of αB from the beginning of the incubation, ThT fluorescence still increased for both mutant and WT HγD-Crys. For WT HγD-Crys, the overall increase in ThT fluorescence was less, with an average fluorescence maximum of 370 a.u. (Figure 3-10 and Table 3-2). The kinetics of ThT binding as well as the final fluorescence maximum were altered for V75D. The increase in fluorescence was slowed and the final the fluorescence maximum was lowered to 1508 a.u. (Figure 3-10 and Table 3-2). Finally, although kinetics were slowed for I90F, the final fluorescence maximum is roughly the same as in the absence of αB (Figure 3-10 and Table 3-2).

For all samples containing αB, the initial ThT fluorescence was higher than for either the WT or mutant HγD in the absence of αB. Control samples containing only αB were incubated at pH 3, and selected time points (0, 60, 120 and 180 minutes) were evaluated for increases in ThT fluorescence. While there was no increase over time for

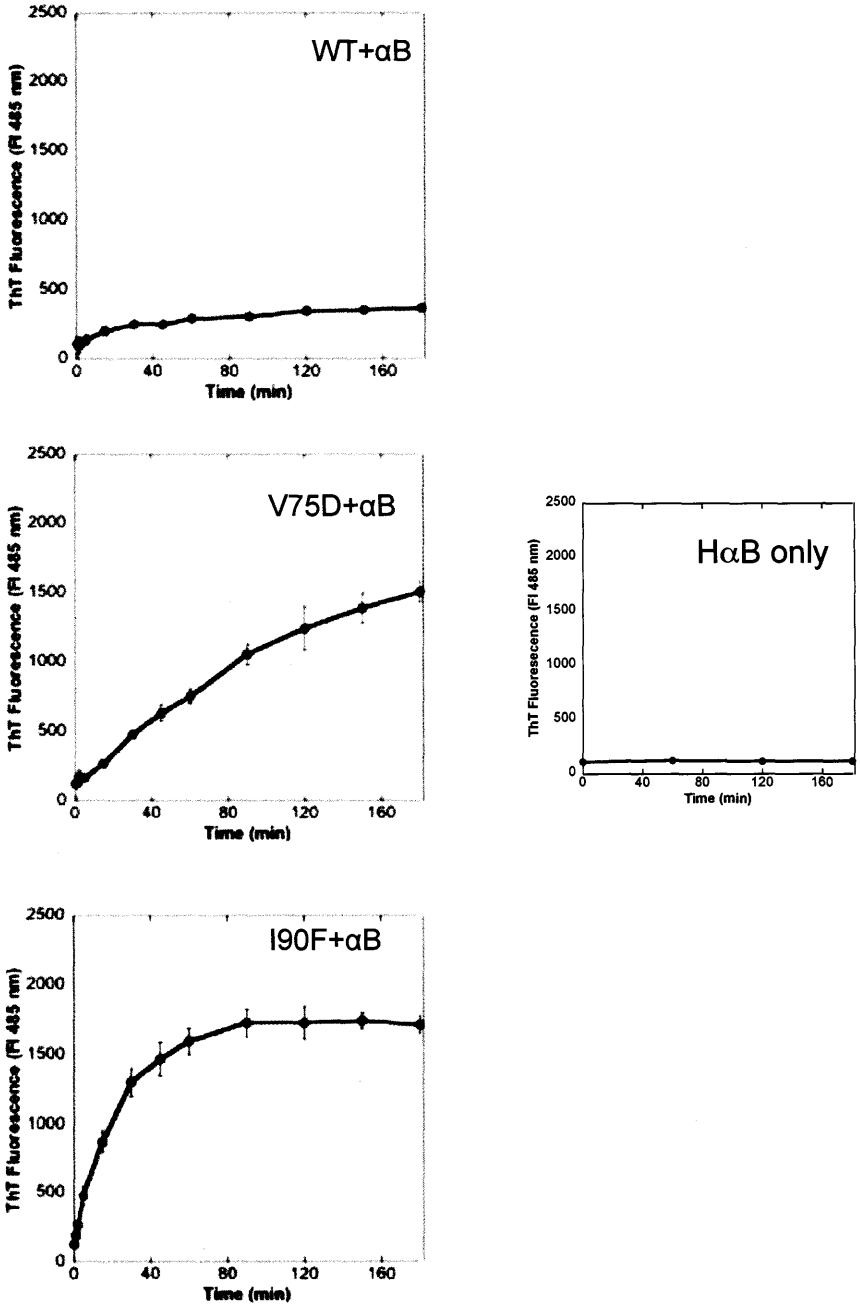

Figure 3-10: Fluorescence increase at 485 nm indicative of ThT binding for WT, V75D and I90F in the presence of αB. Samples were incubated at 37°C for three hours. Data points are shown with connecting lines in black. Error bars represent one standard deviation from the mean. For comparison, ThT fluorescence in the presence of αB alone is shown on the rightmost graph.

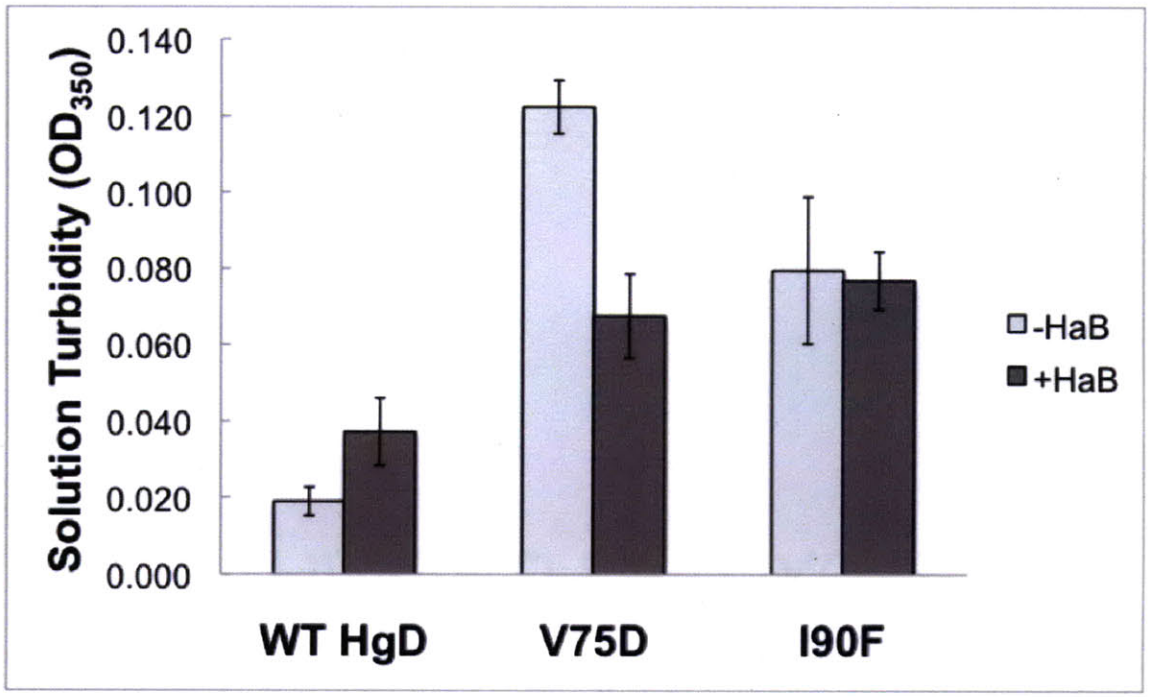

Figure 3-11: Comparison of endpoint turbidity measurements for WT and mutant HγD-Crys proteins in the absence and presence of αB. All measurements were taken after incubation in pH 3 buffer for three hours at 37°C. The average of three trials is shown and error bars represent one standard deviation.

Table 3-2: ThT fluorescence parameters and endpoint turbidity of pH 3 samples in the absence and presence of αB

	ThT Fluorescence$_{Max}$ [a]		Endpoint Turbidity[b]	
Protein	- HαB	+HαB	-HαB	+HαB
WT HγD	495	370	0.02	0.04
V75D	2426	1508	0.12	0.07
I90F	1696	1715	0.08	0.08

[a] Fluorescence measurements are in arbitrary units (a.u.).
[b] Turbidity measurements are in absorbance units (AU).

these samples, the baseline fluorescence was about 110 a.u. (Figure 3-10, *right*). This most likely accounts for the increased initial values observed in the presence of αB. (Compare 0 minute measurements between Figures 3-8 and 3-10.)

Endpoint turbidity was also measured for samples containing both HγD and αB. Results of these measurements were somewhat varied (Figure 3-11 and Table 3-2). For WT HγD-Crys, turbidity was slightly higher in samples that contained αB with an OD_{350} of 0.04 AU. For V75D, turbidity levels were almost 2-fold lower at 0.07 AU, for samples containing αB. A similar trend was observed for the maximum ThT fluorescence measurements for this protein in the presence of chaperone. In the case of I90F, endpoint turbidity levels were virtually identical in the absence and presence of αB at 0.08 AU, and this was again reflected by maximum ThT fluorescence measurements.

5. Both HγD-Crys and αB Underwent Structural Changes Under Acidic Conditions

Many proteins that form amyloid fibers necessarily undergo large structural changes when converting from their native, usually globular, state to the highly regular β-sheet structure characteristic of amyloid (Nelson et al. 2005; Nelson and Eisenberg 2006; Sawaya et al. 2007). WT and mutant HγD-Crys underwent structural transitions at pH 3 that increased solution turbidity and allowed for ThT binding to the proteins, indicating formation of amyloid-like structures. To examine the pH dependence of these transitions, WT HγD-Crys, V75D, and I90F were incubated at 37°C in buffered solutions from pH 3 – 7. After five hours, the Trp fluorescence of the proteins was recorded as a measure of overall tertiary structure. In addition, αB was incubated at pH 7 and pH 3 to determine whether structural changes occur that may affect its chaperone function.

For WT HγD-Crys, no major changes in the Trp fluorescence spectra were observed over the range of pH 7 – 4. At pH 3 the fluorescence maximum increased in intensity although the λ_{max} of ~325 nm did not change (Figure 3-12). V75D exhibited two structural changes with pH (Figure 3-12). At pH 7 – 6, no changes occurred, but there was a reproducible decrease in fluorescence intensity at pH 5, though the λ_{max} did not change. The fluorescence spectrum at pH 4 was nearly identical to those at pH 7 and 6. When the pH was further decreased to 3, a major structural change

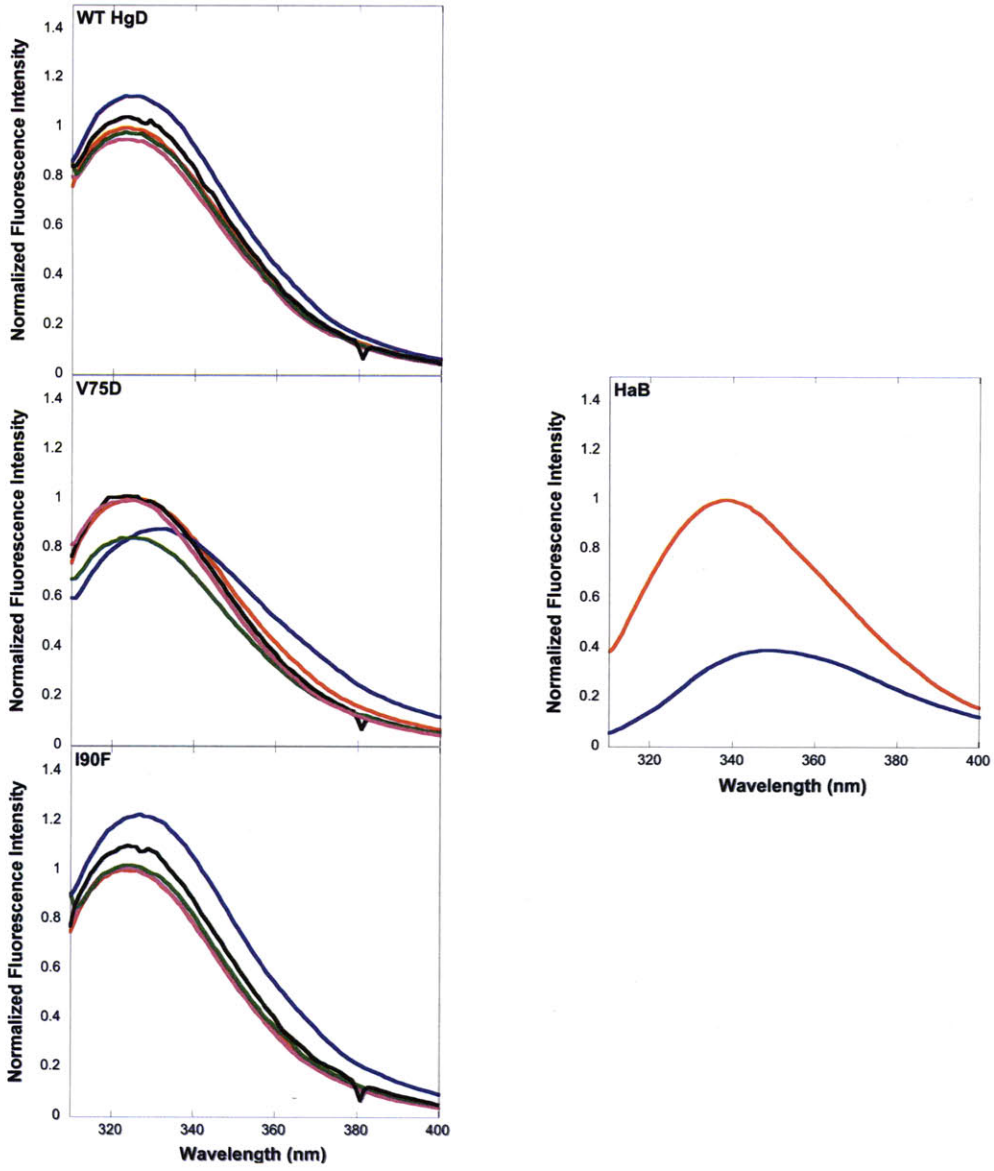

Figure 3-12: pH dependence of tryptophan fluorescence for WT HγD-Crys, V75D, I90F and αB. Curves are defined as follows for all plots: pH 7 – red line; pH 6 – purple line; pH 5 – green line; pH 4 – black line; pH 3 – blue line. Each set of curves is normalized to the maximum fluorescence intensity at pH 7 for the protein of interest. Protein was incubated in appropriate buffers for 5 hours at 37°C. All γD proteins were present at concentrations of 10 μg/ml and αB was present at 50 μg/ml.

occurred with the overall fluorescence intensity dropping and the λ_{max} shifting from ~325 nm to 333 nm. This change is consistent with the partial unfolding of the protein observed in equilibrium unfolding/refolding experiments. Trp fluorescence changes for I90F were more similar to those observed for WT HγD-Crys (Figure 3-12). Fluorescence spectra were the same over the range of pH 7 – 5. At pH 4, the fluorescence intensity was slightly, but reproducibly increased though not shifted. At pH 3, the fluorescence intensity was further increased and the λ_{max} was slightly shifted from 324 to 328 nm.

Although αB slowed the kinetics of fibrillation for both mutant proteins, it did not inhibit fibril formation. One reason for this could be that αB was not stable under such acidic conditions. To examine this, the protein was incubated in both pH 3 and pH 7 buffers at 37°C. Tryptophan fluorescence was then measured for both samples (Figure 3-12). At pH 7, αB displayed native Trp fluorescence with a λ_{max} at 338 nm. This is in agreement with previously published measurements (Acosta-Sampson and King 2010). After incubation at pH 3, the fluorescence spectrum has an overall lower intensity and the λ_{max} was red-shifted to 349 nm. This is the same shift that was observed for αB denatured in GdnHCl (Acosta-Sampson and King 2010), which suggests that at pH 3, the tertiary structure is largely disorganized.

D. Discussion

Protein aggregation can stem from multiple precursor states. In one case (Figure 3-13A), proteins initially in their native states (N), which are only marginally stable in the majority of cases, may become destabilized due to covalent modification or damage, or as the result of amino acid substitutions or other sequence modifications resulting from genetic mutation. Destabilization will drive unfolding of the polypeptide chain and in many cases, especially for large and/or multidomain proteins that do not fold through simple two-state mechanisms, the significant population of a partially unfolded intermediate (I_1). Hydrophobic patches on domain interfaces or portions of the normally buried hydrophobic core may be exposed and instead of refolding to N, these regions may associate to bury these exposed patches forming a non-native

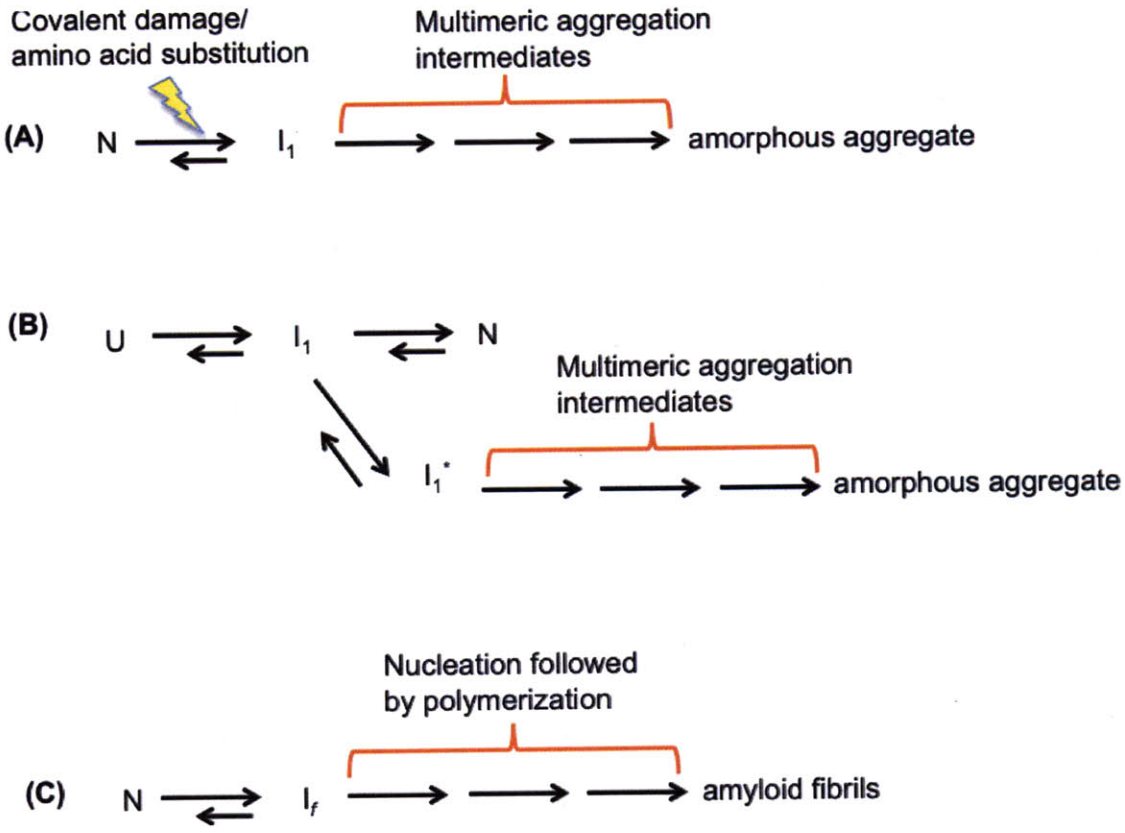

Figure 3-13: Models of γ-crystallin aggregation. **(A)** depicts the native mixing experiments described in Results section 3. **(B)** depicts aggregation that competes with productive refolding, described in Results sections 1 and 2. **(C)** depicts the formation of amyloid fibrils at pH 3 described in Results section 4. See text for details.

aggregate composed of many protein molecules. Aggregation can also occur from an unfolded initial state, U, for example when a nascent chain is exiting the ribosome or if proteins are subjected to high concentrations of denaturant (Figure 3-13B). These two examples of U may behave differently and for purposes of relevance to the experiments presented here, only the latter case will be discussed. In the case of U, the polypeptide chain must pass through at least one intermediate conformation (I_1) to reach N. I_1 is at the juncture of the pathways towards N versus aggregation. For the case of HγD-Crys in particular, upon rapid dilution from denaturant, aggregation is kinetically preferred and this drives the pathway towards the aggregated state.

Figure 3-13C depicts a third case addressed in this chapter, that of amyloid formation. Like the first case, this polymerization pathway begins with N, but specific conditions are required, such as acidic acetate buffer containing sodium chloride for HγD-Crys, to achieve an amyloid-competent intermediate conformation (I_f). In the general case, nucleation proceeds, during which time the critical nucleus is formed, and then fast growth continues. Under appropriate conditions, several protofibrils may associate, wrapping around each other to form wider, rope-like fibers (Jimenez et al. 2002; Meehan et al. 2007).

1. The Differential Aggregation Propensities of HγD-Crys and Its Interaction with the Chaperone αB

WT HγD-Crys displayed a range of aggregation behaviors depending on initial conditions. As previously described, upon dilution from high concentrations of GdnHCl, the partially folded WT protein followed an aggregation pathway that kinetically competes with productive refolding. The majority of molecules in solution were incorporated into amorphous aggregates. The reaction was reliably monitored by light scattering, which reached its plateau in a matter of minutes. In contrast, native WT HγD-Crys was extremely stable and incubation under physiological conditions for up to one month resulted in little aggregation. This is in agreement with the extremely long extrapolated kinetic half-times for the unfolding of the protein in the absence of denaturant (Mills-Henry 2007). Physiologically, this result makes sense as well.

Because the γ-crystallins are present for a lifetime without the possibility of degradation and replenishment of damaged species, it is of utmost importance for the native state to be exceptionally stable, maintaining its structure despite exposure to a host of environmental stresses.

αB effectively suppressed the aggregation of its physiological substrate WT HγD-Crys in experiments where HγD was initially unfolded in 5 M GdnHCl. The ratio of γD:αB for these experiments was 1:5, the optimal ratio for suppression determined by Acosta-Sampson and King (Acosta-Sampson and King 2010). This high ratio of αB was required because of the fast aggregation kinetics under these conditions. Lower ratios were successfully used for proteins whose aggregation proceeded at significantly slower rates (Horwitz et al. 1998). Complexes of αB with HγD intermediate structures were long-lived, similar to complexes formed in the lens, where α-crystallin permanently sequesters aggregation-prone intermediates from participating in aberrant interactions with other molecules. In contrast to the aggregation suppression experiments, mixtures of native αB and HγD-Crys showed no evidence of complex formation between the two proteins. This was expected, because in the lens environment, association of native HγD-Crys with α-crystallin could result in the improper formation of large light-scattering aggregates.

2. V75D and I90F Mutants Exhibit a Range of Aggregation Patterns and are Differentially Recognized by αB

For aggregation reactions initially starting with unfolded protein, both partially folded V75D and I90F chains aggregated to the same extent as WT HγD-Crys. Light-scattering curves had the same shape and intensity (Figure 3-1). This indicates that the reaction proceeded through the same aggregation-prone intermediate as for WT and that population of this conformation was not affected by either mutation. If the aggregation-prone conformation were affected by these mutations a difference in light scattering levels, either lower or higher, would have been expected. Similarly, levels of suppression by αB (1:5 γD:αB) were comparable to those observed for WT. Long-lived complexes

were formed between αB and each of the two mutant proteins in the same manner as WT. This would be expected if the intermediates recognized by αB were the same for WT and the mutants. An alternative case is that the mutants aggregated through a different intermediate, but overall aggregate size and amount of protein incorporation were similar. Because αB recognizes a range of proteins, it is reasonable that it could efficiently bind alternative conformations of these γ-crystallin mutants as well as WT. However, previous results (Moreau and King 2009) demonstrated that the C-td of both the WT and mutant proteins must be partially unfolded for aggregation to occur, making it likely that the same species was recognized by αB in all cases.

For the alternative initial conditions, in which native V75D and I90F were incubated in the absence of denaturant over 28 days, the two proteins behaved quite differently. V75D spontaneously aggregated within 14 days, with little protein remaining in the native state. This end result was very similar to that of V75D initially in the unfolded state, although the aggregation-prone intermediates are likely different. The incubation of αB with native V75D had no effect on the aggregation and the αB peak on SEC traces appeared unchanged over time. αB was an ineffective chaperone for V75D under these conditions and it did not interact with the mutant protein at all. These results are supported by 2-D gel analysis of lens proteins from mice expressing V76D MγD-Crys (Wang et al. 2007). The authors found that although the mutant protein was enriched in the water-insoluble fraction of lens proteins, levels of α-crystallin were unchanged among WT (+/+), heterozygotes (+/V76D) or homozygotes (V76D/V76D). The agreement between these two results also emphasizes that these *in vitro* experiments may serve as suitable models for biochemical analysis of protein stability and protein-protein interactions within the lens, especially in light of the unavailability of lens fiber cell culture.

I90F behaved differently from both WT HγD-Crys and V75D when incubated in the absence of denaturant. When incubated alone, native I90F accumulated aggregated material over the 28-day period. This mutant was globally destabilized both thermodynamically and kinetically and it is likely that over prolonged periods a fraction of the protein unfolds. When incubated in the presence of αB, I90F formed a complex with the chaperone whose population increased over the time course of the experiment.

The slow decrease of I90F with time suggests the slow unfolding and population of an aggregation-prone species. This makes I90F an ideal target for sequestration by αB. Other studies have confirmed that α-crystallin is a better chaperone for slower aggregation processes (Lindner et al. 1997; Carver et al. 2002), supporting this interpretation. A similar interaction with bovine α-crystallin was observed for I4F MγB-Crys in *in vitro* mixing experiments (Liu et al. 2005). However, the chaperone:I4F complex was only formed after incubation at 45°C. Long-term *in vitro* mixing was not examined. In lens extracts from mice harboring this mutation, a complex was formed between α-crystallin and γ-crystallins, although the γ-crystallins were identified using a polyclonal antibody and the presence of I4F MγB-Crys in the complex was not specifically confirmed (Liu et al. 2005).

3. Relevance of Amyloid Formation by HγD-Crys and Interference by αB Under Acidic Conditions

Preliminary studies of amyloid formation by these mutant HγD-Crys proteins are also presented here. Several reports have documented the ability of all three crystallin classes to form amyloid fibrils (Sandilands et al. 2002; Meehan et al. 2004; Meehan et al. 2007; Papanikolopoulou et al. 2008) and in accordance with these reports, WT, V75D and I90F HγD-Crys all formed ThT-binding fibrils that scattered light under destabilizing conditions at pH 3. ThT binds regions of high β-sheet content, and although the γ-crystallins are composed almost exclusively of β-sheets, the native proteins at pH 7 did not bind ThT. Along with the increase in OD_{350} due to light scatter, the increase in ThT fluorescence is indicative of amyloid fibril formation. The ThT fluorescence rose faster and to a greater intensity for both mutant proteins, with I90F samples rising the fastest. This is most likely due to the overall destabilizing effect that the I90F substitution has on the protein. ThT fluorescence for V75D rose slower in a sigmoidal manner and reached the highest overall fluorescence. The slower rise is most likely due to the nature of destabilization by this substitution. Only the N-td of V75D is destabilized and it may take longer for V75D to populate I_f than for I90F to achieve the same conformation.

These results can be accounted for if the aggregation-prone region of I_f is located in the C-td, as it most likely is for the refolding-aggregation pathway.

Both WT and mutant HγD-Crys underwent structural transitions at pH 3. WT and I90F had similar changes in Trp fluorescence, with the increased fluorescence intensity indicating a general loosening of the tertiary structure and some loss of Trp fluorescence quenching. V75D underwent a much more dramatic change under these conditions. The red shift in fluorescence was reminiscent of the partial unfolding observed in equilibrium unfolding experiments. After several hours at these conditions it was apparent that I90F maintained more of its native structure than V75D. This can be reconciled with the ThT results if I90F underwent structural changes faster at pH 3, while V75D, whose structure is more perturbed, took longer to achieve this conformation.

The addition of αB to these samples had different effects on each protein. The overall ThT fluorescence for both WT and V75D was lower than that of samples not containing αB, indicating that the chaperone either suppressed amyloid formation to some extent, or altered the structure of fibrils such that ThT binding was compromised. The shape of the ThT fluorescence curve was altered for V75D and the lag phase was diminished in the presence of αB. I90F saw the most straightforward change, simply a longer $t_{1/2}$, with no changes in the final intensity or overall shape of the ThT fluorescence curve. While it seems that αB suppressed fibril formation somewhat for WT and V75D, it may have only had transient interactions with I90F, slowing its aggregation but ultimately not suppressing it. It could be that αB interacts differently with different "versions" (WT and mutant) of HγD-Crys that can form similar amyloid-like aggregates. αB structure was non-native at pH 3, and so the loss of tertiary structure certainly affected its ability to inhibit amyloid formation.

Amyloid fibril formation by F9S MγS-Crys required incubation for up to 100 hours, although solution conditions were different and longer incubation times may have been necessary (Lee et al. 2010). Based on the red shifted Trp fluorescence of V75D at pH 3, a greater proportion of these molecules may unfold and incorporate into fibrils than for I90F. Even if the rise in ThT fluorescence was slower, this could account for the eventual higher fluorescence intensity for V75D. Alternatively, the differences could be

due to the suprastructure of the fibrils as they continue to grow if certain structures bind ThT more readily than others.

4. Are These Aggregation-Prone Intermediates Similar to One Another?

Similarities, if any, among the intermediates of WT, V75D and I90F for a single set of experiments were discussed above, but what of the similarities and differences of intermediates populated under the different experimental conditions. Could the aggregation pathways depicted in Figure 3-13 converge through similar intermediates? This may be the case for I90F. αB stably bound I90F in both refolding aggregation and native mixing experiments. As described in the previous section, the region of I90F responsible for amyloid formation may be found in the C-td and could be related to the initial aggregation-prone regions exposed upon dilution from denaturant. This same reasoning could be true for WT and V75D in terms of the pH 3 intermediate and the refolding aggregation intermediate. However, these were probably different than the intermediate formed in native mixing experiments for V75D, otherwise interactions with αB would be expected in both the refolding aggregation as well as the native mixing experiments, where aggregation was not inhibited.

5. There are Varied Pathways to Cataract Disease

The two HγD-Crys mutants V75D and I90F were modeled from mutations causing congenital cataract in mice. These mutations were shown in Chapter 2 to differentially destabilize the protein in both equilibrium and kinetic experiments. Just as α-crystallin interacts differently with a variety of substrates, many of which are non-physiological (Horwitz 1992; Horwitz et al. 1998; Rajaraman et al. 2001; Stromer et al. 2003), the experiments presented here demonstrate differential interactions of αB with WT and mutant versions of HγD-Crys.

Native mixing experiments probably provide the most physiologically relevant picture of how these mutations result in cataract disease. While WT HγD-Crys, as expected, does not interact with the chaperone, V75D aggregates to near completion

without recognition by αB. This suggests that in the lens, the aggregation-prone species may evade sequestration by α-crystallin and form aggregates that not only scatter light but may possibly disrupt the complete differentiation of lens fiber cells (Graw et al. 2002b). This would exacerbate the light scattering produced by large protein aggregates, and the cataract would worsen with lens growth. Conversely, I90F was efficiently recognized by αB in these experiments. While analogous behavior *in vivo* would prevent the growth of large aggregates in the lens, the finite supply of α-crystallin would become saturated with mutant proteins much more quickly than in the normal lens. This would most likely also compromise the other functions of α-crystallin in the lens including its associations with the lens-specific cytoskeletal proteins filensin and CP49 (Carter et al. 1995).

Several mutations in HγD-Crys have been identified that cause cataract in humans. Point mutations resulting in single amino acid substitutions lead to very different causes of cataract. The well-characterized P23T HγD substitution as well as R58H HγD both dramatically reduce protein solubility and crystallization is enhanced in the case of R58H (Pande et al. 2001; Basak et al. 2003; Pande et al. 2005; Pande et al. 2010); R14C HγD results in disulfide-mediated aggregation (Pande et al. 2000); R36S HγD increases the propensity for crystallization and crystals actually formed within the lens (Kmoch et al. 2000). The work presented here expands on how the destabilizing mutations V75D and I90F may result in cataract disease. In particular, these results support our proposal that multiple mechanisms may lead to cataract formation, and these biochemical analyses provide adequate models of *in vivo* events.

CHAPTER 4:

FINAL DISCUSSION
AND
FUTURE DIRECTIONS

A. FINAL DISCUSSION

The work comprising this thesis began with the identification of mutations in murine γ-crystallin genes that altered the hydrophobic cores of their protein products. The nature and location of these substitutions were in stark contrast to many of those previously identified in the human γ-crystallins. This motivated the creation of mutant HγD-Crys constructs bearing homologous mutations.

In Chapter 2, I presented a biochemical characterization of the thermodynamic and kinetic stabilities of these mutant proteins and compared their properties with those of WT HγD-Crys. All mutant proteins (L5S, V75D and I90F) were destabilized compared with WT, and the destabilization was directly linked to the three-dimensional location of the amino acid substitution. N-terminal substitutions destabilized only the N-td, while those in the C-td globally disrupted stability. This is most likely because the C-td is used as a template for N-td folding and without a stable C-td, the structure is not maintained. Kinetic unfolding experiments further supported these observations. Both mutant and WT proteins populated a partially unfolded, aggregation-prone intermediate upon dilution from high denaturant concentrations. The requirement for partial disruption of C-td structure was shared among mutant and WT proteins, supporting the hypothesis that the aggregation-prone intermediate is a common off-pathway conformer under these conditions.

In Chapter 3, I continued experiments with WT HγD-Crys, as well as V75D and I90F to represent core mutations within each domain. This chapter focused on the aggregation propensities of these proteins and their interactions with one component of the lenticular chaperone system, human αB-crystallin. I observed differential interactions of αB with the WT and mutant γ-crystallins, which were dependent on the conditions that prompted aggregation. Strikingly, under physiological conditions in the absence of denaturant, both V75D and I90F populated aggregation-prone intermediates, but only I90F was recognized and bound by αB. Based on prior experiments described herein and elsewhere (Acosta-Sampson and King 2010), this result was unexpected and suggested differences in the unfolding pathways of these differentially destabilized mutant proteins. The extremely stable WT protein did not interact with αB under native

conditions, as its structure was most likely unperturbed over the short experimental time course (in comparison to the lifetime of the crystallins within the lens nucleus).

These experiments have shown that different substitutions in the hydrophobic core of HγD-Crys destabilize the protein in different ways and lead to unfolding pathways in which different intermediate conformations are favored. While the aggregation pathway that competes with productive refolding is most likely the same for WT, L5S, V75D and I90F; the unfolding pathway in the absence of denaturant suggests two distinct unfolding pathways for V75D and I90F. Furthermore, αB only interacts with conformers of I90F. While destabilization and protein misfolding are the initial causes of both cataract-associated phenotypes, it was the failure of recognition by αB that led to the large-scale aggregation of V75D observed here under physiological conditions. This is in direct agreement with observations in mice expressing the murine γ-crystallin version of this mutation (Wang et al. 2007), verifying that the *in vitro* model presented here recapitulates the *in vivo* changes in protein behavior. In contrast, I90F was efficiently recognized and bound by αB. Although chaperone function was preserved, the high concentrations of mutant protein in the lens would saturate α-crystallin at a much faster rate than in the normal lens. Aside from the initial identifying studies (Graw et al. 2004), there are no *in vivo* studies on the mechanism of cataract formation for this mouse mutant. We propose that early saturation of α-crystallin through increased interactions with the destabilized protein results in early onset cataract disease.

Studies by Pande and colleagues (Pande et al. 2000; Pande et al. 2001; Pande et al. 2005; Pande et al. 2010) and Benedek and colleagues (Benedek 1997; Basak et al. 2003; McManus et al. 2007) proposed phase separation as the mechanism of cataract formation in several cases of human congenital cataract, as well as the more common age-related manifestation of this disease. It is clear that for several point mutations resulting in surface arginine substitutions, altered phase separation temperatures play a role in protein precipitation; however, these cases do not necessarily capture the main features of age-related cataract disease. The experimental results presented here suggest an alternate mechanism of cataract formation whose roots lay in protein misfolding and altered chaperone interactions; this is distinct from precipitation arising from the native state of WT or mutant HγD-Crys.

Misfolding and subsequent aggregation, coupled with a slow saturation of the α-crystallin chaperone are likely to be the main mechanisms of age-related cataract development. Substitutions mimicking deamidation in both β- and γ-crystallins destabilize the proteins and in some cases, higher chaperone concentrations are required to achieve even partial rescue from aggregation (Kim et al. 2002; Lampi et al. 2002; Flaugh et al. 2006; Lampi et al. 2006; Takata et al. 2007; Takata et al. 2008; Michiel et al. 2010). Paired with the array of other covalent modifications identified in aged and cataractous lenses, the crystallins will eventually suffer from reduced stability and partial unfolding, leading to the population of aggregation-prone species (Figure 4-1). While α-crystallin is active in the young lens, sequestering these species, as the supply becomes limiting protein aggregation will overtake chaperone activity (Figure 4-1). If destabilization and partial unfolding are the key events in tipping the balance towards aggregation, the mutant proteins characterized in this thesis could serve as excellent models for further studies on the detailed aggregation mechanism, as well as the identification of modulators of this process. The following section will suggest some further experimental studies that extend the utility of these proteins.

B. FUTURE DIRECTIONS

The experiments presented in this thesis raise a new set of questions relevant to the molecular mechanism of cataract formation. The most immediate question concerns the aggregation-prone conformation of I90F that is recognized by αB in the absence of denaturant. The protein did not appear to populate kinetic or equilibrium unfolding intermediates; therefore, what is the conformation that is bound by αB? A combination of Trp fluorescence and NMR spectroscopy could provide a relatively detailed answer to this question. And in relation to this, what region of I90F is bound by the chaperone? In the cases of acid-induced and refolding-induced aggregation, where αB interacts with both mutant and WT HγD-Crys, does the chaperone recognize equivalent sites on all proteins? A combination of chemical cross-linking, proteolytic digestion and mass spectrometry may provide answers to these questions.

As discussed above, these hydrophobic core mutations could serve as a model system for the destabilization of lens proteins with age. The specific protein-protein interactions that result in aggregation, like all protein deposition diseases, are critical for cataract formation. These mutant proteins could serve as models for studying the aggregation pathway under physiological conditions. Structural mapping using proteolytic digestion or hydrogen-deuterium exchange coupled with mass spectrometry could identify regions that are protected due to burial within the aggregate. These mutants are also suitable for use in small molecule screens for inhibitors of crystallin aggregation, using the various aggregation assays introduced in Chapter 3. In conjunction with this screening method, small molecule modulators of α-crystallin function could be probed. Potential hits would be informative on several levels, from elucidation of the detailed mechanism of aggregation and chaperone function to development of small molecule pharmaceuticals that prevent or delay the onset of age-related cataract in humans.

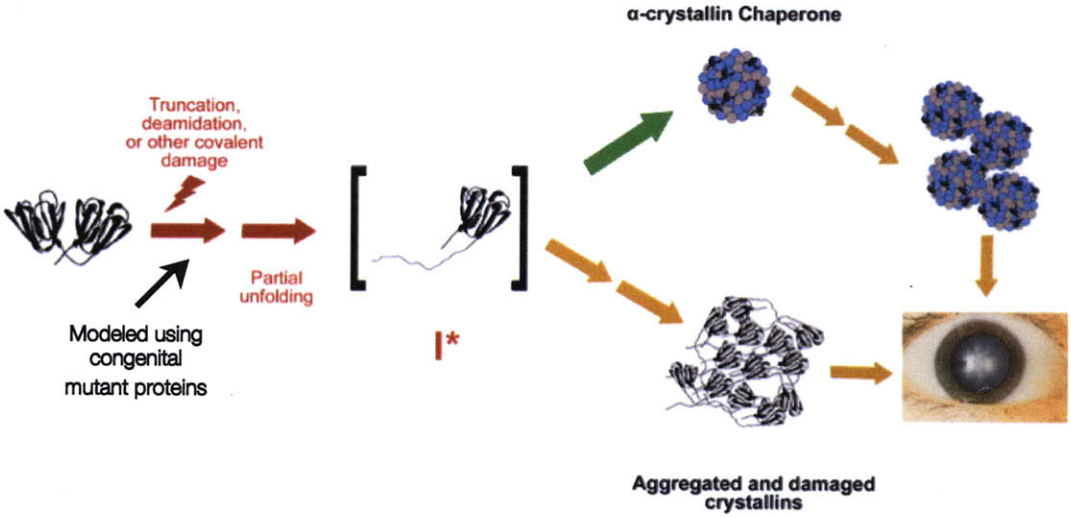

Figure 4-1: A working model of the molecular mechanisms of age-related cataract development. Native crystallins are exposed to environmental stresses through an individual's lifetime. As these damages accumulate, they may destabilize the protein resulting in partial unfolding and population of aggregation-prone species. Without protection in the form of molecular chaperones, these species will aggregate, resulting in light scatter and reduced visual acuity. In young lenses α-crystallin sequesters these conformers, preventing aberrant interactions. However, as the lens ages and the α-crystallin supply is depleted, aggregation is once again favored. In addition, saturated α-crystallin complexes may interact, further forming light-scattering aggregates. The destabilizing damages that accumulate through an individual's lifetime may be modeled through the use of destabilized mutant proteins associated with congenital or early onset cataract disease. Original figure generously provided by Dr. Ligia Acosta-Sampson.

CHAPTER 5:

REFERENCES

Aarts, H.J., Lubsen, N.H., and Schoenmakers, J.G. 1989. Crystallin gene expression during rat lens development. *Eur J Biochem* **183**(1): 31-36.

Abrahamson, M. and Grubb, A. 1994. Increased body temperature accelerates aggregation of the Leu-68-->Gln mutant cystatin C, the amyloid-forming protein in hereditary cystatin C amyloid angiopathy. *Proc Natl Acad Sci U S A* **91**(4): 1416-1420.

Acosta-Sampson, L. and King, J. 2010. Partially folded aggregation intermediates of human gammaD-, gammaC-, and gammaS-crystallin are recognized and bound by human alphaB-crystallin chaperone. *J Mol Biol* **401**(1): 134-152.

Ajaz, M.S., Ma, Z., Smith, D.L., and Smith, J.B. 1997. Size of human lens beta-crystallin aggregates are distinguished by N-terminal truncation of betaB1. *J Biol Chem* **272**(17): 11250-11255.

Anfinsen, C.B. 1973. Principles that govern the folding of protein chains. *Science* **181**(96): 223-230.

Aquilina, J.A., Benesch, J.L.P., Ding, L.L., Yaron, O., Horwitz, J., and Robinson, C.V. 2005. Subunit exchange of polydisperse proteins: mass spectrometry reveals consequences of alphaA-crystallin truncation. *J Biol Chem* **280**(15): 14485-14491.

Aquilina, J.A. and Watt, S.J. 2007. The N-terminal domain of alphaB-crystallin is protected from proteolysis by bound substrate. *Biochem Biophys Res Commun* **353**(4): 1115-1120.

Augusteyn, R.C. 2010. On the growth and internal structure of the human lens. *Exp Eye Res* **90**(6): 643-654.

Azuma, N., Hirakiyama, A., Inoue, T., Asaka, A., and Yamada, M. 2000. Mutations of a human homologue of the Drosophila eyes absent gene (EYA1) detected in patients with congenital cataracts and ocular anterior segment anomalies. *Hum Mol Genet* **9**(3): 363-366.

Bagnéris, C., Bateman, O.A., Naylor, C.E., Cronin, N., Boelens, W.C., Keep, N.H., and Slingsby, C. 2009. Crystal Structures of α-Crystallin Domain Dimers of αB-Crystallin and Hsp20. *Journal of Molecular Biology* **392**(5): 1242-1252.

Baker, D., Sohl, J.L., and Agard, D.A. 1992. A protein-folding reaction under kinetic control. *Nature* **356**(6366): 263-265.

Baldwin, E., Xu, J., Hajiseyedjavadi, O., Baase, W.A., and Matthews, B.W. 1996. Thermodynamic and structural compensation in "size-switch" core repacking variants of bacteriophage T4 lysozyme. *J Mol Biol* **259**(3): 542-559.

Baldwin, E.P., Hajiseyedjavadi, O., Baase, W.A., and Matthews, B.W. 1993. The role of backbone flexibility in the accommodation of variants that repack the core of T4 lysozyme. *Science* **262**(5140): 1715-1718.

Basak, A., Bateman, O., Slingsby, C., Pande, A., Asherie, N., Ogun, O., Benedek, G.B., and Pande, J. 2003. High-resolution X-ray crystal structures of human gammaD crystallin (1.25 A) and the R58H mutant (1.15 A) associated with aculeiform cataract. *J Mol Biol* **328**(5): 1137-1147.

Basha, E., Friedrich, K.L., and Vierling, E. 2006. The N-terminal arm of small heat shock proteins is important for both chaperone activity and substrate specificity. *J Biol Chem* **281**(52): 39943-39952.

Bassnett, S. 2002. Lens organelle degradation. *Exp Eye Res* **74**(1): 1-6.

Bateman, O.A., Sarra, R., van Genesen, S.T., Kappe, G., Lubsen, N.H., and Slingsby, C. 2003. The stability of human acidic beta-crystallin oligomers and hetero-oligomers. *Exp Eye Res* **77**(4): 409-422.

Bax, B., Lapatto, R., Nalini, V., Driessen, H., Lindley, P.F., Mahadevan, D., Blundell, T.L., and Slingsby, C. 1990. X-ray analysis of beta B2-crystallin and evolution of oligomeric lens proteins. *Nature* **347**(6295): 776-780.

Benedek, G.B. 1997. Cataract as a protein condensation disease: the Proctor Lecture. *Invest Ophthalmol Vis Sci* **38**(10): 1911-1921.

Berry, V., Francis, P., Kaushal, S., Moore, A., and Bhattacharya, S. 2000. Missense mutations in MIP underlie autosomal dominant 'polymorphic' and lamellar cataracts linked to 12q. *Nat Genet* **25**(1): 15-17.

Berthoud, V.M., Minogue, P.J., Guo, J., Williamson, E.K., Xu, X., Ebihara, L., and Beyer, E.C. 2003. Loss of function and impaired degradation of a cataract-associated mutant connexin50. *Eur J Cell Biol* **82**(5): 209-221.

Betts, S. and King, J. 1999. There's a right way and a wrong way: in vivo and in vitro folding, misfolding and subunit assembly of the P22 tailspike. *Structure* **7**(6): R131-139.

Bloemendal, H., de Jong, W., Jaenicke, R., Lubsen, N.H., Slingsby, C., and Tardieu, A. 2004. Ageing and vision: structure, stability and function of lens crystallins. *Prog Biophys Mol Biol* **86**(3): 407-485.

Bova, M.P., Ding, L.L., Horwitz, J., and Fung, B.K. 1997. Subunit exchange of alphaA-crystallin. *J Biol Chem* **272**(47): 29511-29517.

Bova, M.P., Huang, Q., Ding, L., and Horwitz, J. 2002. Subunit exchange, conformational stability, and chaperone-like function of the small heat shock protein 16.5 from Methanococcus jannaschii. *J Biol Chem* **277**(41): 38468-38475.

Bova, M.P., McHaourab, H.S., Han, Y., and Fung, B.K. 2000. Subunit exchange of small heat shock proteins. Analysis of oligomer formation of alphaA-crystallin and Hsp27 by fluorescence resonance energy transfer and site-directed truncations. *J Biol Chem* **275**(2): 1035-1042.

Boyle, D. and Takemoto, L. 1994. Characterization of the alpha-gamma and alpha-beta complex: evidence for an in vivo functional role of alpha-crystallin as a molecular chaperone. *Exp Eye Res* **58**(1): 9-15.

Brady, J.P., Garland, D., Duglas-Tabor, Y., Robison, W.G., Jr., Groome, A., and Wawrousek, E.F. 1997. Targeted disruption of the mouse alpha A-crystallin gene induces cataract and cytoplasmic inclusion bodies containing the small heat shock protein alpha B-crystallin. *Proc Natl Acad Sci U S A* **94**(3): 884-889.

Brady, J.P., Garland, D.L., Green, D.E., Tamm, E.R., Giblin, F.J., and Wawrousek, E.F. 2001. AlphaB-crystallin in lens development and muscle integrity: a gene knockout approach. *Invest Ophthalmol Vis Sci* **42**(12): 2924-2934.

Brakenhoff, R.H., Aarts, H.J., Reek, F.H., Lubsen, N.H., and Schoenmakers, J.G. 1990. Human gamma-crystallin genes. A gene family on its way to extinction. *J Mol Biol* **216**(3): 519-532.

Bu, L., Jin, Y., Shi, Y., Chu, R., Ban, A., Eiberg, H., Andres, L., Jiang, H., Zheng, G., Qian, M. et al. 2002. Mutant DNA-binding domain of HSF4 is associated with autosomal dominant lamellar and Marner cataract. *Nat Genet* **31**(3): 276-278.

Buchet, R. and Pikula, S. 2000. Alzheimer's disease: its origin at the membrane, evidence and questions. *Acta Biochim Pol* **47**(3): 725-733.

Burdon, K.P., McKay, J.D., Sale, M.M., Russell-Eggitt, I.M., Mackey, D.A., Wirth, M.G., Elder, J.E., Nicoll, A., Clarke, M.P., FitzGerald, L.M. et al. 2003. Mutations in a novel gene, NHS, cause the pleiotropic effects of Nance-Horan syndrome, including severe congenital cataract, dental anomalies, and mental retardation. *Am J Hum Genet* **73**(5): 1120-1130.

Burdon, K.P., Wirth, M.G., Mackey, D.A., Russell-Eggitt, I.M., Craig, J.E., Elder, J.E., Dickinson, J.L., and Sale, M.M. 2004. Investigation of crystallin genes in familial cataract, and report of two disease associated mutations. *Br J Ophthalmol* **88**(1): 79-83.

Burns, L.L., Dalessio, P.M., and Ropson, I.J. 1998. Folding mechanism of three structurally similar beta-sheet proteins. *Proteins* **33**(1): 107-118.

Burton, R.E., Huang, G.S., Daugherty, M.A., Fullbright, P.W., and Oas, T.G. 1996. Microsecond protein folding through a compact transition state. *J Mol Biol* **263**(2): 311-322.

Byeon, I.J., Louis, J.M., and Gronenborn, A.M. 2003. A protein contortionist: core mutations of GB1 that induce dimerization and domain swapping. *J Mol Biol* **333**(1): 141-152.

Carter, J.M., Hutcheson, A.M., and Quinlan, R.A. 1995. In vitro studies on the assembly properties of the lens proteins CP49, CP115: coassembly with alpha-crystallin but not with vimentin. *Exp Eye Res* **60**(2): 181-192.

Carver, J.A., Guerreiro, N., Nicholls, K.A., and Truscott, R.J. 1995. On the interaction of alpha-crystallin with unfolded proteins. *Biochim Biophys Acta* **1252**(2): 251-260.

Carver, J.A., Lindner, R.A., Lyon, C., Canet, D., Hernandez, H., Dobson, C.M., and Redfield, C. 2002. The interaction of the molecular chaperone alpha-crystallin with unfolding alpha-lactalbumin: a structural and kinetic spectroscopic study. *J Mol Biol* **318**(3): 815-827.

Chaikuad, A., Shafqat, N., Krojer, T., Yue, W.W., Cocking, R., Vollmar, M., Muniz, J.R.C., Pike, A.C.W., von Deift, F., Arrowsmith, C.H. et al. 2010. Crystal structure of human Beta-crystallin A4 (CRYBA4).

Chen, J., Flaugh, S.L., Callis, P.R., and King, J. 2006. Mechanism of the highly efficient quenching of tryptophan fluorescence in human gammaD-crystallin. *Biochemistry* **45**(38): 11552-11563.

Chen, J., Toptygin, D., Brand, L., and King, J. 2008. Mechanism of the efficient tryptophan fluorescence quenching in human gammaD-crystallin studied by time-resolved fluorescence. *Biochemistry* **47**(40): 10705-10721.

Chen, Y.C., Reid, G.E., Simpson, R.J., and Truscott, R.J. 1997. Molecular evidence for the involvement of alpha crystallin in the colouration/crosslinking of crystallins in age-related nuclear cataract. *Exp Eye Res* **65**(6): 835-840.

Chiou, S.H., Chylack, L.T., Jr., Tung, W.H., and Bunn, H.F. 1981. Nonenzymatic glycosylation of bovine lens crystallins. Effect of aging. *J Biol Chem* **256**(10): 5176-5180.

Chung, C.M., Connors, L.H., Benson, M.D., and Walsh, M.T. 2001. Biophysical analysis of normal transthyretin: implications for fibril formation in senile systemic amyloidosis. *Amyloid* **8**(2): 75-83.

Clark, A.C., Sinclair, J.F., and Baldwin, T.O. 1993. Folding of bacterial luciferase involves a non-native heterodimeric intermediate in equilibrium with the native enzyme and the unfolded subunits. *J Biol Chem* **268**(15): 10773-10779.

Clark, P.L., Liu, Z.P., Zhang, J., and Gierasch, L.M. 1996. Intrinsic tryptophans of CRABPI as probes of structure and folding. *Protein Sci* **5**(6): 1108-1117.

Claxton, D.P., Zou, P., and McHaourab, H.S. 2008. Structure and orientation of T4 lysozyme bound to the small heat shock protein alpha-crystallin. *J Mol Biol* **375**(4): 1026-1039.

Cobb, B.A. and Petrash, J.M. 2000. Structural and functional changes in the alpha A-crystallin R116C mutant in hereditary cataracts. *Biochemistry* **39**(51): 15791-15798.

Cobb, N.J., Apetri, A.C., and Surewicz, W.K. 2008. Prion protein amyloid formation under native-like conditions involves refolding of the C-terminal alpha-helical domain. *J Biol Chem* **283**(50): 34704-34711.

Cobb, N.J., Sonnichsen, F.D., McHaourab, H., and Surewicz, W.K. 2007. Molecular architecture of human prion protein amyloid: a parallel, in-register beta-structure. *Proc Natl Acad Sci U S A* **104**(48): 18946-18951.

Colon, W. and Kelly, J.W. 1992. Partial denaturation of transthyretin is sufficient for amyloid fibril formation in vitro. *Biochemistry* **31**(36): 8654-8660.

Conley, Y.P., Erturk, D., Keverline, A., Mah, T.S., Keravala, A., Barnes, L.R., Bruchis, A., Hess, J.F., FitzGerald, P.G., Weeks, D.E. et al. 2000. A juvenile-onset, progressive cataract locus on chromosome 3q21-q22 is associated with a missense mutation in the beaded filament structural protein-2. *Am J Hum Genet* **66**(4): 1426-1431.

Connelly, S., Choi, S., Johnson, S.M., Kelly, J.W., and Wilson, I.A. 2010. Structure-based design of kinetic stabilizers that ameliorate the transthyretin amyloidoses. *Curr Opin Struct Biol* **20**(1): 54-62.

Damas, A.M. and Saraiva, M.J. 2000. Review: TTR amyloidosis-structural features leading to protein aggregation and their implications on therapeutic strategies. *J. Struct. Biol.* **130** (2-3): 290-299.

Dao-pin, S., Anderson, D.E., Baase, W.A., Dahlquist, F.W., and Matthews, B.W. 1991a. Structural and thermodynamic consequences of burying a charged residue within the hydrophobic core of T4 lysozyme. *Biochemistry* **30**(49): 11521-11529.

Dao-pin, S., Soderlind, E., Baase, W.A., Wozniak, J.A., Sauer, U., and Matthews, B.W. 1991b. Cumulative site-directed charge-change replacements in bacteriophage T4 lysozyme suggest that long-range electrostatic interactions contribute little to protein stability. *J Mol Biol* **221**(3): 873-887.

Das, B.K. and Liang, J.J. 1998. Thermodynamic and kinetic characterization of calf lens gammaF-crystallin. *Int J Biol Macromol* **23**(3): 191-197.

Das, K.P. and Surewicz, W.K. 1995. Temperature-induced exposure of hydrophobic surfaces and its effect on the chaperone activity of alpha-crystallin. *FEBS Lett* **369**(2-3): 321-325.

Das, P., King, J.A., and Zhou, R. 2010. beta-Strand interactions at the domain interface critical for the stability of human lens gammaD-crystallin. *Protein Sci* **19**(1): 131-140.

Delaye, M. and Tardieu, A. 1983. Short-range order of crystallin proteins accounts for eye lens transparency. *Nature* **302**(5907): 415-417.
Denisov, V.P., Schlessman, J.L., Garcia-Moreno, E.B., and Halle, B. 2004. Stabilization of internal charges in a protein: water penetration or conformational change? *Biophys J* **87**(6): 3982-3994.
Dill, K.A. and Chan, H.S. 1997. From Levinthal to pathways to funnels. *Nat Struct Biol* **4**(1): 10-19.
Dobson, C.M. 2003. Protein folding and misfolding. *Nature* **426**(6968): 884-890.
-. 2004. Principles of protein folding, misfolding and aggregation. *Semin Cell Dev Biol* **15**(1): 3-16.
Dolgikh, D.A., Gilmanshin, R.I., Brazhnikov, E.V., Bychkova, V.E., Semisotnov, G.V., Venyaminov, S., and Ptitsyn, O.B. 1981. Alpha-Lactalbumin: compact state with fluctuating tertiary structure? *FEBS Lett* **136**(2): 311-315.
Dubin, R.A., Wawrousek, E.F., and Piatigorsky, J. 1989. Expression of the murine alpha B-crystallin gene is not restricted to the lens. *Mol Cell Biol* **9**(3): 1083-1091.
Dyson, H.J., Cross, K.J., Houghten, R.A., Wilson, I.A., Wright, P.E., and Lerner, R.A. 1985. The immunodominant site of a synthetic immunogen has a conformational preference in water for a type-II reverse turn. *Nature* **318**(6045): 480-483.
Eakin, C.M., Attenello, F.J., Morgan, C.J., and Miranker, A.D. 2004. Oligomeric assembly of native-like precursors precedes amyloid formation by beta-2 microglobulin. *Biochemistry* **43**(24): 7808-7815.
Eaton, W.A. and Hofrichter, J. 1990. Sickle cell hemoglobin polymerization. *Adv Protein Chem* **40**: 63-279.
Eriksson, A.E., Baase, W.A., Zhang, X.J., Heinz, D.W., Blaber, M., Baldwin, E.P., and Matthews, B.W. 1992. Response of a protein structure to cavity-creating mutations and its relation to the hydrophobic effect. *Science* **255**(5041): 178-183.
Evans, P., Wyatt, K., Wistow, G.J., Bateman, O.A., Wallace, B.A., and Slingsby, C. 2004. The P23T cataract mutation causes loss of solubility of folded gammaD-crystallin. *J Mol Biol* **343**(2): 435-444.
Everett, C.A., Glenister, P.H., Taylor, D.M., Lyon, M.F., Kratochvilova-Loester, J., and Favor, J. 1994. Mapping of six dominant cataract genes in the mouse. *Genomics* **20**(3): 429-434.
Fagerholm, P., Philipson, B., and Carlstrom, D. 1981. Calcification in the human lens. *Curr Eye Res* **1**(11): 629-633.
Farahbakhsh, Z.T., Huang, Q.L., Ding, L.L., Altenbach, C., Steinhoff, H.J., Horwitz, J., and Hubbell, W.L. 1995. Interaction of alpha-crystallin with spin-labeled peptides. *Biochemistry* **34**(2): 509-516.
Favor, J. 1983. A comparison of the dominant cataract and recessive specific-locus mutation rates induced by treatment of male mice with ethylnitrosourea. *Mutat Res* **110**(2): 367-382.
-. 1984. Characterization of dominant cataract mutations in mice: penetrance, fertility and homozygous viability of mutations recovered after 250 mg/kg ethylnitrosourea paternal treatment. *Genet Res* **44**(2): 183-197.
Ferrao-Gonzales, A.D., Palmieri, L., Valory, M., Silva, J.L., Lashuel, H., Kelly, J.W., and Foguel, D. 2003. Hydration and packing are crucial to amyloidogenesis as

revealed by pressure studies on transthyretin variants that either protect or worsen amyloid disease. *J Mol Biol* **328**(4): 963-974.

Ferrone, F.A., Hofrichter, J., and Eaton, W.A. 1985. Kinetics of sickle hemoglobin polymerization. II. A double nucleation mechanism. *J Mol Biol* **183**(4): 611-631.

Fersht, A.R., Shi, J.P., Knill-Jones, J., Lowe, D.M., Wilkinson, A.J., Blow, D.M., Brick, P., Carter, P., Waye, M.M., and Winter, G. 1985. Hydrogen bonding and biological specificity analysed by protein engineering. *Nature* **314**(6008): 235-238.

Flaugh, S.L. 2006. Folding, Stability and Aggregation of the Long-Lived Eye Lens Protein Human Gamma D Crystallin. In *Biology*, Vol Ph. D. , p. 211. Massachusetts Institute of Technology, Cambridge.

Flaugh, S.L., Kosinski-Collins, M.S., and King, J. 2005a. Contributions of hydrophobic domain interface interactions to the folding and stability of human gammaD-crystallin. *Protein Sci* **14**(3): 569-581.

-. 2005b. Interdomain side-chain interactions in human γD crystallin influencing folding and stability. *Protein Sci* **14**(8): 2030-2043.

Flaugh, S.L., Mills, I.A., and King, J. 2006. Glutamine deamidation destabilizes human gammaD-crystallin and lowers the kinetic barrier to unfolding. *J Biol Chem* **281**(41): 30782-30793.

Fort, P.E., Freeman, W.M., Losiewicz, M.K., Singh, R.S., and Gardner, T.W. 2009. The retinal proteome in experimental diabetic retinopathy: up-regulation of crystallins and reversal by systemic and periocular insulin. *Mol Cell Proteomics* **8**(4): 767-779.

Francis, P., Berry, V., Bhattacharya, S., and Moore, A. 2000a. Congenital progressive polymorphic cataract caused by a mutation in the major intrinsic protein of the lens, MIP (AQP0). *Br J Ophthalmol* **84**(12): 1376-1379.

Francis, P., Chung, J.J., Yasui, M., Berry, V., Moore, A., Wyatt, M.K., Wistow, G., Bhattacharya, S.S., and Agre, P. 2000b. Functional impairment of lens aquaporin in two families with dominantly inherited cataracts. *Hum Mol Genet* **9**(15): 2329-2334.

Fu, L. and Liang, J.J. 2001. Spectroscopic analysis of lens recombinant betaB2- and gammaC-crystallin. *Mol Vis* **7**: 178-183.

-. 2002a. Unfolding of human lens recombinant betaB2- and gammaC-crystallins. *J Struct Biol* **139**(3): 191-198.

-. 2003. Alteration of protein-protein interactions of congenital cataract crystallin mutants. *Invest Ophthalmol Vis Sci* **44**(3): 1155-1159.

Fu, L. and Liang, J.J.N. 2002b. Conformational change and destabilization of cataract gammaC-crystallin T5P mutant. *FEBS Lett* **513**(2-3): 213-216.

Gasteiger, E., Hoogland, C., Gattiker, A., Duvaud, S., Wilkins, M.R., Appel, R.D., and Bairoch, A. 2005. Protein Identification and Analysis Tools on the ExPASy Server. In *The Proteomics Protocols Handbook*, (ed. J.M. Walker), pp. 571-607. Humana Press.

Geyer, D.D., Spence, M.A., Johannes, M., Flodman, P., Clancy, K.P., Berry, R., Sparkes, R.S., Jonsen, M.D., Isenberg, S.J., and Bateman, J.B. 2006. Novel single-base deletional mutation in major intrinsic protein (MIP) in autosomal dominant cataract. *Am J Ophthalmol* **141**(4): 761-763.

Ghosh, J.G., Estrada, M.R., and Clark, J.I. 2005. Interactive domains for chaperone activity in the small heat shock protein, human alphaB crystallin. *Biochemistry* **44**(45): 14854-14869.

Govaerts, C., Wille, H., Prusiner, S.B., and Cohen, F.E. 2004. Evidence for assembly of prions with left-handed beta-helices into trimers. *Proc Natl Acad Sci U S A* **101**(22): 8342-8347.

Graw, J., Klopp, N., Neuhauser-Klaus, A., Favor, J., and Loster, J. 2002a. Crygf(Rop): the first mutation in the Crygf gene causing a unique radial lens opacity. *Invest Ophthalmol Vis Sci* **43**(9): 2998-3002.

Graw, J., Löster, J., Soewarto, D., Fuchs, H., Reis, A., Wolf, E., Balling, R., and Hrabé de Angelis, M. 2002b. V76D mutation in a conserved gD-crystallin region leads to dominant cataracts in mice. *Mamm Genome* **13**(8): 452-455.

Graw, J., Neuhauser-Klaus, A., Klopp, N., Selby, P.B., Loster, J., and Favor, J. 2004. Genetic and allelic heterogeneity of Cryg mutations in eight distinct forms of dominant cataract in the mouse. *Invest Ophthalmol Vis Sci* **45**(4): 1202-1213.

Greene, R.F., Jr. and Pace, C.N. 1974. Urea and guanidine hydrochloride denaturation of ribonuclease, lysozyme, alpha-chymotrypsin, and beta-lactoglobulin. *J Biol Chem* **249**(17): 5388-5393.

Gronenborn, A.M. 2009. Protein acrobatics in pairs--dimerization via domain swapping. *Curr Opin Struct Biol* **19**(1): 39-49.

Guijarro, J.I., Morton, C.J., Plaxco, K.W., Campbell, I.D., and Dobson, C.M. 1998. Folding kinetics of the SH3 domain of PI3 kinase by real-time NMR combined with optical spectroscopy. *J Mol Biol* **276**(3): 657-667.

Hains, P. and Truscott, R.J. 2010. AGE-DEPENDENT DEAMIDATION OF LIFE-LONG PROTEINS IN THE HUMAN LENS. *Investigative Ophthalmology & Visual Science*.

Hains, P.G. and Truscott, R.J. 2007. Post-translational modifications in the nuclear region of young, aged, and cataract human lenses. *J Proteome Res* **6**(10): 3935-3943.

-. 2008. Proteomic analysis of the oxidation of cysteine residues in human age-related nuclear cataract lenses. *Biochim Biophys Acta* **1784**(12): 1959-1964.

Hamill, S.J., Cota, E., Chothia, C., and Clarke, J. 2000a. Conservation of folding and stability within a protein family: the tyrosine corner as an evolutionary cul-de-sac. *J Mol Biol* **295**(3): 641-649.

Hamill, S.J., Steward, A., and Clarke, J. 2000b. The folding of an immunoglobulin-like Greek key protein is defined by a common-core nucleus and regions constrained by topology. *J Mol Biol* **297**(1): 165-178.

Hamilton, J.A., Steinrauf, L.K., Braden, B.C., Liepnieks, J., Benson, M.D., Holmgren, G., Sandgren, O., and Steen, L. 1993. The x-ray crystal structure refinements of normal human transthyretin and the amyloidogenic Val-30-->Met variant to 1.7-A resolution. *J Biol Chem* **268**(4): 2416-2424.

Hammarstrom, P., Wiseman, R.L., Powers, E.T., and Kelly, J.W. 2003. Prevention of transthyretin amyloid disease by changing protein misfolding energetics. *Science* **299**(5607): 713-716.

Hansen, L., Yao, W., Eiberg, H., Kjaer, K.W., Baggesen, K., Hejtmancik, J.F., and Rosenberg, T. 2007. Genetic heterogeneity in microcornea-cataract: five novel

mutations in CRYAA, CRYGD, and GJA8. *Invest Ophthalmol Vis Sci* **48**(9): 3937-3944.

Hanson, S.R., Hasan, A., Smith, D.L., and Smith, J.B. 2000. The major in vivo modifications of the human water-insoluble lens crystallins are disulfide bonds, deamidation, methionine oxidation and backbone cleavage. *Exp Eye Res* **71**(2): 195-207.

Hanson, S.R., Smith, D.L., and Smith, J.B. 1998. Deamidation and disulfide bonding in human lens gamma-crystallins. *Exp Eye Res* **67**(3): 301-312.

Harper, J.D. and Lansbury, P.T., Jr. 1997. Models of amyloid seeding in Alzheimer's disease and scrapie: mechanistic truths and physiological consequences of the time-dependent solubility of amyloid proteins. *Annu Rev Biochem* **66**: 385-407.

Harrington, V., McCall, S., Huynh, S., Srivastava, K., and Srivastava, O.P. 2004. Crystallins in water soluble-high molecular weight protein fractions and water insoluble protein fractions in aging and cataractous human lenses. *Mol Vis* **10**: 476-489.

Harrington, V., Srivastava, O.P., and Kirk, M. 2007. Proteomic analysis of water insoluble proteins from normal and cataractous human lenses. *Mol Vis* **13**: 1680-1694.

Hartl, F.U. and Hayer-Hartl, M. 2009. Converging concepts of protein folding in vitro and in vivo. *Nat Struct Mol Biol* **16**(6): 574-581.

Haslbeck, M., Franzmann, T., Weinfurtner, D., and Buchner, J. 2005. Some like it hot: the structure and function of small heat-shock proteins. *Nat Struct Mol Biol* **12**(10): 842-846.

Hatters, D.M., Lindner, R.A., Carver, J.A., and Howlett, G.J. 2001. The molecular chaperone, alpha-crystallin, inhibits amyloid formation by apolipoprotein C-II. *J Biol Chem* **276**(36): 33755-33761.

Heidary, D.K., Gross, L.A., Roy, M., and Jennings, P.A. 1997. Evidence for an obligatory intermediate in the folding of interleukin-1 beta. *Nat Struct Biol* **4**(9): 725-731.

Hejtmancik, J.F. 2008. Congenital cataracts and their molecular genetics. *Semin Cell Dev Biol* **19**(2): 134-149.

Hemmingsen, J.M., Gernert, K.M., Richardson, J.S., and Richardson, D.C. 1994. The tyrosine corner: a feature of most Greek key beta-barrel proteins. *Protein Sci* **3**(11): 1927-1937.

Heon, E., Priston, M., Schorderet, D.F., Billingsley, G.D., Girard, P.O., Lubsen, N., and Munier, F.L. 1999. The gamma-crystallins and human cataracts: a puzzle made clearer. *Am J Hum Genet* **65**(5): 1261-1267.

Hoenders, H.J. and Bloemendal, H. 1983. Lens proteins and aging. *J Gerontol* **38**(3): 278-286.

Hogg, D., Tsui, L.C., Gorin, M., and Breitman, M.L. 1986. Characterization of the human beta-crystallin gene Hu beta A3/A1 reveals ancestral relationships among the beta gamma-crystallin superfamily. *J Biol Chem* **261**(26): 12420-12427.

Horwich, A.L. and Fenton, W.A. 2009. Chaperonin-mediated protein folding: using a central cavity to kinetically assist polypeptide chain folding. *Q Rev Biophys* **42**(2): 83-116.

Horwitz, J. 1992. Alpha-crystallin can function as a molecular chaperone. *Proc Natl Acad Sci U S A* **89**(21): 10449-10453.
Horwitz, J., Huang, Q.L., Ding, L., and Bova, M.P. 1998. Lens alpha-crystallin: chaperone-like properties. *Methods Enzymol* **290**: 365-383.
Huntington, J.A., Read, R.J., and Carrell, R.W. 2000. Structure of a serpin-protease complex shows inhibition by deformation. *Nature* **407**(6806): 923-926.
Ishikawa, K., Nakamura, H., Morikawa, K., and Kanaya, S. 1993. Stabilization of Escherichia coli ribonuclease HI by cavity-filling mutations within a hydrophobic core. *Biochemistry* **32**(24): 6171-6178.
Isom, D.G., Castaneda, C.A., Cannon, B.R., Velu, P.D., and Garcia-Moreno, E.B. 2010. Charges in the hydrophobic interior of proteins. *Proc Natl Acad Sci U S A*.
Iwaki, T., Kume-Iwaki, A., and Goldman, J.E. 1990. Cellular distribution of alpha B-crystallin in non-lenticular tissues. *J Histochem Cytochem* **38**(1): 31-39.
Jaenicke, R. 1994. Eye-lens proteins: structure, superstructure, stability, genetics. *Naturwissenschaften* **81**(10): 423-429.
-. 1999. Stability and folding of domain proteins. *Prog Biophys Mol Biol* **71**(2): 155-241.
Jaenicke, R. and Slingsby, C. 2001. Lens crystallins and their microbial homologs: structure, stability, and function. *Crit Rev Biochem Mol Biol* **36**(5): 435-499.
Jager, M., Nguyen, H., Crane, J.C., Kelly, J.W., and Gruebele, M. 2001. The folding mechanism of a beta-sheet: the WW domain. *J Mol Biol* **311**(2): 373-393.
Jager, M., Zhang, Y., Bieschke, J., Nguyen, H., Dendle, M., Bowman, M.E., Noel, J.P., Gruebele, M., and Kelly, J.W. 2006. Structure-function-folding relationship in a WW domain. *Proc Natl Acad Sci U S A* **103**(28): 10648-10653.
Jakob, U., Gaestel, M., Engel, K., and Buchner, J. 1993. Small heat shock proteins are molecular chaperones. *J Biol Chem* **268**(3): 1517-1520.
Jakobs, P.M., Hess, J.F., FitzGerald, P.G., Kramer, P., Weleber, R.G., and Litt, M. 2000. Autosomal-dominant congenital cataract associated with a deletion mutation in the human beaded filament protein gene BFSP2. *Am J Hum Genet* **66**(4): 1432-1436.
Janowski, R., Kozak, M., Jankowska, E., Grzonka, Z., Grubb, A., Abrahamson, M., and Jaskolski, M. 2001. Human cystatin C, an amyloidogenic protein, dimerizes through three-dimensional domain swapping. *Nat Struct Biol* **8**(4): 316-320.
Jarrett, J.T., Berger, E.P., and Lansbury, P.T., Jr. 1993. The carboxy terminus of the beta amyloid protein is critical for the seeding of amyloid formation: implications for the pathogenesis of Alzheimer's disease. *Biochemistry* **32**(18): 4693-4697.
Jaya, N., Garcia, V., and Vierling, E. 2009. Substrate binding site flexibility of the small heat shock protein molecular chaperones. *Proc Natl Acad Sci USA* **106**(37): 15604-15609.
Jiang, X., Smith, C.S., Petrassi, H.M., Hammarstrom, P., White, J.T., Sacchettini, J.C., and Kelly, J.W. 2001. An engineered transthyretin monomer that is nonamyloidogenic, unless it is partially denatured. *Biochemistry* **40**(38): 11442-11452.
Jimenez, J.L., Nettleton, E.J., Bouchard, M., Robinson, C.V., Dobson, C.M., and Saibil, H.R. 2002. The protofilament structure of insulin amyloid fibrils. *Proc Natl Acad Sci U S A* **99**(14): 9196-9201.

Jung, J., Byeon, I.J., Wang, Y., King, J., and Gronenborn, A.M. 2009. The structure of the cataract-causing P23T mutant of human gammaD-crystallin exhibits distinctive local conformational and dynamic changes. *Biochemistry* **48**(12): 2597-2609.

Kallur, L.S., Aziz, A., and Abraham, E.C. 2008. C-Terminal truncation affects subunit exchange of human alphaA-crystallin with alphaB-crystallin. *Mol Cell Biochem* **308**(1-2): 85-91.

Karp, D.A., Gittis, A.G., Stahley, M.R., Fitch, C.A., Stites, W.E., and Garcia-Moreno, E.B. 2007. High apparent dielectric constant inside a protein reflects structural reorganization coupled to the ionization of an internal Asp. *Biophys J* **92**(6): 2041-2053.

Karpusas, M., Baase, W.A., Matsumura, M., and Matthews, B.W. 1989. Hydrophobic packing in T4 lysozyme probed by cavity-filling mutants. *Proc Natl Acad Sci U S A* **86**(21): 8237-8241.

Kelly, J.W. and Lansbury, P.T.J. 1994. A chemical approach to elucidate the mechanism of transthyretin and beta-protein amyloid fibril formation *Amyloid* **1**: 186-205.

Kim, K.K., Kim, R., and Kim, S.H. 1998. Crystal structure of a small heat-shock protein. *Nature* **394**(6693): 595-599.

Kim, Y.H., Kapfer, D.M., Boekhorst, J., Lubsen, N.H., Bachinger, H.P., Shearer, T.R., David, L.L., Feix, J.B., and Lampi, K.J. 2002. Deamidation, but not truncation, decreases the urea stability of a lens structural protein, betaB1-crystallin. *Biochemistry* **41**(47): 14076-14084.

Kirsten Frank, M., Dyda, F., Dobrodumov, A., and Gronenborn, A.M. 2002. Core mutations switch monomeric protein GB1 into an intertwined tetramer. *Nat Struct Biol* **9**(11): 877-885.

Kitamura, A. and Kubota, H. 2010. Amyloid oligomers: dynamics and toxicity in the cytosol and nucleus. *FEBS J* **277**(6): 1369-1379.

Kmoch, S., Brynda, J., Asfaw, B., Bezouska, K., Novak, P., Rezacova, P., Ondrova, L., Filipec, M., Sedlacek, J., and Elleder, M. 2000. Link between a novel human gammaD-crystallin allele and a unique cataract phenotype explained by protein crystallography. *Hum Mol Genet* **9**(12): 1779-1786.

Knaus, K.J., Morillas, M., Swietnicki, W., Malone, M., Surewicz, W.K., and Yee, V.C. 2001. Crystal structure of the human prion protein reveals a mechanism for oligomerization. *Nat Struct Biol* **8**(9): 770-774.

Kopito, R.R. 2000. Aggresomes, inclusion bodies and protein aggregation. *Trends Cell Biol* **10**(12): 524-530.

Kosinski-Collins, M.S. 2004. Characterization of the unfolding, refolding, and aggregation pathways of two proteins implicated in cataractogenesis: human gamma D and human gamma S crystallin. In *Biology*, p. 217. Massachusetts Institute of Technology, Cambridge, MA.

Kosinski-Collins, M.S., Flaugh, S.L., and King, J. 2004. Probing folding and fluorescence quenching in human gammaD crystallin Greek key domains using triple tryptophan mutant proteins. *Protein Sci* **13**(8): 2223-2235.

Kosinski-Collins, M.S. and King, J. 2003. In vitro unfolding, refolding, and polymerization of human gammaD crystallin, a protein involved in cataract formation. *Protein Sci* **12**(3): 480-490.

Koteiche, H.A. and McHaourab, H.S. 2003. Mechanism of chaperone function in small heat-shock proteins. Phosphorylation-induced activation of two-mode binding in alphaB-crystallin. *J Biol Chem* **278**(12): 10361-10367.

Kudva, Y.C., Hiddinga, H.J., Butler, P.C., Mueske, C.S., and Eberhardt, N.L. 1997. Small heat shock proteins inhibit in vitro A beta(1-42) amyloidogenesis. *FEBS Lett* **416**(1): 117-121.

Kumar, M.S., Kapoor, M., Sinha, S., and Reddy, G.B. 2005. Insights into hydrophobicity and the chaperone-like function of alphaA- and alphaB-crystallins: an isothermal titration calorimetric study. *J Biol Chem* **280**(23): 21726-21730.

Laganowsky, A., Benesch, J.L., Landau, M., Ding, L., Sawaya, M.R., Cascio, D., Huang, Q., Robinson, C.V., Horwitz, J., and Eisenberg, D. 2010. Crystal structures of truncated alphaA and alphaB crystallins reveal structural mechanisms of polydispersity important for eye lens function. *Protein Sci* **19**(5): 1031-1043.

Lampi, K.J., Amyx, K.K., Ahmann, P., and Steel, E.A. 2006. Deamidation in human lens betaB2-crystallin destabilizes the dimer. *Biochemistry* **45**(10): 3146-3153.

Lampi, K.J., Kim, Y.H., Bachinger, H.P., Boswell, B.A., Lindner, R.A., Carver, J.A., Shearer, T.R., David, L.L., and Kapfer, D.M. 2002. Decreased heat stability and increased chaperone requirement of modified human betaB1-crystallins. *Mol Vis* **8**: 359-366.

Lampi, K.J., Ma, Z., Hanson, S.R., Azuma, M., Shih, M., Shearer, T.R., Smith, D.L., Smith, J.B., and David, L.L. 1998. Age-related changes in human lens crystallins identified by two-dimensional electrophoresis and mass spectrometry. *Exp Eye Res* **67**(1): 31-43.

Lampi, K.J., Ma, Z., Shih, M., Shearer, T.R., Smith, J.B., Smith, D.L., and David, L.L. 1997. Sequence analysis of betaA3, betaB3, and betaA4 crystallins completes the identification of the major proteins in young human lens. *J Biol Chem* **272**(4): 2268-2275.

Lee, G.J., Roseman, A.M., Saibil, H.R., and Vierling, E. 1997. A small heat shock protein stably binds heat-denatured model substrates and can maintain a substrate in a folding-competent state. *EMBO J* **16**(3): 659-671.

Lee, S. and Eisenberg, D. 2003. Seeded conversion of recombinant prion protein to a disulfide-bonded oligomer by a reduction-oxidation process. *Nat Struct Biol* **10**(9): 725-730.

Lee, S., Mahler, B., Toward, J., Jones, B., Wyatt, K., Dong, L., Wistow, G., and Wu, Z. 2010. A Single Destabilizing Mutation (F9S) Promotes Concerted Unfolding of an Entire Globular Domain in gammaS-Crystallin. *Journal of molecular biology.*

Levinthal, C. 1968. Are there pathways for protein folding? *J Chem Phys* **65**: 44-45.

Liang, J.J. 2000. Interaction between beta-amyloid and lens alphaB-crystallin. *FEBS Lett* **484**(2): 98-101.

Liang, J.J. and Liu, B.F. 2006. Fluorescence resonance energy transfer study of subunit exchange in human lens crystallins and congenital cataract crystallin mutants. *Protein Sci* **15**(7): 1619-1627.

Lim, W.A., Farruggio, D.C., and Sauer, R.T. 1992. Structural and energetic consequences of disruptive mutations in a protein core. *Biochemistry* **31**(17): 4324-4333.

Lindner, R.A., Kapur, A., and Carver, J.A. 1997. The interaction of the molecular chaperone, alpha-crystallin, with molten globule states of bovine alpha-lactalbumin. *J Biol Chem* **272**(44): 27722-27729.

Litt, M., Carrero-Valenzuela, R., LaMorticella, D.M., Schultz, D.W., Mitchell, T.N., Kramer, P., and Maumenee, I.H. 1997. Autosomal dominant cerulean cataract is associated with a chain termination mutation in the human beta-crystallin gene CRYBB2. *Hum Mol Genet* **6**(5): 665-668.

Litt, M., Kramer, P., LaMorticella, D.M., Murphey, W., Lovrien, E.W., and Weleber, R.G. 1998. Autosomal dominant congenital cataract associated with a missense mutation in the human alpha crystallin gene CRYAA. *Hum Mol Genet* **7**(3): 471-474.

Liu, B.F., Song, S., Hanson, M., and Liang, J.J. 2008. Protein-protein interactions involving congenital cataract T5P gammaC-crystallin mutant: a confocal fluorescence microscopy study. *Exp Eye Res* **87**(6): 515-520.

Liu, H., Du, X., Wang, M., Huang, Q., Ding, L., McDonald, H.W., Yates, J.R., 3rd, Beutler, B., Horwitz, J., and Gong, X. 2005. Crystallin {gamma}B-I4F mutant protein binds to {alpha}-crystallin and affects lens transparency. *J Biol Chem* **280**(26): 25071-25078.

Liu, Y. and Eisenberg, D. 2002. 3D domain swapping: as domains continue to swap. *Protein Sci* **11**(6): 1285-1299.

Lomas, D.A. and Carrell, R.W. 2002. Serpinopathies and the conformational dementias. *Nat Rev Genet* **3**(10): 759-768.

Lomas, D.A., Evans, D.L., Finch, J.T., and Carrell, R.W. 1992. The mechanism of Z alpha 1-antitrypsin accumulation in the liver. *Nature* **357**(6379): 605-607.

Ma, Z., Hanson, S.R., Lampi, K.J., David, L.L., Smith, D.L., and Smith, J.B. 1998. Age-related changes in human lens crystallins identified by HPLC and mass spectrometry. *Exp Eye Res* **67**(1): 21-30.

Ma, Z., Piszczek, G., Wingfield, P.T., Sergeev, Y.V., and Hejtmancik, J.F. 2009. The G18V CRYGS mutation associated with human cataracts increases gammaS-crystallin sensitivity to thermal and chemical stress. *Biochemistry* **48**(30): 7334-7341.

Mackay, D.S., Andley, U.P., and Shiels, A. 2003. Cell death triggered by a novel mutation in the alphaA-crystallin gene underlies autosomal dominant cataract linked to chromosome 21q. *Eur J Hum Genet* **11**(10): 784-793.

Mackay, D.S., Boskovska, O.B., Knopf, H.L., Lampi, K.J., and Shiels, A. 2002. A nonsense mutation in CRYBB1 associated with autosomal dominant cataract linked to human chromosome 22q. *Am J Hum Genet* **71**(5): 1216-1221.

Magabo, K.S., Horwitz, J., Piatigorsky, J., and Kantorow, M. 2000. Expression of betaB(2)-crystallin mRNA and protein in retina, brain, and testis. *Invest Ophthalmol Vis Sci* **41**(10): 3056-3060.

Marcelino, A.M. and Gierasch, L.M. 2008. Roles of beta-turns in protein folding: from peptide models to protein engineering. *Biopolymers* **89**(5): 380-391.

Marsili, S., Salganik, R.I., Albright, C.D., Freel, C.D., Johnsen, S., Peiffer, R.L., and Costello, M.J. 2004. Cataract formation in a strain of rats selected for high oxidative stress. *Exp Eye Res* **79**(5): 595-612.

Mayor, U., Johnson, C.M., Daggett, V., and Fersht, A.R. 2000. Protein folding and unfolding in microseconds to nanoseconds by experiment and simulation. *Proc Natl Acad Sci U S A* **97**(25): 13518-13522.

Mayr, E.M., Jaenicke, R., and Glockshuber, R. 1997. The domains in gammaB-crystallin: identical fold-different stabilities. *J Mol Biol* **269**(2): 260-269.

McAvoy, J.W. 1978. Cell division, cell elongation and distribution of alpha-, beta- and gamma-crystallins in the rat lens. *J Embryol Exp Morphol* **44**: 149-165.

McHaourab, H.S., Dodson, E.K., and Koteiche, H.A. 2002. Mechanism of chaperone function in small heat shock proteins. Two-mode binding of the excited states of T4 lysozyme mutants by alphaA-crystallin. *J Biol Chem* **277**(43): 40557-40566.

McHaourab, H.S., Kumar, M.S., and Koteiche, H.A. 2007. Specificity of alphaA-crystallin binding to destabilized mutants of betaB1-crystallin. *FEBS Lett* **581**(10): 1939-1943.

McManus, J.J., Lomakin, A., Ogun, O., Pande, A., Basan, M., Pande, J., and Benedek, G.B. 2007. Altered phase diagram due to a single point mutation in human gammaD-crystallin. *Proc Natl Acad Sci USA* **104**(43): 16856-16861.

Meehan, S., Berry, Y., Luisi, B., Dobson, C.M., Carver, J.A., and MacPhee, C.E. 2004. Amyloid fibril formation by lens crystallin proteins and its implications for cataract formation. *J Biol Chem* **279**(5): 3413-3419.

Meehan, S., Knowles, T.P., Baldwin, A.J., Smith, J.F., Squires, A.M., Clements, P., Treweek, T.M., Ecroyd, H., Tartaglia, G.G., Vendruscolo, M. et al. 2007. Characterisation of amyloid fibril formation by small heat-shock chaperone proteins human alphaA-, alphaB- and R120G alphaB-crystallins. *J Mol Biol* **372**(2): 470-484.

Messina-Baas, O.M., Gonzalez-Huerta, L.M., and Cuevas-Covarrubias, S.A. 2006. Two affected siblings with nuclear cataract associated with a novel missense mutation in the CRYGD gene. *Mol Vis* **12**: 995-1000.

Michael, R., van Marle, J., Vrensen, G.F., and van den Berg, T.J. 2003. Changes in the refractive index of lens fibre membranes during maturation--impact on lens transparency. *Exp Eye Res* **77**(1): 93-99.

Michiel, M., Duprat, E., Skouri-Panet, F., Lampi, J.A., Tardieu, A., Lampi, K.J., and Finet, S. 2010. Aggregation of deamidated human betaB2-crystallin and incomplete rescue by alpha-crystallin chaperone. *Exp Eye Res* **90**(6): 688-698.

Michiel, M., Skouri-Panet, F., Duprat, E., Simon, S., Ferard, C., Tardieu, A., and Finet, S. 2009. Abnormal assemblies and subunit exchange of alphaB-crystallin R120 mutants could be associated with destabilization of the dimeric substructure. *Biochemistry* **48**(2): 442-453.

Milla, M.E., Brown, B.M., and Sauer, R.T. 1994. Protein stability effects of a complete set of alanine substitutions in Arc repressor. *Nat Struct Biol* **1**(8): 518-523.

Mills, I.A., Flaugh, S.L., Kosinski-Collins, M.S., and King, J.A. 2007. Folding and stability of the isolated Greek key domains of the long-lived human lens proteins gammaD-crystallin and gammaS-crystallin. *Protein Sci* **16**(11): 2427-2444.

Mills-Henry, I. 2007. Stability, Unfolding, and Aggregation of the gamma D and gamma S Human Eye Lens Crystallins. In *Biology*, Vol Ph.D., p. 219. Massachusetts Institute of Technology, Cambridge.

Minogue, P.J., Liu, X., Ebihara, L., Beyer, E.C., and Berthoud, V.M. 2005. An aberrant sequence in a connexin46 mutant underlies congenital cataracts. *J Biol Chem* **280**(49): 40788-40795.

Mitraki, A., and King, J. 1989. Protein folding intermediates and inclusion body formation. *Biotechnology* **7**: 690-697.

Moreau, K.L. and King, J. 2009. Hydrophobic Core Mutations Associated with Cataract Development in Mice Destabilize Human D-Crystallin. *Journal of Biological Chemistry* **284**(48): 33285-33295.

Murthy, G.V., Gupta, S.K., Maraini, G., Camparini, M., Price, G.M., Dherani, M., John, N., Chakravarthy, U., and Fletcher, A.E. 2007. Prevalence of lens opacities in North India: the INDEYE feasibility study. *Invest Ophthalmol Vis Sci* **48**(1): 88-95.

Nandrot, E., Slingsby, C., Basak, A., Cherif-Chefchaouni, M., Benazzouz, B., Hajaji, Y., Boutayeb, S., Gribouval, O., Arbogast, L., Berraho, A. et al. 2003. Gamma-D crystallin gene (CRYGD) mutation causes autosomal dominant congenital cerulean cataracts. *J Med Genet* **40**(4): 262-267.

Narberhaus, F. 2002. Alpha-crystallin-type heat shock proteins: socializing minichaperones in the context of a multichaperone network. *Microbiol Mol Biol Rev* **66**(1): 64-93; table of contents.

Nelson, R. and Eisenberg, D. 2006. Recent atomic models of amyloid fibril structure. *Curr Opin Struct Biol* **16**(2): 260-265.

Nelson, R., Sawaya, M.R., Balbirnie, M., Madsen, A.O., Riekel, C., Grothe, R., and Eisenberg, D. 2005. Structure of the cross-beta spine of amyloid-like fibrils. *Nature* **435**(7043): 773-778.

Nicholson, H., Anderson, D.E., Dao-pin, S., and Matthews, B.W. 1991. Analysis of the interaction between charged side chains and the alpha-helix dipole using designed thermostable mutants of phage T4 lysozyme. *Biochemistry* **30**(41): 9816-9828.

Nilsson, M., Wang, X., Rodziewicz-Motowidlo, S., Janowski, R., Lindstrom, V., Onnerfjord, P., Westermark, G., Grzonka, Z., Jaskolski, M., and Grubb, A. 2004. Prevention of domain swapping inhibits dimerization and amyloid fibril formation of cystatin C: use of engineered disulfide bridges, antibodies, and carboxymethylpapain to stabilize the monomeric form of cystatin C. *J Biol Chem* **279**(23): 24236-24245.

Nirmalan, P.K., Krishnadas, R., Ramakrishnan, R., Thulasiraj, R.D., Katz, J., Tielsch, J.M., and Robin, A.L. 2003. Lens opacities in a rural population of southern India: the Aravind Comprehensive Eye Study. *Invest Ophthalmol Vis Sci* **44**(11): 4639-4643.

Olafsson, I. and Grubb, A. 2000. Hereditary cystatin C amyloid angiopathy. *Amyloid* **7**(1): 70-79.

Olofsson, A., Ippel, J.H., Wijmenga, S.S., Lundgren, E., and Ohman, A. 2004. Probing solvent accessibility of transthyretin amyloid by solution NMR spectroscopy. *J Biol Chem* **279**(7): 5699-5707.

Oyster, C.W. 1999. *The human eye: structure and function.* Sinauer Associates, Inc, Sunderland, MA.

Pal, J.D., Liu, X., Mackay, D., Shiels, A., Berthoud, V.M., Beyer, E.C., and Ebihara, L. 2000. Connexin46 mutations linked to congenital cataract show loss of gap junction channel function. *Am J Physiol Cell Physiol* **279**(3): C596-602.

Pande, A., Annunziata, O., Asherie, N., Ogun, O., Benedek, G.B., and Pande, J. 2005. Decrease in protein solubility and cataract formation caused by the Pro23 to Thr mutation in human gamma D-crystallin. *Biochemistry* **44**(7): 2491-2500.

Pande, A., Ghosh, K.S., Banerjee, P.R., and Pande, J. 2010. Increase in Surface Hydrophobicity of the Cataract-Associated P23T Mutant of Human gammaD-Crystallin Is Responsible for Its Dramatically Lower, Retrograde Solubility. *Biochemistry*.

Pande, A., Pande, J., Asherie, N., Lomakin, A., Ogun, O., King, J., and Benedek, G.B. 2001. Crystal cataracts: human genetic cataract caused by protein crystallization. *Proc Natl Acad Sci U S A* **98**(11): 6116-6120.

Pande, A., Pande, J., Asherie, N., Lomakin, A., Ogun, O., King, J.A., Lubsen, N.H., Walton, D., and Benedek, G.B. 2000. Molecular basis of a progressive juvenile-onset hereditary cataract. *Proc Natl Acad Sci U S A* **97**(5): 1993-1998.

Papanikolopoulou, K., Mills-Henry, I., Thol, S.L., Wang, Y., Gross, A.A., Kirschner, D.A., Decatur, S.M., and King, J. 2008. Formation of amyloid fibrils in vitro by human gammaD-crystallin and its isolated domains. *Mol Vis* **14**: 81-89.

Pasta, S.Y., Raman, B., Ramakrishna, T., and Rao Ch, M. 2003. Role of the conserved SRLFDQFFG region of alpha-crystallin, a small heat shock protein. Effect on oligomeric size, subunit exchange, and chaperone-like activity. *J Biol Chem* **278**(51): 51159-51166.

Pauli, S., Soker, T., Klopp, N., Illig, T., Engel, W., and Graw, J. 2007. Mutation analysis in a German family identified a new cataract-causing allele in the CRYBB2 gene. *Mol Vis* **13**: 962-967.

Peschek, J., Braun, N., Franzmann, T.M., Georgalis, Y., Haslbeck, M., Weinkauf, S., and Buchner, J. 2009. The eye lens chaperone alpha-crystallin forms defined globular assemblies. *Proc Natl Acad Sci USA* **106**(32): 13272-13277.

Plater, M.L., Goode, D., and Crabbe, M.J. 1996. Effects of site-directed mutations on the chaperone-like activity of alphaB-crystallin. *J Biol Chem* **271**(45): 28558-28566.

Plaxco, K.W., Guijarro, J.I., Morton, C.J., Pitkeathly, M., Campbell, I.D., and Dobson, C.M. 1998. The folding kinetics and thermodynamics of the Fyn-SH3 domain. *Biochemistry* **37**(8): 2529-2537.

Prevent Blindness America, N.E.I. 2008. Vision Problems in the U.S.: Prevalence of adult vision impairment and age-related eye disease in America. pp. 22-25. Published in conjuction with the National Eye Institute.

Purkiss, A.G., Bateman, O.A., Goodfellow, J.M., Lubsen, N.H., and Slingsby, C. 2002. The X-ray crystal structure of human gamma S-crystallin C-terminal domain. *J Biol Chem* **277**(6): 4199-4205.

Purkiss, A.G., Bateman, O.A., Wyatt, K., Wilmarth, P.A., David, L.L., Wistow, G.J., and Slingsby, C. 2007. Biophysical properties of gammaC-crystallin in human and mouse eye lens: the role of molecular dipoles. *J Mol Biol* **372**(1): 205-222.

Rajan, R.S., Illing, M.E., Bence, N.F., and Kopito, R.R. 2001. Specificity in intracellular protein aggregation and inclusion body formation. *Proc Natl Acad Sci U S A* **98**(23): 13060-13065.

Rajaraman, K., Raman, B., Ramakrishna, T., and Rao, C.M. 2001. Interaction of human recombinant alphaA- and alphaB-crystallins with early and late unfolding intermediates of citrate synthase on its thermal denaturation. *FEBS Lett* **497**(2-3): 118-123.

Ramachandran, R.D., Perumalsamy, V., and Hejtmancik, J.F. 2007. Autosomal recessive juvenile onset cataract associated with mutation in BFSP1. *Hum Genet* **121**(3-4): 475-482.

Raman, B., Ban, T., Sakai, M., Pasta, S.Y., Ramakrishna, T., Naiki, H., Goto, Y., and Rao Ch, M. 2005. AlphaB-crystallin, a small heat-shock protein, prevents the amyloid fibril growth of an amyloid beta-peptide and beta2-microglobulin. *Biochem J* **392**(Pt 3): 573-581.

Raman, B., Ramakrishna, T., and Rao, C.M. 1995. Temperature dependent chaperone-like activity of alpha-crystallin. *FEBS Lett* **365**(2-3): 133-136.

Rao, G., Santhoshkumar, P., and Sharma, K.K. 2008. Anti-chaperone betaA3/A1(102-117) peptide interacting sites in human alphaB-crystallin. *Mol Vis* **14**: 666-674.

Reddy, G.B., Das, K.P., Petrash, J.M., and Surewicz, W.K. 2000. Temperature-dependent chaperone activity and structural properties of human alphaA- and alphaB-crystallins. *J Biol Chem* **275**(7): 4565-4570.

Reddy, G.B., Kumar, P.A., and Kumar, M.S. 2006. Chaperone-like activity and hydrophobicity of alpha-crystallin. *IUBMB Life* **58**(11): 632-641.

Rekas, A., Jankova, L., Thorn, D.C., Cappai, R., and Carver, J.A. 2007. Monitoring the prevention of amyloid fibril formation by alpha-crystallin. Temperature dependence and the nature of the aggregating species. *FEBS J* **274**(24): 6290-6304.

Richards, F.M. 1977. Areas, volumes, packing and protein structure. *Annu Rev Biophys Bioeng* **6**: 151-176.

Robinson, N.E., Lampi, K.J., Speir, J.P., Kruppa, G., Easterling, M., and Robinson, A.B. 2006. Quantitative measurement of young human eye lens crystallins by direct injection Fourier transform ion cyclotron resonance mass spectrometry. *Mol Vis* **12**: 704-711.

Rose, G.D. and Wolfenden, R. 1993. Hydrogen bonding, hydrophobicity, packing, and protein folding. *Annu Rev Biophys Biomol Struct* **22**: 381-415.

Rotondi, K.S. and Gierasch, L.M. 2003. Role of local sequence in the folding of cellular retinoic abinding protein I: structural propensities of reverse turns. *Biochemistry* **42**(26): 7976-7985.

Rudolph, R., Siebendritt, R., Nesslauer, G., Sharma, A.K., and Jaenicke, R. 1990. Folding of an all-beta protein: independent domain folding in gamma II-crystallin from calf eye lens. *Proc Natl Acad Sci U S A* **87**(12): 4625-4629.

Sandilands, A., Hutcheson, A.M., Long, H.A., Prescott, A.R., Vrensen, G., Löster, J., Klopp, N., Lutz, R.B., Graw, J., Masaki, S. et al. 2002. Altered aggregation properties of mutant gamma-crystallins cause inherited cataract. *EMBO J* **21**(22): 6005-6014.

Santhiya, S.T., Manisastry, S.M., Rawlley, D., Malathi, R., Anishetty, S., Gopinath, P.M., Vijayalakshmi, P., Namperumalsamy, P., Adamski, J., and Graw, J. 2004. Mutation analysis of congenital cataracts in Indian families: identification of

SNPS and a new causative allele in CRYBB2 gene. *Invest Ophthalmol Vis Sci* **45**(10): 3599-3607.

Santhiya, S.T., Shyam Manohar, M., Rawlley, D., Vijayalakshmi, P., Namperumalsamy, P., Gopinath, P.M., Löster, J., and Graw, J. 2002. Novel mutations in the gamma-crystallin genes cause autosomal dominant congenital cataracts. *J Med Genet* **39**(5): 352-358.

Santhoshkumar, P. and Sharma, K.K. 2002. Identification of a region in alcohol dehydrogenase that binds to alpha-crystallin during chaperone action. *Biochim Biophys Acta* **1598**(1-2): 115-121.

Sathish, H.A., Koteiche, H.A., and McHaourab, H.S. 2004. Binding of destabilized betaB2-crystallin mutants to alpha-crystallin: the role of a folding intermediate. *J Biol Chem* **279**(16): 16425-16432.

Sawaya, M.R., Sambashivan, S., Nelson, R., Ivanova, M.I., Sievers, S.A., Apostol, M.I., Thompson, M.J., Balbirnie, M., Wiltzius, J.J.W., McFarlane, H.T. et al. 2007. Atomic structures of amyloid cross-beta spines reveal varied steric zippers. *Nature* **447**(7143): 453-457.

Schindler, T., Herrler, M., Marahiel, M.A., and Schmid, F.X. 1995. Extremely rapid protein folding in the absence of intermediates. *Nat Struct Biol* **2**(8): 663-673.

Schindler, T. and Schmid, F.X. 1996. Thermodynamic properties of an extremely rapid protein folding reaction. *Biochemistry* **35**(51): 16833-16842.

Schonbrunner, N., Koller, K.P., and Kiefhaber, T. 1997. Folding of the disulfide-bonded beta-sheet protein tendamistat: rapid two-state folding without hydrophobic collapse. *J Mol Biol* **268**(2): 526-538.

Semina, E.V., Brownell, I., Mintz-Hittner, H.A., Murray, J.C., and Jamrich, M. 2001. Mutations in the human forkhead transcription factor FOXE3 associated with anterior segment ocular dysgenesis and cataracts. *Hum Mol Genet* **10**(3): 231-236.

Serpell, L.C., Goldstein, G., Dacklin, I., Lundgren, E., and Blake, C.C.F. 1996. The 'edge strand' hypothesis: prediction and test of a mutational 'hot-spot' on the transthyretin molecule associated with FAP amyloidogenesis. *Amyloid* **3**(75-85).

Sharma, K.K., Kaur, H., and Kester, K. 1997. Functional elements in molecular chaperone alpha-crystallin: identification of binding sites in alpha B-crystallin. *Biochem Biophys Res Commun* **239**(1): 217-222.

Shiloh, Y., Donlon, T., Bruns, G., Breitman, M.L., and Tsui, L.C. 1986. Assignment of the human gamma-crystallin gene cluster (CRYG) to the long arm of chromosome 2, region q33-36. *Hum Genet* **73**(1): 17-19.

Shimeld, S.M., Purkiss, A.G., Dirks, R.P., Bateman, O.A., Slingsby, C., and Lubsen, N.H. 2005. Urochordate betagamma-crystallin and the evolutionary origin of the vertebrate eye lens. *Curr Biol* **15**(18): 1684-1689.

Shirley, B.A., Stanssens, P., Hahn, U., and Pace, C.N. 1992. Contribution of hydrogen bonding to the conformational stability of ribonuclease T1. *Biochemistry* **31**(3): 725-732.

Siezen, R.J., Wu, E., Kaplan, E.D., Thomson, J.A., and Benedek, G.B. 1988. Rat lens gamma-crystallins. Characterization of the six gene products and their spatial and temporal distribution resulting from differential synthesis. *J Mol Biol* **199**(3): 475-490.

Simkovsky, R. and King, J. 2006. An elongated spine of buried core residues necessary for in vivo folding of the parallel beta-helix of P22 tailspike adhesin. *Proc Natl Acad Sci U S A* **103**(10): 3575-3580.

Sinha, D., Esumi, N., Jaworski, C., Kozak, C.A., Pierce, E., and Wistow, G. 1998. Cloning and mapping the mouse Crygs gene and non-lens expression of [gamma]S-crystallin. *Mol Vis* **4**: 8.

Sinha, D., Wyatt, M.K., Sarra, R., Jaworski, C., Slingsby, C., Thaung, C., Pannell, L., Robison, W.G., Favor, J., Lyon, M. et al. 2001. A temperature-sensitive mutation of Crygs in the murine Opj cataract. *J Biol Chem* **276**(12): 9308-9315.

Slingsby, C. and Clout, N.J. 1999. Structure of the crystallins. *Eye* **13 (Pt 3b)**: 395-402.

Smulders, R., Carver, J.A., Lindner, R.A., van Boekel, M.A., Bloemendal, H., and de Jong, W.W. 1996. Immobilization of the C-terminal extension of bovine alphaA-crystallin reduces chaperone-like activity. *J Biol Chem* **271**(46): 29060-29066.

Sobott, F., Benesch, J.L., Vierling, E., and Robinson, C.V. 2002. Subunit exchange of multimeric protein complexes. Real-time monitoring of subunit exchange between small heat shock proteins by using electrospray mass spectrometry. *J Biol Chem* **277**(41): 38921-38929.

Song, S., Landsbury, A., Dahm, R., Liu, Y., Zhang, Q., and Quinlan, R.A. 2009. Functions of the intermediate filament cytoskeleton in the eye lens. *J Clin Invest* **119**(7): 1837-1848.

Speed, M.A., Wang, D.I., and King, J. 1996. Specific aggregation of partially folded polypeptide chains: the molecular basis of inclusion body composition. *Nat Biotechnol* **14**(10): 1283-1287.

Stege, G.J., Renkawek, K., Overkamp, P.S., Verschuure, P., van Rijk, A.F., Reijnen-Aalbers, A., Boelens, W.C., Bosman, G.J., and de Jong, W.W. 1999. The molecular chaperone alphaB-crystallin enhances amyloid beta neurotoxicity. *Biochem Biophys Res Commun* **262**(1): 152-156.

Stephan, D.A., Gillanders, E., Vanderveen, D., Freas-Lutz, D., Wistow, G., Baxevanis, A.D., Robbins, C.M., VanAuken, A., Quesenberry, M.I., Bailey-Wilson, J. et al. 1999. Progressive juvenile-onset punctate cataracts caused by mutation of the gammaD-crystallin gene. *Proc Natl Acad Sci U S A* **96**(3): 1008-1012.

Stromer, T., Ehrnsperger, M., Gaestel, M., and Buchner, J. 2003. Analysis of the interaction of small heat shock proteins with unfolding proteins. *J Biol Chem* **278**(20): 18015-18021.

Stroup, A.N. and Gierasch, L.M. 1990. Reduced tendency to form a beta turn in peptides from the P22 tailspike protein correlates with a temperature-sensitive folding defect. *Biochemistry* **29**(42): 9765-9771.

Sun, D.P., Sauer, U., Nicholson, H., and Matthews, B.W. 1991. Contributions of engineered surface salt bridges to the stability of T4 lysozyme determined by directed mutagenesis. *Biochemistry* **30**(29): 7142-7153.

Sun, H., Ma, Z., Li, Y., Liu, B., Li, Z., Ding, X., Gao, Y., Ma, W., Tang, X., Li, X. et al. 2005. Gamma-S crystallin gene (CRYGS) mutation causes dominant progressive cortical cataract in humans. *J Med Genet* **42**(9): 706-710.

Sun, T.X., Akhtar, N.J., and Liang, J.J. 1998. Subunit exchange of lens alpha-crystallin: a fluorescence energy transfer study with the fluorescent labeled alphaA-crystallin mutant W9F as a probe. *FEBS Lett* **430**(3): 401-404.

Sun, T.X., Das, B.K., and Liang, J.J. 1997. Conformational and functional differences between recombinant human lens alphaA- and alphaB-crystallin. *J Biol Chem* **272**(10): 6220-6225.

Takata, T., Oxford, J.T., Brandon, T.R., and Lampi, K.J. 2007. Deamidation alters the structure and decreases the stability of human lens betaA3-crystallin. *Biochemistry* **46**(30): 8861-8871.

Takata, T., Oxford, J.T., Demeler, B., and Lampi, K.J. 2008. Deamidation destabilizes and triggers aggregation of a lens protein, betaA3-crystallin. *Protein Sci* **17**(9): 1565-1575.

Takemoto, L. and Emmons, T. 1991. Truncation of alpha A-crystallin from the human lens. *Exp Eye Res* **53**(6): 811-813.

Talla, V., Srinivasan, N., and Balasubramanian, D. 2008. Visualization of in situ intracellular aggregation of two cataract-associated human gamma-crystallin mutants: lose a tail, lose transparency. *Invest Ophthalmol Vis Sci* **49**(8): 3483-3490.

Tanksale, A., Ghatge, M., and Deshpande, V. 2002. Alpha-crystallin binds to the aggregation-prone molten-globule state of alkaline protease: implications for preventing irreversible thermal denaturation. *Protein Sci* **11**(7): 1720-1728.

Truhlar, S.M. and Agard, D.A. 2005. The folding landscape of an alpha-lytic protease variant reveals the role of a conserved beta-hairpin in the development of kinetic stability. *Proteins* **61**(1): 105-114.

Truscott, R.J. and Augusteyn, R.C. 1977a. Oxidative changes in human lens proteins during senile nuclear cataract formation. *Biochim Biophys Acta* **492**(1): 43-52.

-. 1977b. The state of sulphydryl groups in normal and cataractous human lenses. *Exp Eye Res* **25**(2): 139-148.

Tsutsui, Y., Kuri, B., Sengupta, T., and Wintrode, P.L. 2008. The structural basis of serpin polymerization studied by hydrogen/deuterium exchange and mass spectrometry. *J Biol Chem* **283**(45): 30804-30811.

Udupa, E.G. and Sharma, K.K. 2005a. Effect of oxidized betaB3-crystallin peptide on lens betaL-crystallin: interaction with betaB2-crystallin. *Invest Ophthalmol Vis Sci* **46**(7): 2514-2521.

Udupa, P.E. and Sharma, K.K. 2005b. Effect of oxidized betaB3-crystallin peptide (152-166) on thermal aggregation of bovine lens gamma-crystallins: identification of peptide interacting sites. *Exp Eye Res* **80**(2): 185-196.

Van Leen, R.W., Breuer, M.L., Lubsen, N.H., and Schoenmakers, J.G. 1987. Developmental expression of crystallin genes: in situ hybridization reveals a differential localization of specific mRNAs. *Dev Biol* **123**(2): 338-345.

van Montfort, R.L., Basha, E., Friedrich, K.L., Slingsby, C., and Vierling, E. 2001. Crystal structure and assembly of a eukaryotic small heat shock protein. *Nat Struct Biol* **8**(12): 1025-1030.

Van Montfort, R.L., Bateman, O.A., Lubsen, N.H., and Slingsby, C. 2003. Crystal structure of truncated human betaB1-crystallin. *Protein Sci* **12**(11): 2606-2612.

Villafane, R. and King, J. 1988. Nature and distribution of sites of temperature-sensitive folding mutations in the gene for the P22 tailspike polypeptide chain. *J Mol Biol* **204**(3): 607-619.

Wahlbom, M., Wang, X., Lindstrom, V., Carlemalm, E., Jaskolski, M., and Grubb, A. 2007. Fibrillogenic oligomers of human cystatin C are formed by propagated domain swapping. *J Biol Chem* **282**(25): 18318-18326.

Waldburger, C.D., Jonsson, T., and Sauer, R.T. 1996. Barriers to protein folding: formation of buried polar interactions is a slow step in acquisition of structure. *Proc Natl Acad Sci U S A* **93**(7): 2629-2634.

Wang, K., Cheng, C., Li, L., Liu, H., Huang, Q., Xia, C.-H., Yao, K., Sun, P., Horwitz, J., and Gong, X. 2007. GammaD-crystallin associated protein aggregation and lens fiber cell denucleation. *Invest Ophthalmol Vis Sci* **48**(8): 3719-3728.

Wang, Y., Petty, S., Trojanowski, A., Knee, K., Goulet, D., Mukerji, I., and King, J. 2010. Formation of Amyloid Fibrils In Vitro from Partially Unfolded Intermediates of Human C-Crystallin. *Investigative Ophthalmology & Visual Science* **51**(2): 672-678.

Waudby, C.A., Knowles, T.P., Devlin, G.L., Skepper, J.N., Ecroyd, H., Carver, J.A., Welland, M.E., Christodoulou, J., Dobson, C.M., and Meehan, S. 2010. The interaction of alphaB-crystallin with mature alpha-synuclein amyloid fibrils inhibits their elongation. *Biophys J* **98**(5): 843-851.

Wieligmann, K., Mayr, E.M., and Jaenicke, R. 1999. Folding and self-assembly of the domains of betaB2-crystallin from rat eye lens. *J Mol Biol* **286**(4): 989-994.

Wijnen, J.T., Oldenburg, M., Bloemendal, H., and Meera Khan, P. 1989. GS(gamma-S)-crystallin (CRYGS) assignment to chromosome 3. *Cytogenet Cell Genet* **51**: 1108.

Wilhelmus, M.M., Boelens, W.C., Otte-Holler, I., Kamps, B., de Waal, R.M., and Verbeek, M.M. 2006. Small heat shock proteins inhibit amyloid-beta protein aggregation and cerebrovascular amyloid-beta protein toxicity. *Brain Res* **1089**(1): 67-78.

Wilmarth, P.A., Tanner, S., Dasari, S., Nagalla, S.R., Riviere, M.A., Bafna, V., Pevzner, P.A., and David, L.L. 2006. Age-related changes in human crystallins determined from comparative analysis of post-translational modifications in young and aged lens: does deamidation contribute to crystallin insolubility? *J Proteome Res* **5**(10): 2554-2566.

Wistow, G., Bernstein, S.L., Wyatt, M.K., Behal, A., Touchman, J.W., Bouffard, G., Smith, D., and Peterson, K. 2002. Expressed sequence tag analysis of adult human lens for the NEIBank Project: over 2000 non-redundant transcripts, novel genes and splice variants. *Mol Vis* **8**: 171-184.

Wistow, G., Wyatt, K., David, L., Gao, C., Bateman, O., Bernstein, S., Tomarev, S., Segovia, L., Slingsby, C., and Vihtelic, T. 2005. gammaN-crystallin and the evolution of the betagamma-crystallin superfamily in vertebrates. *FEBS J* **272**(9): 2276-2291.

Wormstone, I.M. 2002. Posterior capsule opacification: a cell biological perspective. *Exp Eye Res* **74**(3): 337-347.

Wu, Z., Delaglio, F., Wyatt, K., Wistow, G., and Bax, A. 2005. Solution structure of (gamma)S-crystallin by molecular fragment replacement NMR. *Protein Sci* **14**(12): 3101-3114.

Xu, J., Baase, W.A., Baldwin, E., and Matthews, B.W. 1998. The response of T4 lysozyme to large-to-small substitutions within the core and its relation to the hydrophobic effect. *Protein Sci* **7**(1): 158-177.

Yamasaki, M., Li, W., Johnson, D.J.D., and Huntington, J.A. 2008. Crystal structure of a stable dimer reveals the molecular basis of serpin polymerization. *Nature* **455**(7217): 1255-1258.

Zampighi, G.A., Hall, J.E., Ehring, G.R., and Simon, S.A. 1989. The structural organization and protein composition of lens fiber junctions. *J Cell Biol* **108**(6): 2255-2275.

Zhang, Z., Smith, D.L., and Smith, J.B. 2003. Human beta-crystallins modified by backbone cleavage, deamidation and oxidation are prone to associate. *Exp Eye Res* **77**(3): 259-272.

Zigler, J.S., Jr., Horwitz, J., and Kinoshita, J.H. 1980. Human beta-crystallin. I. Comparative studies on the beta 1, beta 2 and beta 3-crystallins. *Exp Eye Res* **31**(1): 41-55.

CHAPTER 6:

APPENDICES

APPENDIX A: NMR ANALYSIS OF THE POPULATED FOLDING INTERMEDIATE OF V75D HγD-CRYS

1. Statement of Collaboration

The work described in Appendix A was performed in collaboration with Dr. Jinwon Jung in the laboratory of Dr. Angela Gronenborn (University of Pittsburgh School of Medicine). I prepared both unlabeled and isotope-labeled protein and performed all equilibrium unfolding/refolding experiments. All NMR data were collected and analyzed in the Gronenborn laboratory.

2. Background

WT HγD-Crys folds through an intermediate, although it is not present over a wide range of denaturant concentrations. Studies using triple-tryptophan mutants (Kosinski-Collins et al. 2004) in combination with mutational analysis of the domain interface (Flaugh et al. 2005a) found that the first equilibrium unfolding transition corresponded to unfolding of the N-td, while the second transition corresponded to unfolding of the C-td. Thus, the folding intermediate should have an unfolded N-td while maintaining a fully folded C-td. Due to the high thermodynamic stability of WT HγD-Crys, high-resolution structural studies on this intermediate were not accessible.

In comparison, a stable intermediate was observed in equilibrium unfolding/refolding experiments for both L5S and V75D. This intermediate was populated over a wide range of GdnHCl concentrations. (See Chapter 2 for the full discussion of these mutants.) Based on these and other mutational studies of HγD-Crys (Flaugh et al. 2005a; Flaugh et al. 2005b; Flaugh et al. 2006), the intermediate observed for both L5S and V75D was most likely the same folding intermediate populated by the WT protein. Our interest in the detailed structure of the folding intermediate led to the following studies, and our long-standing collaboration with the laboratory of Dr. Angela Gronenborn, a pioneer in the study of folding intermediates and alternative structures using NMR spectroscopy, facilitated the experiments described below.

3. Preliminary Results and Discussion

Both L5S and V75D appear to populate the same structural intermediate over a similar range of GdnHCl concentrations. V75D was selected for further structural studies due to its ability to fold to the native state at 37°C and the conservation of amino acid identity at this position between the human and murine γD-crystallins. NMR spectroscopy was selected as the method for studying this intermediate because x-ray crystallography is not suitable for the analysis of unstructured or mobile non-native regions of this intermediate.

The charged nature of guanidinium hydrochloride is incompatible with high-resolution NMR structural studies; therefore urea was utilized as the denaturant in all experiments. Initially, it was necessary to determine the experimental conditions for NMR analysis of the intermediate state in urea. Equilibrium unfolding/refolding experiments were performed at 37°C as described in Chapter 2, with the substitution of urea for GdnHCl. Under equilibrium conditions, the N-td of V75D unfolded with a transition midpoint of 2.6 ± 0.06 M urea (Figure 6-1). The folding intermediate was populated from 3.6-7 M urea (Figure 6-1). Tryptophan fluorescence at 360 nm began to increase around 7 M urea, indicating the start of unfolding of the C-terminal domain. However, under these conditions the C-td does not unfold in the range of experimentally accessible urea concentrations. Based on these observations, 3.6 M urea was selected as the denaturant concentration for NMR studies of the folding intermediate. This was chosen in order to significantly populate the intermediate while minimizing the urea concentration.

Both ^{15}N- and $^{15}N,^{13}C$-V75D were expressed in *E. coli* grown in M9 media containing 100% isotope-labeled nitrogen and/or carbon. The protein contained an N-terminal His-tag and was purified by Ni-affinity chromatography as described in Chapter 2. Samples were prepared for NMR first by dialysis into NMR buffer (20 mM NaPi, 5 mM DTT, pH 6.2) followed by concentration of the sample to roughly 0.25 mM (~5 mg/ml). NaN_3 was added to a final concentration of 0.02% to inhibit bacterial growth.

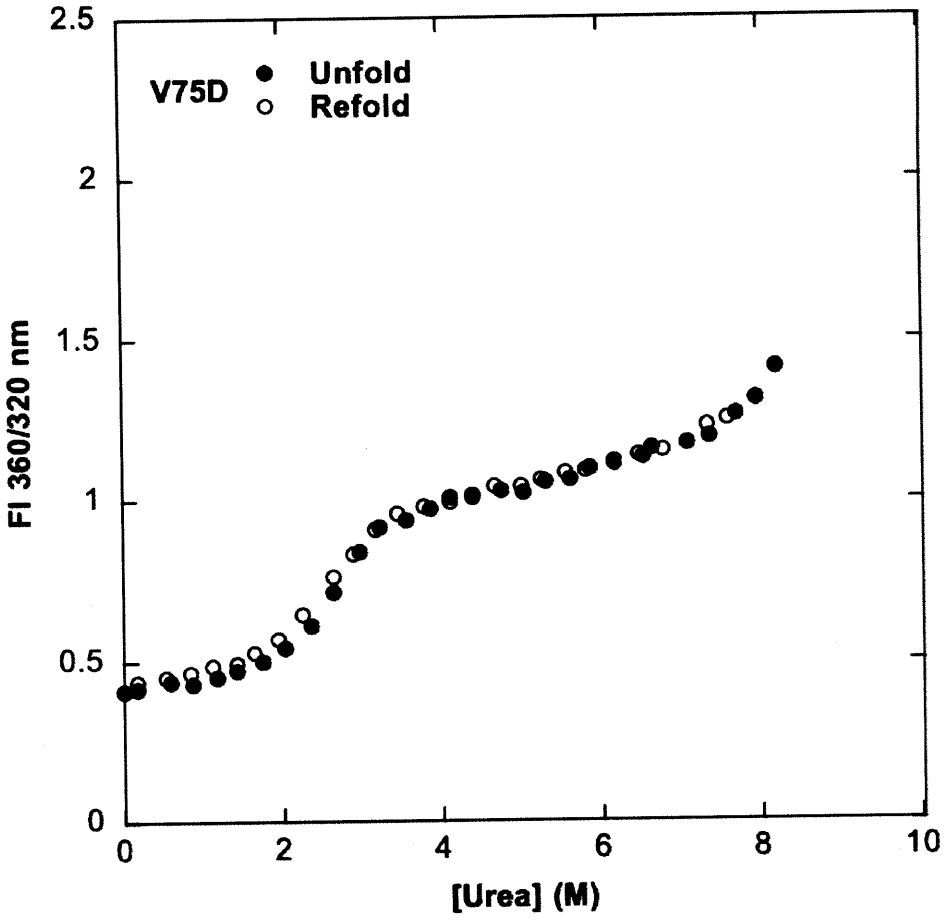

Figure 6-1: Urea equilibrium unfolding/refolding of V75D HγD-Crys. Experiments were performed at pH 7, 37°C after incubation for either 24 or 48 hours at 37°C. Both incubation times yielded the same transition midpoints. Note that the protein is not fully unfolded, even when incubated in 8 M urea.

Initial analyses were conducted to determine the quality of the ^{15}N-V75D sample under native conditions using heteronuclear single quantum coherence (HSQC). This method results in a spectrum containing a peak for every amide proton in the backbone, as well as applicable side chains. If a protein is folded and monodisperse this analysis yields well-resolved peaks for each residue (except proline which does not contain an amide proton), making it an excellent screening method before labor intensive multidimensional NMR experiments are performed. The ^{15}N-^{1}H HSQC spectrum for WT HγD-Crys was collected previously for experiments on the WT protein and the P23T mutant (Jung et al. 2009). HSQC data were collected for V75D and compared with the WT protein under native conditions in identical buffer. The overlaid spectra are shown in Figure 6-2. Both spectra are well resolved under native conditions and most peaks overlay well between the two proteins. As expected the largest deviation is for the mutated position. Next, the same experiment was performed after unfolding V75D in 3.6 M urea. The HSQC spectra of the overlaid native (blue) and partially unfolded (red) V75D are compared (Figure 6-3). Although the resolution of many peaks was diminished and peak broadening was observed upon partial unfolding, several peaks corresponding to residues in the C-td were still well resolved in the presence of 3.6 M urea (Figure 6-4, arrows). This suggests that the N-td loses its native structure upon incubation in 3.6 M urea while the C-td structure is maintained. Further confirmation of this was given by measurement of residual dipolar couplings (RDC). RDCs provide long-range structural information on the orientation of different regions of the protein. Figure 6-5 gives the RDC measurements for each residue of V75D HγD-Crys in 3.6 M urea. Small values (near zero) in the majority of the N-td resulted from the lack of a specific orientation of these residues. The larger values observed for the majority of residues in the C-td suggest a well-ordered structure in this region. Taken with the alignment of peaks in the HSQC in 3.6 M urea, these data suggest a folded, well-ordered C-td with a structure like that of native WT HγD-Crys. The N-td contains little native-like structure. These data support the previous conclusions of King and colleagues regarding the structural nature of the folding intermediate of WT HγD-Crys.

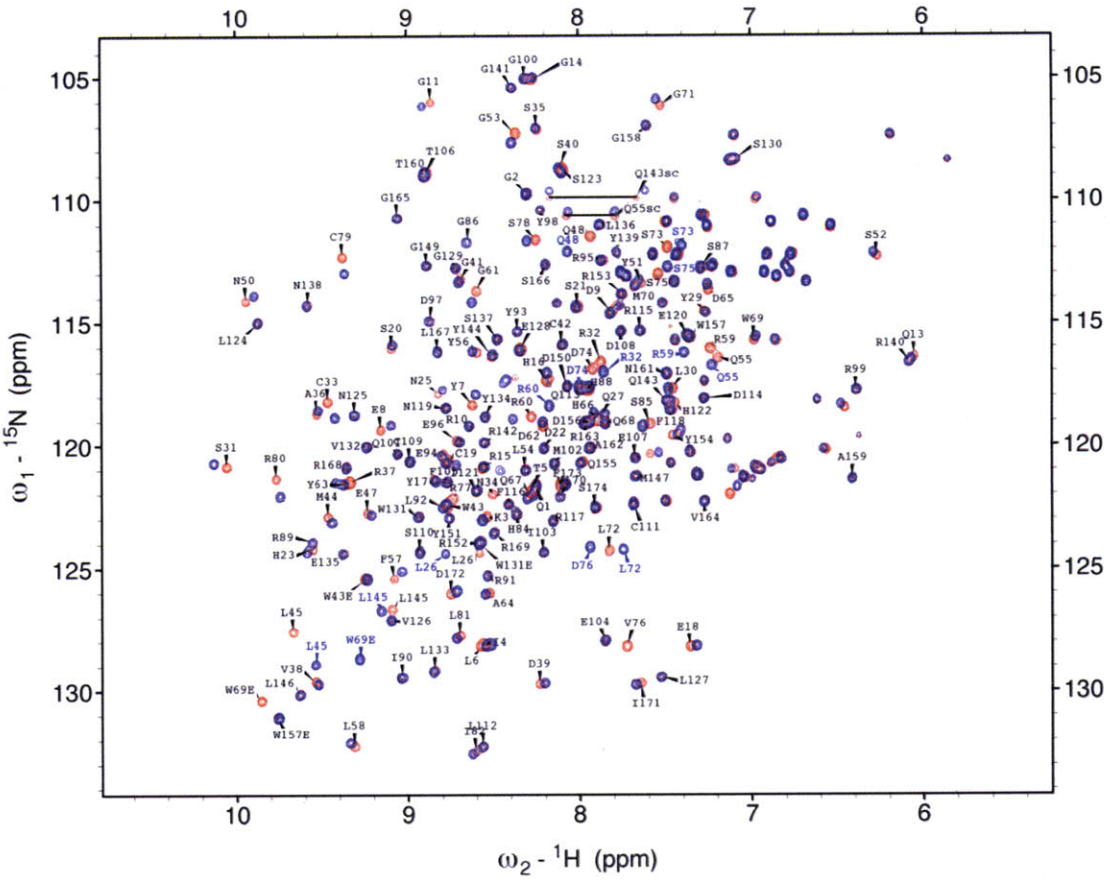

Figure 6-2: ^{1}H-^{15}N HSQC comparison of WT and V75D HγD-Crys in NMR buffer (20 mM NaPi, 5 mM DTT pH 6.2). Red peaks are WT HγD-Crys and blue peaks are V75D. This figure was generously provided by Dr. Jinwon Jung (Gronenborn lab).

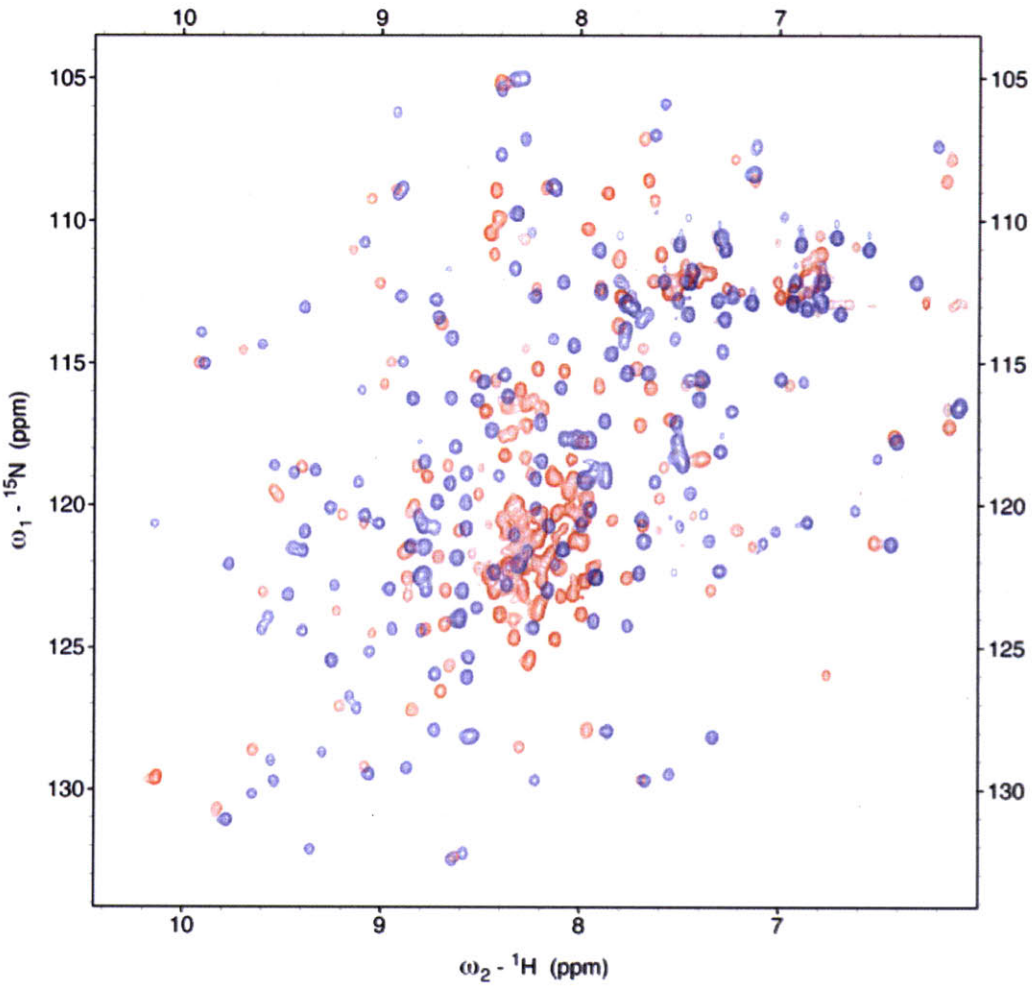

Figure 6-3: Comparison of ^{1}H-^{15}N HSQC spectra for V75D. Spectrum in NMR buffer is shown in blue. Spectrum in NMR buffer containing 3.6 M urea is shown in red. This figure was generously provided by Dr. Jinwon Jung (Gronenborn lab).

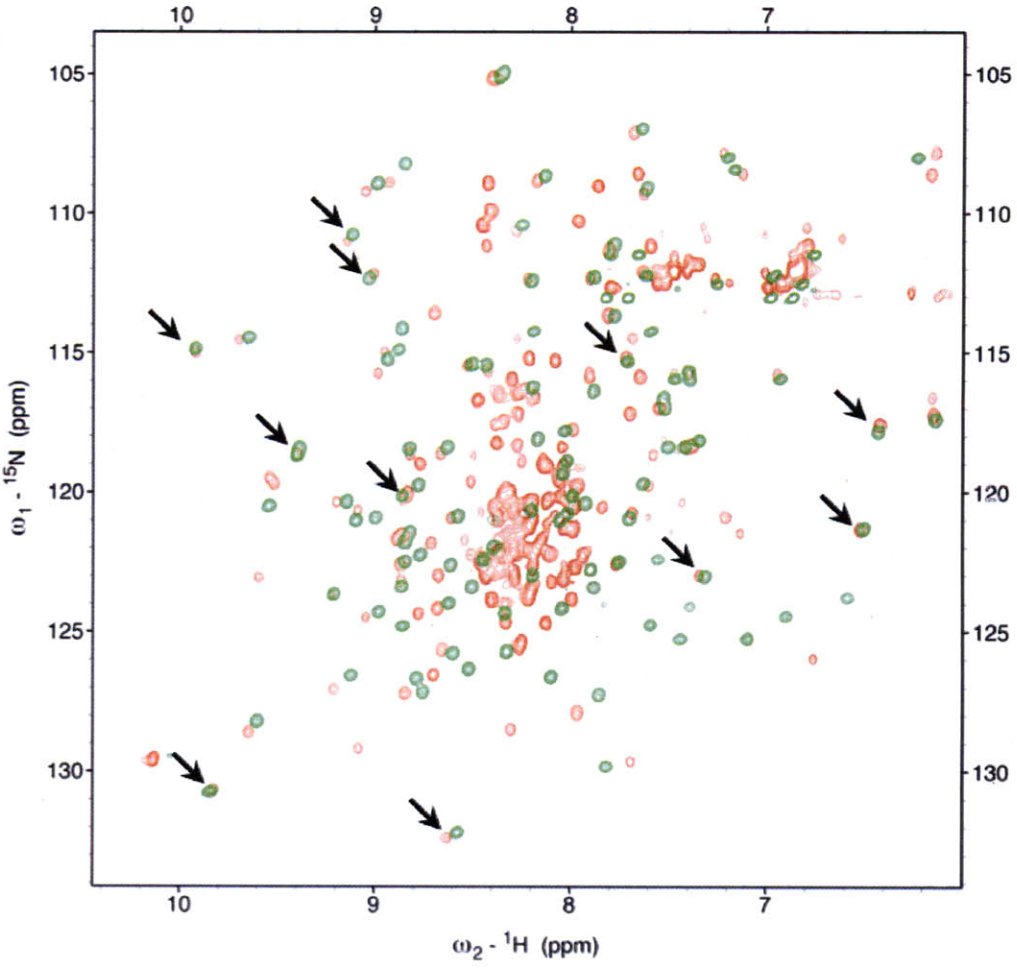

Figure 6-4: Comparison of HSQC spectra of V75D partially unfolded in 3.6 M urea (red) and the isolated C-td of WT HγD-Crys under native conditions (green). The arrows highlight residues in the C-terminal domain whose peaks vary little between the native C-td and the C-td of V75D in 3.6 M urea. This figure was generously provided by Dr. Jinwon Jung (Gronenborn lab).

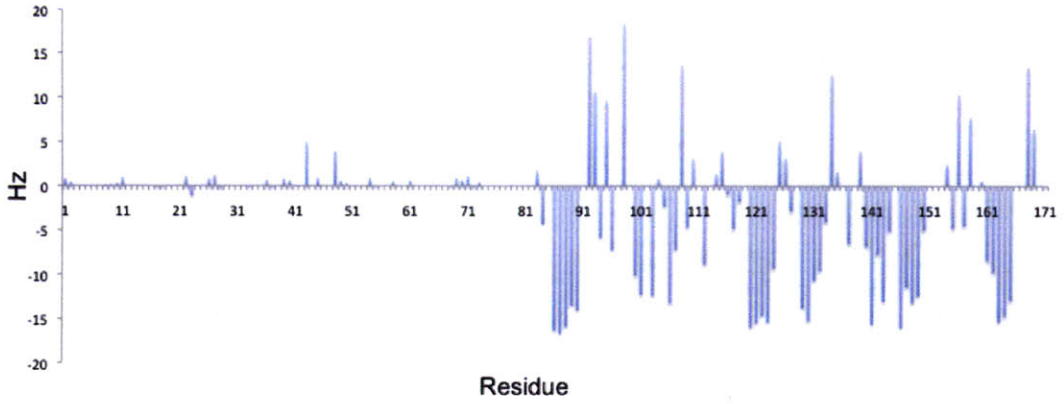

Figure 6-5: ^{1}H-^{15}N residual dipolar couplings for V75D in 3.6 M urea. NMR buffer was as previously described. This figure was generously provided by Dr. Jinwon Jung (Gronenborn lab).

Further data collection under partially denaturing conditions could provide atomic-level details on residues in the C-td. Many important questions remain, such as: (1) What are the differences between the C-td of V75D in 3.6 M urea and in buffer? (2) Are there differences in the presumably exposed C-td interface residues, which form a hydrophobic patch? (3) Are there any regions of residual, non-native structure in the N-td of V75D in 3.6 M urea? Preliminary backbone resonance assignment covered 64% of the N-td (compared with 91% of the C-td) even in 3.6 M urea (J. Jung, personal communication), which suggests some local structure may be present, even under these destabilizing conditions.

The study of this structure is valuable on several levels. First, intermediates by nature are somewhat transient. The dramatic stabilization of this folding intermediate will enable a detailed atomic-level analysis of what is likely an obligate folding intermediate for WT HγD-Crys under physiological conditions. Second, the presence of structure in the unfolded state of a protein is still an open question in biochemistry (McCarney et al. 2005). The unfolded chains are unlikely to be fully extended and they may take on many different conformations involving regions of local structure, which may or may not be native-like. Elucidation of the conformation(s) of the N-td of V75D in 3.6 M urea will shed light on any regions of local structure populated in the "unfolded" state of this protein. In addition, the study of the unfolding of V75D in urea may provide experimental results to complement theoretical and modeling studies on the mechanisms of urea unfolding of proteins (Hua et al. 2008).

APPENDIX B: pK_A ALTERATION IN THE BURIED CORE OF HγS-CRYS

1. Statement of Collaboration

The experiments described in Appendix B were performed in collaboration with Dr. Michael Harms in the laboratory of Dr. Bertrand Garcia-Moreno E. (Johns Hopkins University). I prepared all protein samples and performed all equilibrium unfolding experiments. Continuum calculations were performed in the Garcia-Moreno laboratory.

2. Background

One of the contributing factors to protein stability is formation of the core through the burial of hydrophobic residues (discussed in more detail in Chapter 1). The hydrophobic core is incompatible with buried, charged residues; however, it has been shown that charged residues in an otherwise nonpolar environment are biologically important (for example Luecke et al. 1998; Jiang et al. 2003). The two domains of the γ-crystallins interact through an interface composed of a buried hydrophobic patch. In HγD-Crys a pair of interacting glutamine residues (Q54/Q143) are found above this patch, and at homologous positions in MγS-Crys (and presumably HγS-Crys, no crystal structure is available) a single glutamine residue is conserved (M58/Q148). Deamidation, one of the most common covalent modifications found in the crystallins (Wilmarth et al. 2006), introduces a negative charge at the modified residue. Flaugh *et al.* demonstrated that single and double deamidation at the interface of HγD-Crys led to thermodynamic and kinetic destabilization of the protein (Flaugh et al. 2006). The difference in thermodynamic stability between WT HγD-Crys and the deamidated mutants was minimized at pH 3.0, suggesting that protonation of glutamate at low pH resulted in a WT-like protein, and the destabilization at pH 7 was due to the introduction of a charge in the buried domain interface. The deamidated proteins did however, fold and achieve native-like conformations as measured by far-UV CD and Trp emission

fluorescence spectroscopy. An important question then is how a charged residue could be maintained in the buried core of a protein.

3. Preliminary Results and Discussion

In an attempt to study the properties of the buried charge in deamidated crystallin models, equilibrium unfolding/refolding experiments were performed using urea as the denaturant. Urea is required in these experiments to rule out charge effects that may be associated with denaturation in GdnHCl. Because HγD-Crys does not fully unfold in urea, HγS-Crys was utilized. Thermodynamic stability was measured over the range of pH 4-8 for WT and the deamidated mutant protein Q148E HγS-Crys (summarized in Table 6-1). At pH 6-8, the WT protein is more stable that Q148E, as demonstrated by the left-shifted unfolding curves of Q148E corresponding to lower transition midpoints of urea unfolding (Figure 6-6). At pH 4-5, the difference is completely abolished and the transition regions overlay with one another (Figure 6-6). Destabilization of Q148E relative to WT HγS-Crys is lost at pH 5 and below, suggesting that the glutamate introduced to the interface region becomes protonated at these pH values. The pK_a of free glutamate in water is ~ 4.4 and if this value holds in the context of the buried protein interface, the relative destabilization observed from pH 6-8 would be expected to be maintained at pH 5 where ~ 90% of molecules would be deprotonated. Therefore, it seems that in the relatively protected hydrophobic environment of the HγS-Crys domain interface, the pK_a of glutamate is elevated. Based on the transition midpoint overlap the pK_a of this buried glutamate in the native state must be between 5 and 6. A more stringent method of calculating the pK_a utilizes the $\Delta\Delta G^{\circ}_{H2O\,(pH)}$ (Karp et al. 2007):

$$\Delta\Delta G^{\circ}_{H2O(pH)} = \Delta\Delta G^{\circ}_{H2O(mut)} - RT*\ln((1 + 10^{(pK_a^D - pH)})/(1 + 10^{(pK_a^N - pH)})) \quad \text{(Eqn. 1)}$$

Where $\Delta\Delta G^{\circ}_{H2O\,(mut)}$ represents the energetic cost of the mutation irrespective of charge, pK_a^D is the pK_a of the introduced residue in the denatured state and pK_a^N is the pK_a of the introduced residue in the native state. However, a preliminary analysis of the data with

Table 6-1: Equilibrium unfolding parameters for WT and Q148E HγS-Crys in urea.

	WT HγS-Crys			Q148E HγS-Crys		
pH	C_m [a]	*m*-value [b]	ΔG_{H2O}° [c]	C_m [a]	*m*-value [b]	ΔG_{H2O}° [c]
8	6.2±0.06	2.2±0.3	13.4±1.9	5.6±0.1	1.4±0.2	7.9±0.07
7	6.7±0.06	2.4±0.6	16.4±3.9	6.1±0.07	1.9±0.3	11.5±1.5
6	6.8±0.02	2.5±0.6	16.7±3.8	6.3±0.07	2.3±0.1	14.6±0.06
5	5.9±0.1	3.3±0.5	19.5±2.7	5.9±0.01	2.8±0.2	16.7±1.2
4	4.1±0.06	3.6±0.8	15.0±3.4	4.3±0.04	3.0±0.4	13.0±1.6

[a] Transition midpoints are in units of M urea.
[b] *m*-Values are in units of kcal mol^{-1} M^{-1}.
[c] ΔG_{H2O}° values are in units of kcal mol^{-1}.

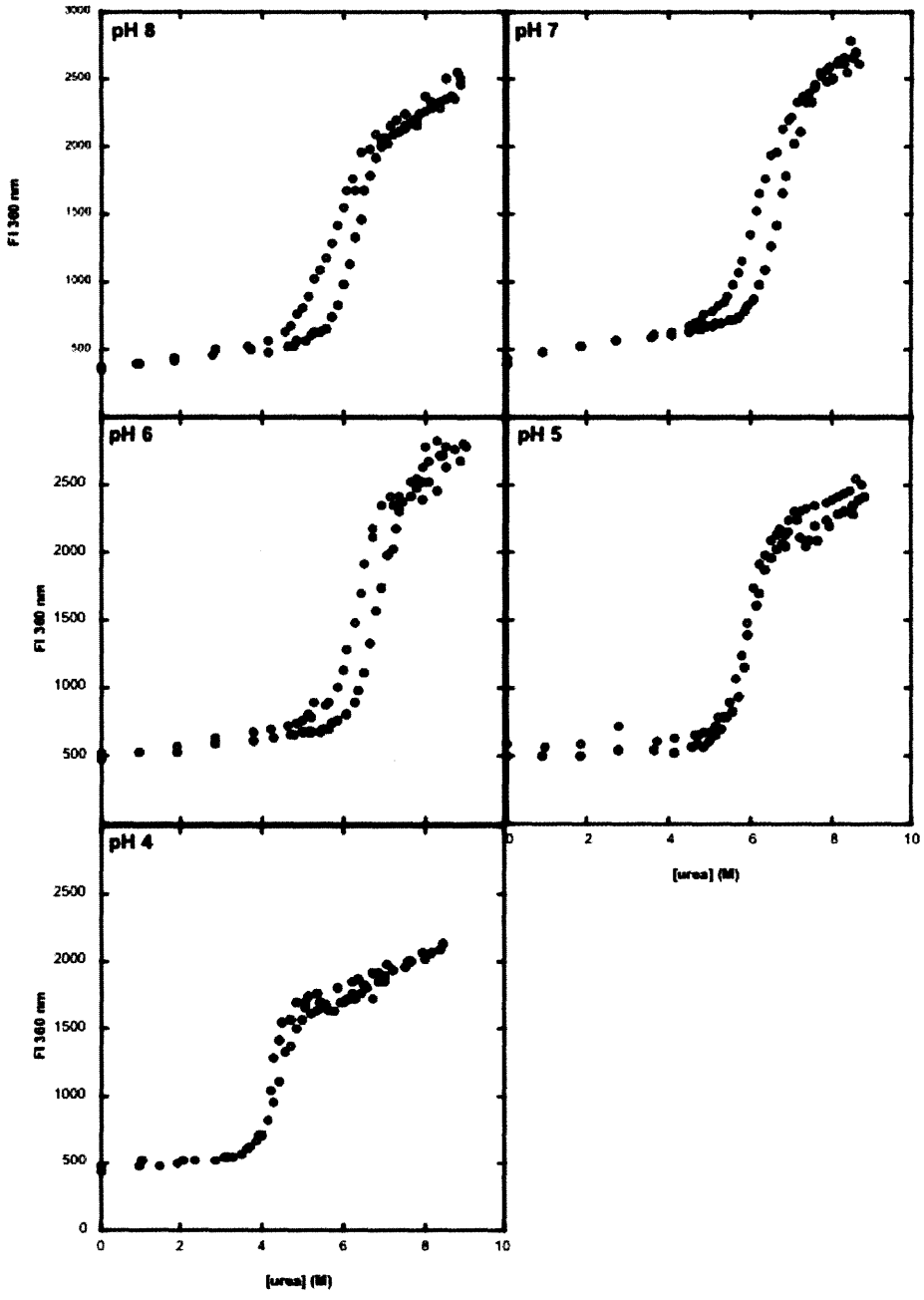

Figure 6-6: Urea equilibrium unfolding of WT and Q148E HγS-Crys over a range of pH values. The destabilizing effect of the deamidation mimic Q148E is lost with decreasing pH. For each plot, (•) is WT HγS-Crys and (o) is Q148E HγS-Crys. All experiments were performed at 37°C and 10 μg/ml protein concentration. Samples were incubated for 24 hours prior to fluorescence measurements.

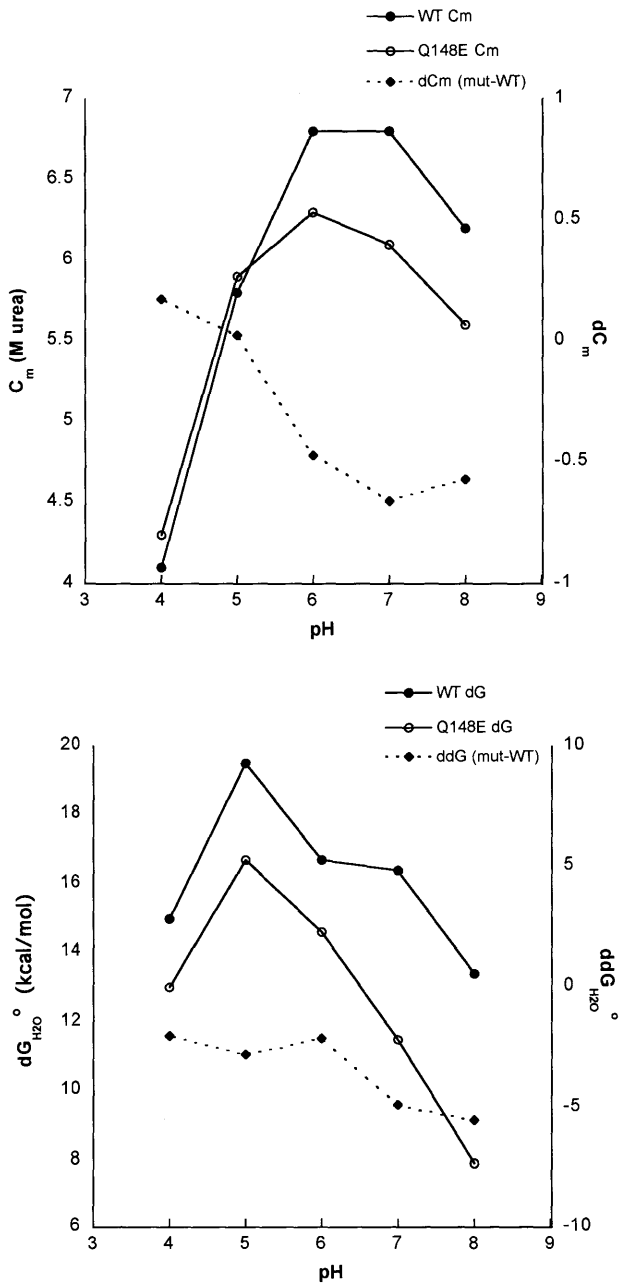

Figure 6-7: (*upper*) Comparison of C_m values versus pH on the left axis and ΔC_m on the right axis, where $\Delta C_m = C_m(Q148E) - C_m(WT)$. (*lower*) Comparison of $\Delta G_{N\text{-}U}^{o}$ versus pH on the left axis and $\Delta\Delta G$ on the right axis, where $\Delta\Delta G = \Delta G(Q148E) - \Delta G(WT)$. See figure legends above.

Eqn. 1 did not produce a good fit. One problem may be the changing *m*-value for each protein with pH, which affects the calculated $\Delta G^{\circ}_{N\text{-}U}$. The *m*-value represents the amount of solvent exposure of buried residues during the unfolding/folding transition and it very well may change with variations in pH. Using a constant *m*-value directly relates the $\Delta G^{\circ}_{N\text{-}U}$ with only changes in the values for C_m at a given pH, however true variations in the *m*-value representing physical changes are then lost. Although the difference in transitions midpoints (ΔC_m) becomes approximately constant by pH 8 (Figure 6-7, *upper panel*), the $\Delta\Delta G^{\circ}_{N\text{-}U}$ appears to still be changing (Figure 6-7, *lower panel*). Experiments at extended high pH values could help to determine if the $\Delta\Delta G^{\circ}_{N\text{-}U}$ baseline truly flattens, and if so, this data would most likely yield a better fit from Eqn. 1.

Calculations made in the Garcia-Moreno laboratory based on C_m values yielded a pK_a of 5.7 for Q148E in the native state. These same calculations gave a pK_a of 5.1 in the denatured state, although this second value is error-prone and the actual physical value is often lower than that estimated by calculation. The more likely pK_a of Q148E in the denatured state is 4.3-4.4 (M. Harms, personal communication). In either case, it is clear that the pK_a of the interface glutamate residue in Q148E HγS-Crys is elevated favoring the neutral state of this side chain within buried regions. The elevation is most likely due to dehydration at these interface residues and it minimizes the energetic cost of burying the charge. However, the elevation is not large enough to neutralize the side chain at physiological pH. Therefore, deamidation *in vivo* would result in the introduction of a charge at the interface and reduce the barrier to unfolding. This could be a viable pathway to crystallin destabilization and age-related cataract development.

APPENDIX C: APPENDIX REFERENCES

Flaugh, S.L., Kosinski-Collins, M.S., and King, J. 2005a. Contributions of hydrophobic domain interface interactions to the folding and stability of human gammaD-crystallin. *Protein Sci* **14**(3): 569-581.

-. 2005b. Interdomain side-chain interactions in human γD crystallin influencing folding and stability. *Protein Sci* **14**(8): 2030-2043.

Flaugh, S.L., Mills, I.A., and King, J. 2006. Glutamine deamidation destabilizes human gammaD-crystallin and lowers the kinetic barrier to unfolding. *J Biol Chem* **281**(41): 30782-30793.

Hua, L., Zhou, R., Thirumalai, D., and Berne, B.J. 2008. Urea denaturation by stronger dispersion interactions with proteins than water implies a 2-stage unfolding. *Proc Natl Acad Sci USA* **105**(44): 16928-16933.

Jiang, Y., Lee, A., Chen, J., Ruta, V., Cadene, M., Chait, B.T., and MacKinnon, R. 2003. X-ray structure of a voltage-dependent K+ channel. *Nature* **423**(6935): 33-41.

Jung, J., Byeon, I.J., Wang, Y., King, J., and Gronenborn, A.M. 2009. The structure of the cataract-causing P23T mutant of human gammaD-crystallin exhibits distinctive local conformational and dynamic changes. *Biochemistry* **48**(12): 2597-2609.

Karp, D.A., Gittis, A.G., Stahley, M.R., Fitch, C.A., Stites, W.E., and Garcia-Moreno, E.B. 2007. High apparent dielectric constant inside a protein reflects structural reorganization coupled to the ionization of an internal Asp. *Biophys J* **92**(6): 2041-2053.

Kosinski-Collins, M.S., Flaugh, S.L., and King, J. 2004. Probing folding and fluorescence quenching in human gammaD crystallin Greek key domains using triple tryptophan mutant proteins. *Protein Sci* **13**(8): 2223-2235.

Luecke, H., Richter, H.T., and Lanyi, J.K. 1998. Proton transfer pathways in bacteriorhodopsin at 2.3 angstrom resolution. *Science* **280**(5371): 1934-1937.

McCarney, E.R., Kohn, J.E., and Plaxco, K.W. 2005. Is there or isn't there? The case for (and against) residual structure in chemically denatured proteins. *Crit Rev Biochem Mol Biol* **40**(4): 181-189.

Wilmarth, P.A., Tanner, S., Dasari, S., Nagalla, S.R., Riviere, M.A., Bafna, V., Pevzner, P.A., and David, L.L. 2006. Age-related changes in human crystallins determined from comparative analysis of post-translational modifications in young and aged lens: does deamidation contribute to crystallin insolubility? *J Proteome Res* **5**(10): 2554-2566.

APPENDIX D: ANALYSIS OF EQUILIBRIUM UNFOLDING/REFOLDING DATA

1. Calculating guanidinium hydrochloride concentration

The concentration of GdnHCl was determined by measuring the refractive indices of samples and applying the following equation:

$$[\text{GdnHCl}] = 57.147*\Delta N + 38.68*\Delta N^2 - 91.60*\Delta N^3$$

where ΔN is the refractive index of the sample minus the refractive index of buffer.

2. Calculating Urea Concentration

The concentration of urea was determined similarly to that of GdnHCl, using the following equation:

$$[\text{Urea}] = 117.66*\Delta N + 29.753*\Delta N^2 + 185.56*\Delta N^3$$

where ΔN is the refractive index of the sample minus the refractive index of buffer.

3. Two-State Equilibrium Unfolding/Refolding

$$\text{Native (N)} \overset{K_1}{\leftrightarrow} \text{Unfolded (U)}$$

$$K_1 = [U]/[N]$$

K_1 is the equilibrium constant for the reaction.
The following equation was used to describe an equilibrium reaction with no intermediates:

$$Y = (Y_N^{\circ} + S_N*[den])*(1/(1 + \exp((m*[den] - \Delta G_1)/RT))) +$$
$$(Y_U^{\circ} + S_U*[den])*(1/(1/\exp((m*[den] - \Delta G_1^{\circ})/RT) + 1))$$

Where Y is the spectroscopic signal of a mixture of native and unfolded protein. Y_N° and Y_U° are the signals of the native and unfolded proteins in the absence of denaturant, respectively, and S_N and S_U are the slopes of the native and unfolded baselines, respectively. ΔG_1° and *m*-value are the equilibrium values of the transition.

$$\Delta G_1^{\circ} = - RT*\ln(K_1)$$

Data were fit to the two-state equilibrium model using the curve-fitting feature of KaleidaGraph. The following algorithm was used for experiments performed at 37°C (310 K). The gas constant is in units of $cal*mol^{-1}*K^{-1}$.

x=m0;
a=ml;
b=m2;
c=m3;
d=m4;

```
e=m5;
f=m6;
;
K1() = exp((c*x-d)/(1.987*310))
;
twost(a0, b0, c0, d0, e0, f0) = (a+b*x)*(1/(1+K1))+(e+f*x)*(1/(1/K1+1))\;
a=a0\; b=b0\; c=c0\; d=d0\; e=e0\; f=f0\;
```

4. Three-State Equilibrium Unfolding/Refolding

$$\text{Native (N)} \overset{K_1}{\leftrightarrow} \text{Intermediate (I)} \overset{K_2}{\leftrightarrow} \text{Unfolded (U)}$$

K_1 and K_2 are the equilibrium constants for the native to intermediate and intermediate to unfolded transitions, respectively. They are related to the concentration of native, intermediate and unfolded protein in the following manner:

$$K_1 = [I]/[N]$$

$$K_2 = [U]/[I]$$

The following equation was used to describe an equilibrium reaction with one intermediate:

$$Y = (Y_N^{\circ} + S_N*[den])(1/(1 + \exp((m_1*[den] - \Delta G_1)/RT) + \exp((m_1*[den] - \Delta G_1)/RT)* \exp((m_2*[den] - \Delta G_2)/RT)) + Y_I*(\exp((m_1*[den] - \Delta G_1)/RT)/(1 + \exp((m_1*[den] - \Delta G_I)/RT) + \exp((m_1*[den] - \Delta G_1)/RT)* \exp((m_2*[den] - \Delta G_2)/RT))) + (Y_U^{\circ} + S_U*[den])((\exp((m_1*[den] - \Delta G_1)/RT)* \exp((m_2*[den] - \Delta G_2)/RT))/(1 + \exp((m_1*[den] - \Delta G_I)/RT) + \exp((m_1*[den] - \Delta G_1)/RT)* \exp((m_2*[den] - \Delta G_2)/RT))$$

Y_N° and Y_U° are the intercepts of the native and unfolded conformations in the absence of denaturant, respectively. S_N and S_U are the slopes of the native and unfolded baselines, respectively. The signal of the intermediate was treated as a single value to reduce the number of unknown variables during the fitting.

$\Delta G_1^{\circ} = - RT*\ln(K_1)$

$\Delta G_2^{\circ} = - RT*\ln(K_2)$

Data were fit to the three-state equilibrium model using the curve-fitting feature of KaleidaGraph. The following algorithm was used for experiments performed at 37°C (310 K). The gas constant is in units of $cal*mol^{-1}*K^{-1}$.

```
x=m0;
a=ml;
b=m2;
c=m3;
d=m4;
e=m5;
f=m6;
g=m7;
h=m8;
i=m9;
;
K1() = exp((c*x-d)/(1.987*310));
;
K2() = exp((e*x-f)/(1.987*310));
;
threest(a0, b0, c0, d0, e0, f0, g0, h0, i0) =
((a+b*x)+g*K1()+((h+i*x)*K1()*K2()))/(1+K1() +K1()*K2())
\;a=a0\; b=b0\; c=c0\; d=d0\; e=e0\; f=f0\; g=g0\; h=h0\; i=i0;
```

APPENDIX E: ANALYSIS OF KINETIC UNFOLDING DATA

1. Two-State Kinetics

The following equation was used to describe a kinetic reaction with no intermediates:

$$A \xrightarrow{k_1} B$$

$$Y = Y_B - (Y_B - Y_A)*\exp(-k_1*t)$$

Data were fit to the two-state kinetic model (single exponential) with the curve-fitting feature of KaleidaGraph using the following algorithm:

```
x=m0;
a=ml;
b=m2;
c=m3;
;
Twokin(a0, b0, c0)=
a*exp(-b*x)+c
\; a=a0\; b=b0\; c=c0\;
```

2. Three-State Kinetics

The following equation was used to describe a kinetic reaction with one intermediate:

$$A \xrightarrow{k_1} B \xrightarrow{k_2} C$$

$$Y = Y_C - (Y_B - Y_A)*\exp(-k_1*t) + (Y_C - Y_B)*\exp(-k_2*t)$$

Data were fit to the three-state kinetic model (double exponential) with the curve-fitting feature of KaleidaGraph using the following algorithm:

```
x=m0;
a=ml;
b=m2;
c=m3;
d=m4;
e=m5;
;
Threekin(a0, b0, c0, d0, e0)=
a*exp(-b*x)+c*exp(-d*x)+e
\; a=a0\; b=b0\; c=c0\; d=d0\; e=e0\;
```

You sound like you're chickensh!t.